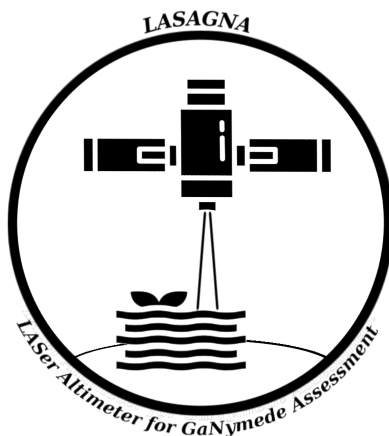


POLITECNICO
MILANO 1863

LASAGNA mission System Design Report



Group 2

Alex Yousef Al Naber 939915
Silvia Bonfanti 952900
Christian Di Lazzaro 945857
Sofia Grusovin 940015
Stefano Mascetti 940314

Claudia Balossi 952954
Mario Corradetti 952839
Marco Di Vitto 952855
Gianluca Lardo 945857

Final Report

Course of Payload Design
School of Industrial Engineering
Academic Year 2020-2021

Contents

1	Introduction	1
1.1	Purpose of the system	1
1.2	Design goals	1
2	Design Guidelines/Approach	2
2.1	Approach	2
2.2	Preliminary trade off analysis	2
2.3	Design drivers	3
2.4	Technical measures	4
2.5	Choice of the orbit	4
3	Environment	6
3.1	Ganymede	6
3.2	Radiative Environment	8
3.3	Ionizing Dose and Shielding Results	10
3.4	Further improvements	14
4	System Architecture	15
5	Operational Scenarios	17
5.1	Safe Mode	17
5.2	Operative Mode	17
5.3	Data Transfer Mode	18
5.4	Focus Mode	18
6	Components Design	19
6.1	Transmitter Unit	19
6.1.1	Transmitter Baffle Unit and Straylight Protection Unit	20
6.1.2	Laser Head Box and Laser Electronic Unit	20
6.1.3	Transmitter Optics and Beam Expander	23
6.2	Receiver Unit	25
6.2.1	Receiver Baffle Unit	26
6.2.2	Receiver Telescope	27
6.2.3	Back-End Optics	28
6.2.4	Avalanche Photo Diode-Assembly	30
6.2.5	Analog Electronic Unit	33
6.3	Electronic Unit	34
6.3.1	Digital Processing Module	34
6.3.2	Range-finder Module	35
6.3.3	Power Converter Unit	35
6.3.4	Data volume	35

7 Thermal Analysis	37
8 Structural Analysis	42
8.1 3D model	42
8.2 Materials selection	43
8.3 Launcher	43
8.4 Stress analysis	44
8.4.1 Static loads	44
8.4.2 Random loads	45
8.4.3 Acoustic loads	45
8.4.4 Design loads	46
8.4.5 Results	46
8.5 Frequency analysis	51
9 Conclusions	54
9.1 Mass and power budget	54
9.2 Final considerations	55
A Mass budget graphical representations	57
B <i>Excelitas</i> Long Wavelength Enhanced Silicon Avalanche Photodiodes	60
C <i>Montfort Laser GmbH</i> M-NANO	63
D <i>Texas Instrument</i> ADS5474-SP	66

List of Figures

2.1	Nearly orbit at 500 km altitude ($i = 87^\circ$)	4
2.2	Groundtracks	5
(a)	1 orbit	5
(b)	1 year	5
3.1	Ganymede surface view	7
3.2	Ganymede internal layers	7
3.3	Ganymede magnetic dipole	8
3.4	Jupiter magnetic environment	9
3.5	Energy spectrum of proton and electron fluxes	9
3.6	Ganymede orbit electron flux spectrum	10
3.7	Ganymede orbit proton flux spectrum	11
3.8	Doses into Ganymede orbit on Al components	11
3.9	Doses into Ganymede orbit on electronics components (Si)	12
3.10	Venus-Earth-Earth gravity assist sequence of interplanetary transfer to Jupiter	12
3.11	Doses during 8 year interplanetary transfer on electronics components (Si)	13
3.12	Doses during 8 years interplanetary transfer on Al components	13
3.13	Tantalum-based shielding	14
4.1	Overall system architecture	16
5.1	Power budget for every mode	18
6.1	Architecture of transmitter unit	20
6.2	Transmitter baffle and straylight protection unit	20
6.3	Laser Electronic Unit	21
6.4	M-NANO 80mJ 10Hz Nd:YAG DPSSL w/ Separate Compact Driver [PR179]	21
6.5	Laser scheme	22
6.6	M-NANO Power consumption	22
6.7	Transmitter optics	23
6.8	Beam expander data	23
6.9	Beam expander architecture	24
6.10	Beam expander 3D architecture	24
6.11	Architecture of receiver and electronic unit	26
6.12	Baffle construction	26
6.13	Stavroudis baffle design	27
6.14	Telescope architecture	28
6.15	Back-End Optics architecture	29
6.16	3D model of Receiver Telescope and Back-End Optics	30
6.17	Excelitas' 1064 nm Si APD	30
6.18	Typical Responsivity at 1060 nm as a function of Operating Voltage	31
6.19	Typical Dark Current as a function of Operating Voltage	31
6.20	Typical Responsivity of APD as function of wavelength	32

6.21	Typical Noise Current as function of gain	32
6.22	Back End Optics Footprint	33
6.23	Texas Instrument ADS5474-S	33
6.24	Laser cycle timing	35
6.25	ELU	36
7.1	Payload configuration in the thermal model	38
7.2	Thermal Control Scheme	39
7.3	MLI composition	40
7.4	Thermal analysis for hot case	41
7.5	Thermal analysis for cold case	41
8.1	Assembly model	43
(a)	3D view	43
(b)	Lateral view	43
8.2	Ariane 5 launcher vehicle by Arianespace	44
8.3	Typical longitudinal static acceleration	45
8.4	Sine excitation at spacecraft base	45
8.5	Acoustic noise load	46
(a)	Sound Pressure Level table	46
(b)	Acoustic noise spectrum	46
8.6	Design loads	46
8.7	Von Mises stresses due to longitudinal acceleration	47
8.8	Zoom on maximum stress	47
8.9	Stress-strain curve of Al 2014-T6	48
8.10	Displacements due to longitudinal acceleration	48
(a)	Displacements	48
(b)	Zoom on laser footprint on the detector	48
8.11	Von Mises stresses due to lateral acceleration	49
8.12	Zoom on maximum stress	49
8.13	Stress-strain curve of Ti-6Al-4V	50
8.14	Displacements due to lateral acceleration	50
(a)	Displacements due to lateral acceleration	50
(b)	Zoom on laser footprint on the detector	50
8.15	Modal frequency analysis of the receiver telescope: fixed at bottom side	51
(a)	$f_1 = 99.04$ Hz	51
(b)	$f_2 = 144.78$ Hz	51
(c)	$f_3 = 148.62$ Hz	51
8.16	Modal frequency analysis of the receiver telescope: fixed on lateral ring	51
(a)	$f_1 = 146.97$ Hz	51
(b)	$f_2 = 560.67$ Hz	51
(c)	$f_3 = 589.82$	51
8.17	Modal frequency analysis of the assembly: fixed at bottom side	52
(a)	$f_1 = 147.83$ Hz	52
(b)	$f_2 = 404.56.36$ Hz	52
(c)	$f_3 = 406.22$ Hz	52
(d)	$f_4 = 479.76$ Hz	52
8.18	Modal frequency analysis of the assembly: fixed on lateral plate	53
(a)	$f_1 = 148.05$ Hz	53
(b)	$f_2 = 255.36$ Hz	53
(c)	$f_3 = 416.72$ Hz	53
(d)	$f_4 = 482.22$ Hz	53

8.19 Final assembly with a close up on the mounting supports	53
9.1 Final assembly and section view	56
9.2 Details of transmitter and receiver units	56
A.1 Components mass	57
A.2 Marginated components mass divided in sub-systems	58
A.3 Sub-systems mass	59
B.1 C30954EH, C30955EH and C30956EH Series	60
B.2 Mechanical and Optical Characteristics	61
B.3 Electro-Optical Characteristics - Case Temperature TA = 22 °C; at the DC reverse operating voltage V, V_{op}	61
B.4 Absolute - Maximum Ratings, Limiting Values	62
B.5 Approximate Field of View	62
B.6 Dimensional Outline (C30954EH, C30955EH Types) Low-Profile TO-5 Package, dimensions in mm (inch)	62
C.1 Introduction	63
C.2 Characteristics	63
C.3 Specifications	64
C.4 Laser Head dimensions	65
C.5 Controller dimensions	65
D.1 A/D converter features	66
D.2 A/D converter block scheme	67
D.3 A/D converter recommended operating conditions	67
D.4 A/D converter electrical characteristics at $T = 25^\circ$	67
D.5 A/D converter architecture	68

List of Tables

2.1	Design guidelines requirements	2
2.2	Design drivers	3
2.3	Technical Measures	4
3.1	Environment requirements	6
3.2	Equivalent Tantalum shielding	14
4.1	Interface Requirements	15
5.1	Operational scenarios requirements	17
5.2	Operative modes	18
6.1	Transmitter Unit requirements	19
6.2	Receiver Unit Requirements	25
6.3	Receiver reflective baffle data	27
6.4	Telescope Data	28
6.5	Back End Optics Data	29
6.6	Avalanche Photo Diode specifications	32
6.7	Electronic Unit Requirements	34
7.1	Thermal requirements	37
7.2	Heat Fluxes	39
7.3	MLI materials properties	40
7.4	Equilibrium Temperatures	40
8.1	Structural Requirements	42
8.2	Materials properties	43
9.1	Mass budget: Transmitter Unit	54
9.2	Mass budget: Receiver Unit	54
9.3	Mass budget: Electronic Unit	54
9.4	Mass budget: Structural Unit	55
9.5	Mass budget: Subsystems	55
9.6	Operative Mode Power Budget	55
9.7	Margined power budget for different operational modes	55

Nomenclature

A/D	Analog to Digital converter
AEU	Analog Electronic Unit
APD	Avalanche Photo-Diode
APD-A	Avalanche Photo-Diode Assembly
AU	Astronomical Unit
BEO	Back-End Optics
BEX	Beam Expander
c	Light speed in vacuum
CGS	Centre Spacial Guyanais
DPM	Digital Processing Module
DPSSL	Diode Pumped Solid State Laser
E	Young modulus
ELU	Electronic unit
ENV	Environment Requirement
FOV	Field Of View
FPA	Focal Plane Assembly
FUN	Functional Requirement
G	Shear modulus
g	Gravity acceleration
HLR	High Level Requirement
INT	Interface Requirement
L/V	Launch Vehicle
LAN	Launcher Requirement
LEU	Laser Electronic Unit
LHB	Laser Head Box
MIS	Mission Requirement

MLI	Multi-Layer Insulator
MOE	Measure Of Effectiveness
MOP	Measure Of Performance
OASPL	Overall acoustic Sound Pressure Level
PCM	Power Converter Module
PER	Performance Requirement
QSL	Quasi-Static Loads
R_J	Jupiter's mean Radius
RBU	Receiver Baffle Unit
REL	Reliability Requirement
RFM	Range-Finder Module
RTL	Receiver Telescope
RX	Receiver
S/C	Spacecraft
SAF	Safety Requirement
SPU	Straylight Protection Unit
STR	Structural Requirement
TBU	Transmitter Baffle Unit
TCU	Thermal Control Unit
THE	Thermal Requirement
TPM	Technical Performance Measure
TT&C	Telemetry and Telecommand unit
TX	Transmitter

1. Introduction

In this report, the development of the preliminary design for the LASAGNA (LASer Altimeter for Ganymede Assessment) mission will be exposed, covering the design guidelines and the approach chosen for the problem. This regards the environmental analysis, the system architecture, the components design, the thermal analysis, the operational scenarios of the mission, and the structural analysis of the instrument.

The purpose of this introduction is to provide a brief overview on the functions of the system and the reasons for its development, its scope, and references to the development context.

1.1 Purpose of the system

The objective of the LASAGNA mission is to perform an altimetric mapping of Ganymede's surface. Obtaining this type of mapping is a necessary step for future missions on the surface of the moon, which is of scientific interest because of Ganymede's unique features and environment.

The system will have to endure the launch phase and the interplanetary transfer, then to be able to operate in the harsh environment of the Jovian system, and finally to send the acquired altimetric data back to the ground station on Earth. To fulfill such goals, the preliminary design of the system has to take into account the various phases of the mission, the environmental and structural constraints, and the interfacing of the instrument with the spacecraft that will carry it. In the development of the preliminary design, previous mission plans with interest in the Jovian system and similar environmental analysis, have been studied.

1.2 Design goals

The horizontal resolution required for mapping is 70 m; the instrument shall be able to achieve it and to cover the highest possible percentage of the surface. In order to achieve this goal, the spacecraft must be in the appropriate orbit around Ganymede, but most importantly the instrument must be able to survive in the Jovian environment for a sufficient time, which is set to be at least two years.[19]

It is possible to divide the mission in three phases: launch, interplanetary travel, and operative time in the Jovian system. While the first phase is negligible from the time point of view, the second will take about eight years. Therefore the minimum lifetime of the instrument shall be ten years.

2. Design Guidelines/Approach

Table 2.1: Design guidelines requirements

ID	Statement	Subsection
R-HLR-010	The instrument shall perform the altimetric mapping of Ganymede's surface	2.2
R-HLR-020	The horizontal resolution of the mapping shall be at least 70 m	2.2
R-MIS-010	The orbit around Ganymede should maximize the coverage of the instrument	2.5
R-MIS-010.1	The orbit around Ganymede should be polar	2.5
R-MIS-020	The orbit around Ganymede shall have an altitude of 500 km	2.5

2.1 Approach

As anticipated in the introduction, the first step in the preliminary design is an overview of other mission plans having similar objectives (destination, necessary environmental studies or type of mapping) to the LASAGNA mission. From there, preliminary estimations on some expected values for the instrument and possible issues for the mission can be deduced. This previous missions analysis allows also to find a baseline for the mission plan and the instrument, which is a very powerful tool since it allows comparison during the initial phases of the design and gives a first estimation of the values that have to be imposed.

2.2 Preliminary trade off analysis

The first design issue is the choice of the type of instrument most suited for the mission. Altimetry satellites determine their distance from the target sources by emitting a pulse, then measuring the satellite-to-surface round trip time. From this time measure, the instrument is able to compute the satellite-to-surface range. Surface height is the difference between the position of the orbiting satellite, with respect to an arbitrary reference surface, and the satellite-to-surface range. This kind of altimetric measures can be obtained using both a laser and a radar altimeter.

A laser altimeter transmits laser pulses towards planetary surfaces with a very narrow beam, which allows for the mapping of surface features with high spatial resolution. The instrument measures the round-trip time of the light pulse between the emission and the returned reflection to determine the distance of the spacecraft, with respect to the surface itself, as in Eq. (2.1).

$$z = \frac{c\Delta t}{2} \quad (2.1)$$

Where $c = 299792458$ m/s, and Δt is the difference between the return and the emitted pulse time.

An optical telescope is used to collect the detected laser photons onto an avalanche photodiode. A very precise time measurement between pulse emission and return signal detection is used for the precise altitude estimations.

The working principle of a radar altimeter is very similar, but in this case the antenna emits microwave pulses. When these pulses interact with the rough surface, part of the incident radiation is reflected back to the altimeter and it is collected by the receiving antenna. The altitude is determined from the roundtrip time and waveform of the returned signal.

In order to choose the proper technology, a preliminary trade-off between the two candidates must be performed. The laser altimeter has a smaller footprint with respect to the radar and this will lead to a smaller coverage of the surface. However, the laser will obtain a higher resolution of the altimetry. In addition to this, the laser will have a lower mass and will occupy a lower volume with respect to the radar. On the other hand, the laser has a bad atmosphere penetration, compared to the radar. Another important difference between the two technologies is the fact that the radar is more subjected to the magnetic perturbation and the radio noises from Jupiter. This will translate in more power required by the radar in order to compensate for the losses. The laser altimeter allows for a higher vertical resolution with higher energy saving. Furthermore, it is known, from previous mission projects, that the radio noise from Jupiter will make it very difficult for the radar to operate nominally for most of the time spent in orbit. This nullifies the advantage of a faster mapping given by the larger covered area. The other main benefit of the radar is the atmosphere penetration, which is not so relevant in this mission scenario, since Ganymede presents a very rarefied atmosphere. All these considerations led to the choice of the laser altimeter as the best solution for this mission.

2.3 Design drivers

Once the baseline and the type of technology for the instrument are established, it is important to state the design drivers for the project (see Table 2.2): these parameters will be optimized because of their high influence on performance, mass, power and cost of the mission.

Table 2.2: Design drivers

Driver	What limits driver	What driver limits	Where discussed
Mass	Launcher requirements, integration with spacecraft	Components design	chapter 6
Size	Launcher requirements integration with spacecraft	Components design	chapter 6
Surface coverage	Lifetime, orbit, FOV	Shielding, materials choice	section 2.5, 3.3
Power	Size, mass	Lifetime, bus design, components design	chapter 6
Data rate	Storage, processing	Communication time and capabilities	section 6.3.4
Temperature	Components	Components design, materials choice	chapter 7

2.4 Technical measures

After the design drivers, a list of technical measures is set: this measures, reported in Table 2.3, will be precisely tracked and assessed throughout the entire design process to ensure the product effectiveness and the customer's satisfaction.

Table 2.3: Technical Measures

Measure	Type	Motivation	Where discussed
Mapping resolution	MOP	Good quality mapping and results	section 6.2.5
Equilibrium temperatures	TPM	Survival needs, operational needs	chapter 7
Natural vibration frequencies	TPM	Launcher requirements	chapter 8
Telescope dimensions	MOE	Launcher requirements	section 6.2.2
Data storage	MOE	Power and mass budget	section 6.3.4

2.5 Choice of the orbit

When approaching the choice of the orbit, it is important to take into account both the desired coverage of the instrument and the environmental characteristics that may affect orbit stability. The main goal, as anticipated in the introduction, is to allow the instrument to acquire data on the highest possible percentage of the moon's surface. The presence of Jupiter's perturbation would tend to circularize the orbit around Ganymede, making it very expensive from a maneuvering point of view to maintain a highly eccentric path. Also the radius of the orbit with respect to Ganymede's magnetosphere is an important parameter to evaluate.

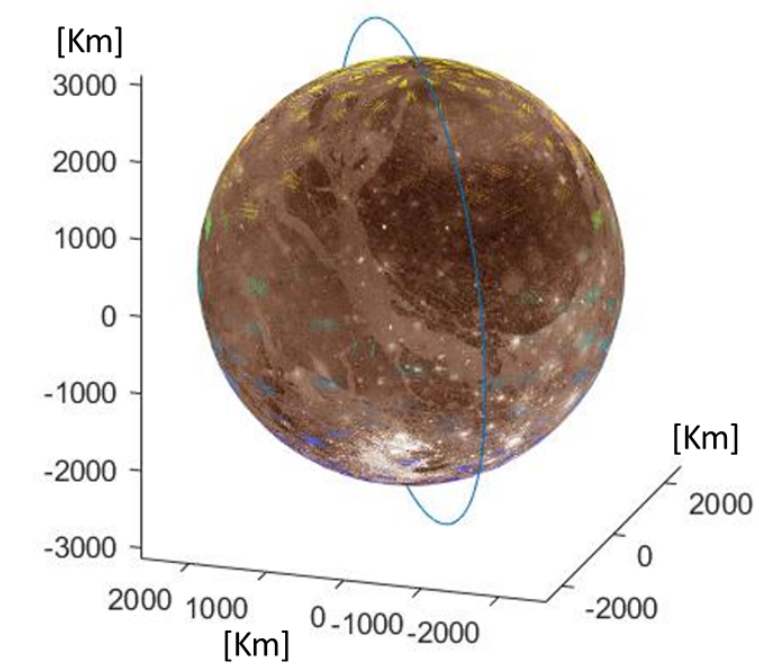


Figure 2.1: Nearly orbit at 500 km altitude ($i = 87^\circ$)

After the previous considerations, a circular nearly polar orbit at 500 km altitude has been selected (Fig. 2.1); its theoretical ground track on Ganymede's surface shows that the coverage is satisfactory considering the use of a single laser beam, as depicted in Fig. 2.2. It is known from literature that from 500 km altitude, the spot size on the surface of a laser altimeter can be around 50 m, which is in line with the customer requirement on the horizontal resolution.

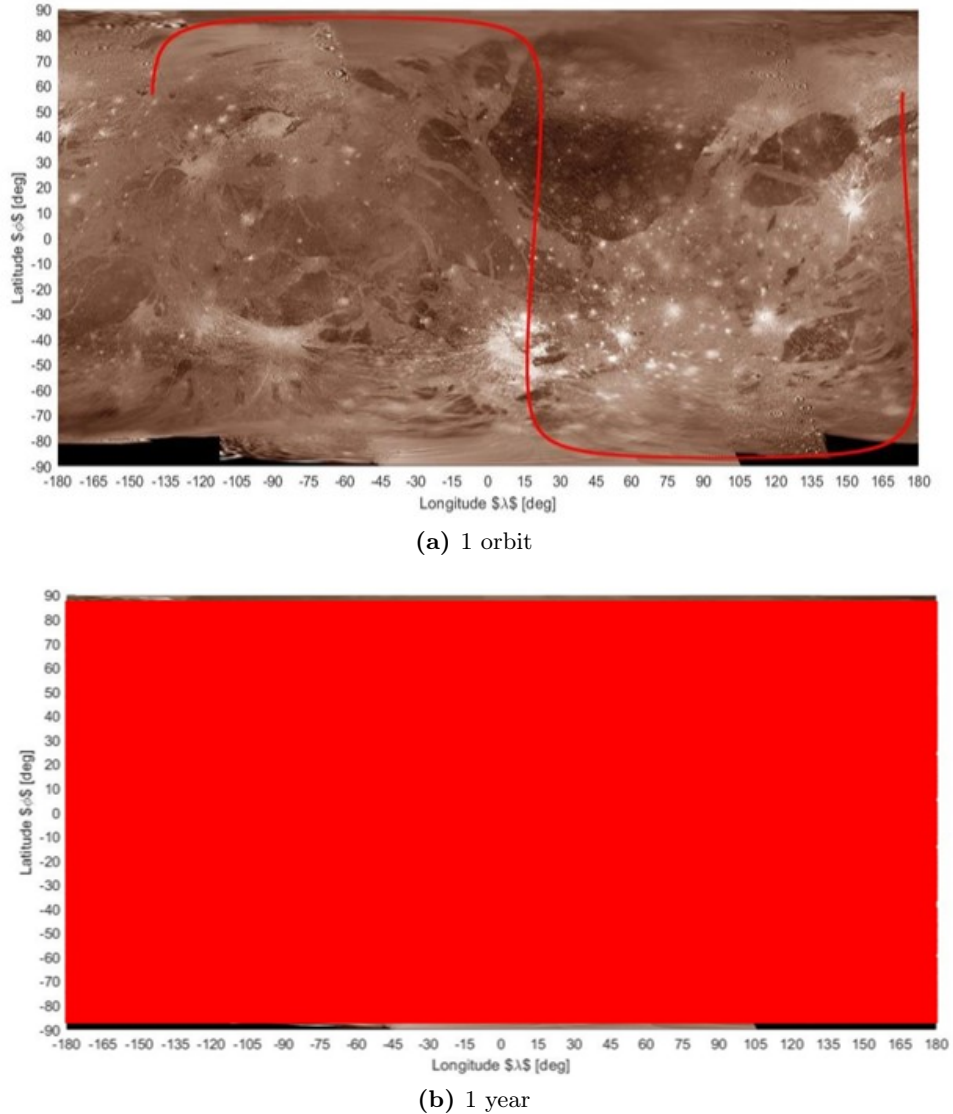


Figure 2.2: Groundtracks

3. Environment

Table 3.1: Environment requirements

ID	Statement	Section
R-HLR-030	The minimum lifetime of the spacecraft shall be 10 years	3.3
R-MIS-020	The orbit around Ganymede shall have an altitude of 500 km	3.3
R-REL-030	The electronic components shall resist the highest radiation encountered during the mission	3.3
R-ENV-010	The instrument shall operate in jovian environment	3.2
R-ENV-020	The instrument shall survive to the interplanetary transfer to Ganymede	3.3
R-ENV-030	The instrument shall survive to the hottest Venus fly-by	3.3
R-ENV-040	The instrument shall survive to the coldest position in Jupiter shadow	3.3
R-ENV-070	The spacecraft TCU shall cope with the space environment	3.2, 3.3
R-SAF-010	The instrument shall be designed according to the standards	3.3

3.1 Ganymede

The Jovian System is often compared to a miniature solar system as a result of its dynamism, the massive amount of emitted energy, the huge magnetosphere, and its large number of satellites. This combination makes it a very interesting destination for scientific missions. Ganymede is a unique and interesting satellite of Jupiter and the most massive moon of the Solar System. Despite all the recent interest and missions to the Jovian System, its topographic data are of relatively coarse resolution and very limited areal extent. The moon is most likely composed by equal parts of rocky material and of water ice, up to a mass fraction of 50-90%. Its surface is very asymmetric, composed by a mix of light, younger regions, and dark, older terrain. Ganymede's dark terrain contains clays and organic materials, which may indicate the composition of the impactors from which Jovian satellites accreted. This might give clues about the formation of the Jovian System.

Concerning the internal layers, Ganymede is made by a subsurface salt-water ocean, making it a candidate location for life. Its liquid iron–nickel-rich core explains the intrinsic magnetic moment of the moon (three times larger than the magnetic moment of Mercury). Ganymede is in fact the only satellite with its own dynamo magnetic field as a dipole. The magnetosphere is unique, being the only known example of magnetosphere created by superimposition with the background magnetic field of Jupiter.

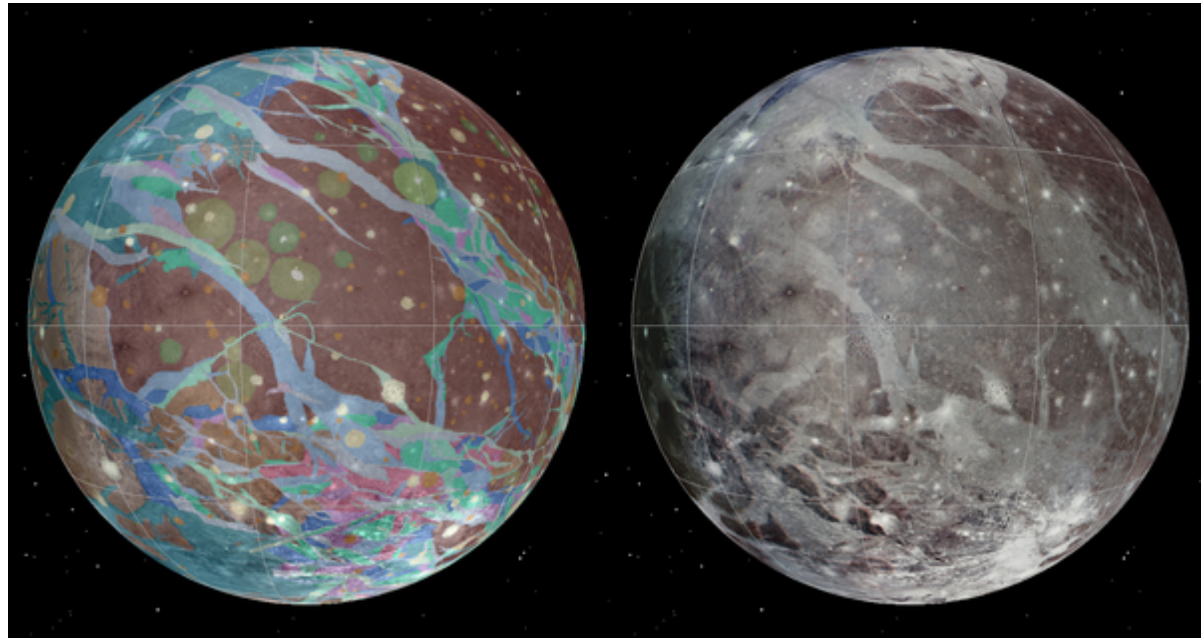


Figure 3.1: Ganymede surface view

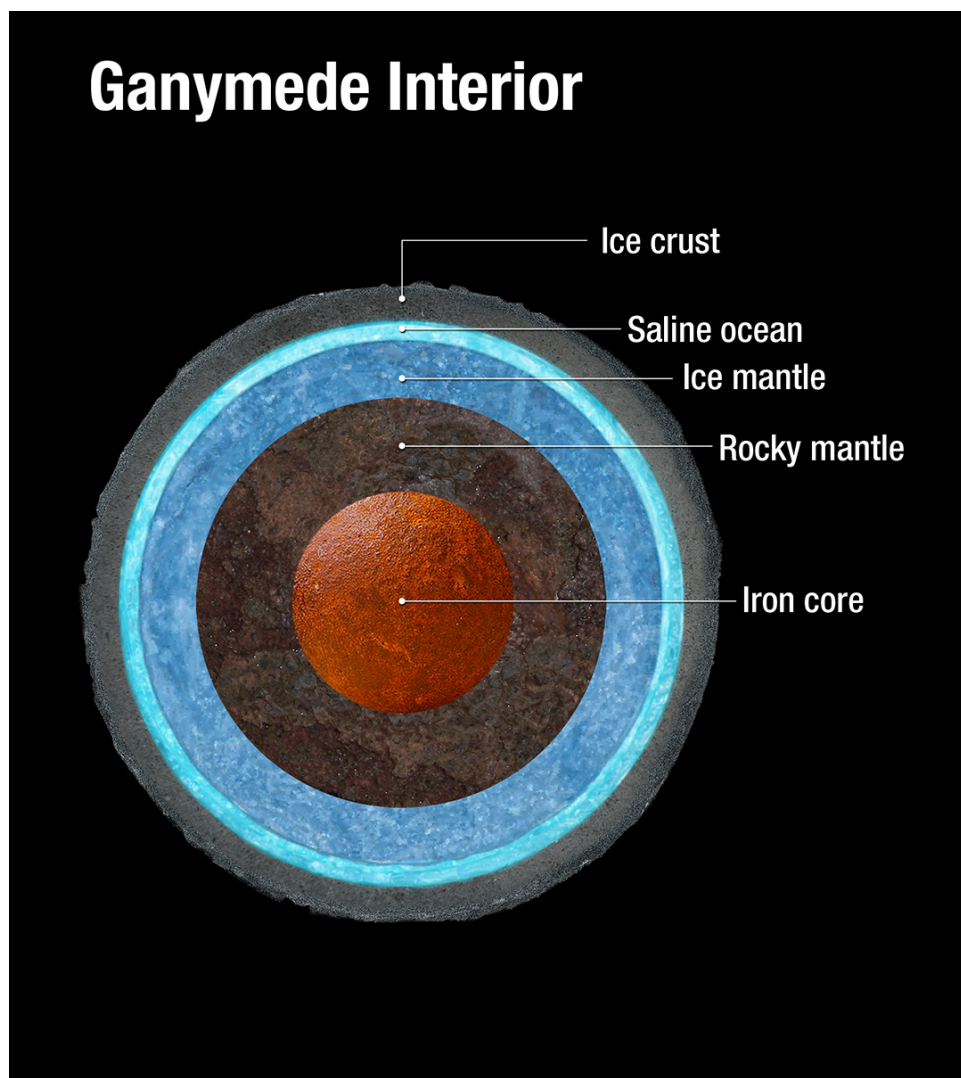


Figure 3.2: Ganymede internal layers

3.2 Radiative Environment

The radiative environment of Jupiter, depicted in Fig. 3.3 and Fig. 3.4, is considered to be one of the most aggressive, in terms of ionising radiation in our Solar System. The latest researches by ONERA developed a theoretical model of the trapped electrons and protons in Jupiter's radiation belts. It is based on the Earth's Salammbô code and the resultant energy spectrum is underlined in Fig. 3.5, compared with other available models. The Salammbô model is valid for ranges up to the orbit of Europa (distance from Jupiter: $9.4 R_J$) for electrons, and up to the orbit of Io ($6 R_J$) for protons, but Ganymede ($15 R_J$) is outside this range and a complete model is not available yet [16]. It is important to note that the current models only describe the trapped particles in Jupiter's radiation belt and exclude solar energetic particles, cosmic rays, and heavy ions from the Jovian System. The combination of this effect with the dipole of Ganymede creates specific conditions, which need to be carefully studied in terms of radiations on spacecrafts and instruments.

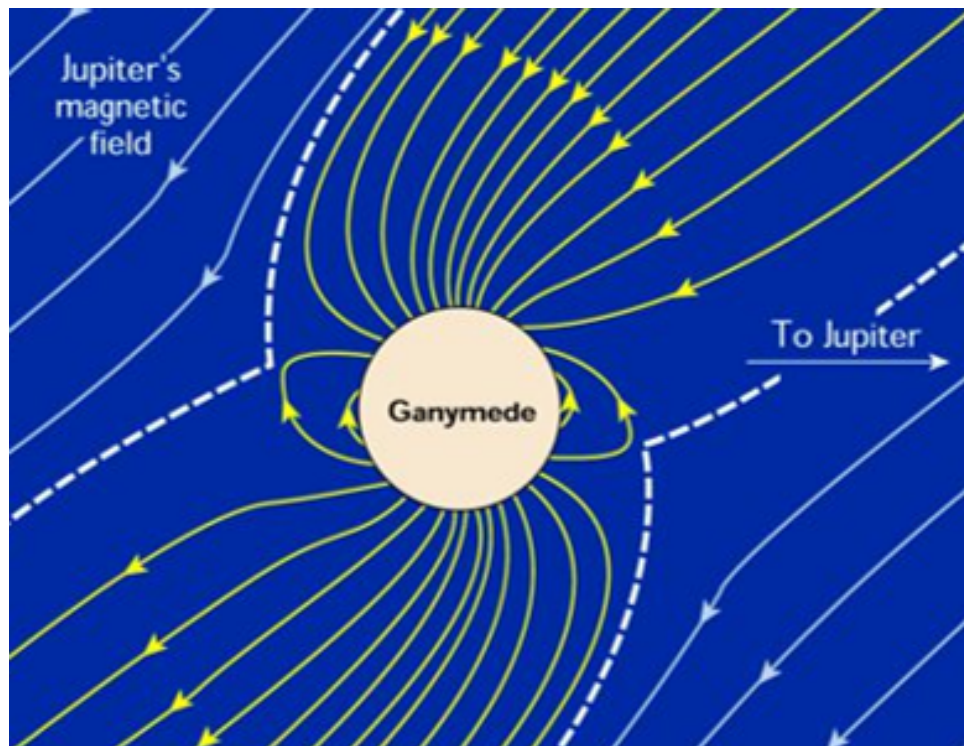


Figure 3.3: Ganymede magnetic dipole

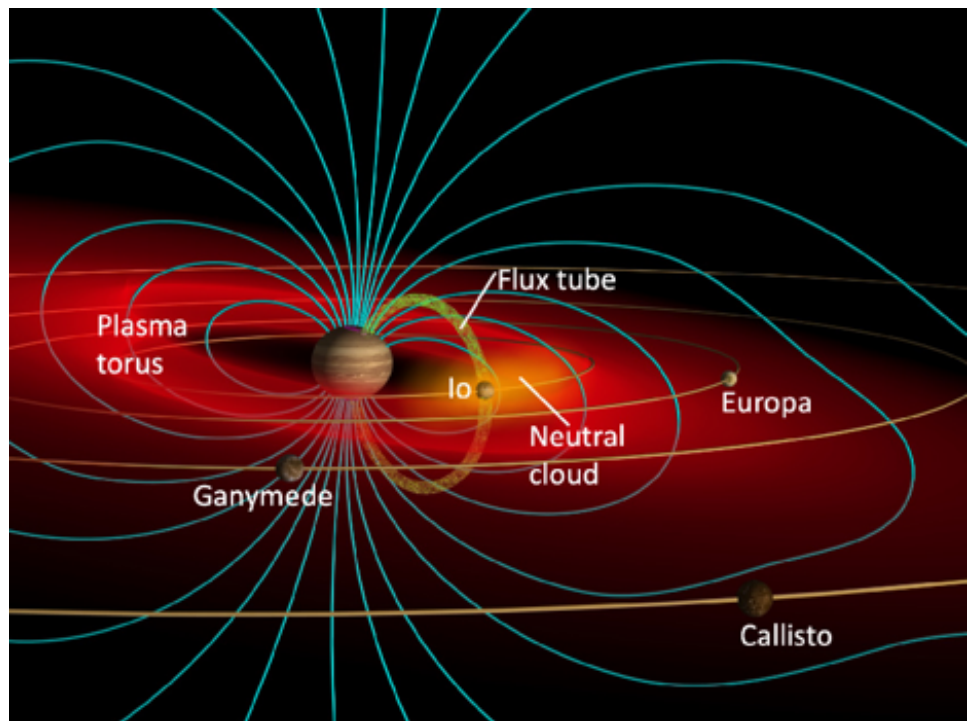


Figure 3.4: Jupiter magnetic environment

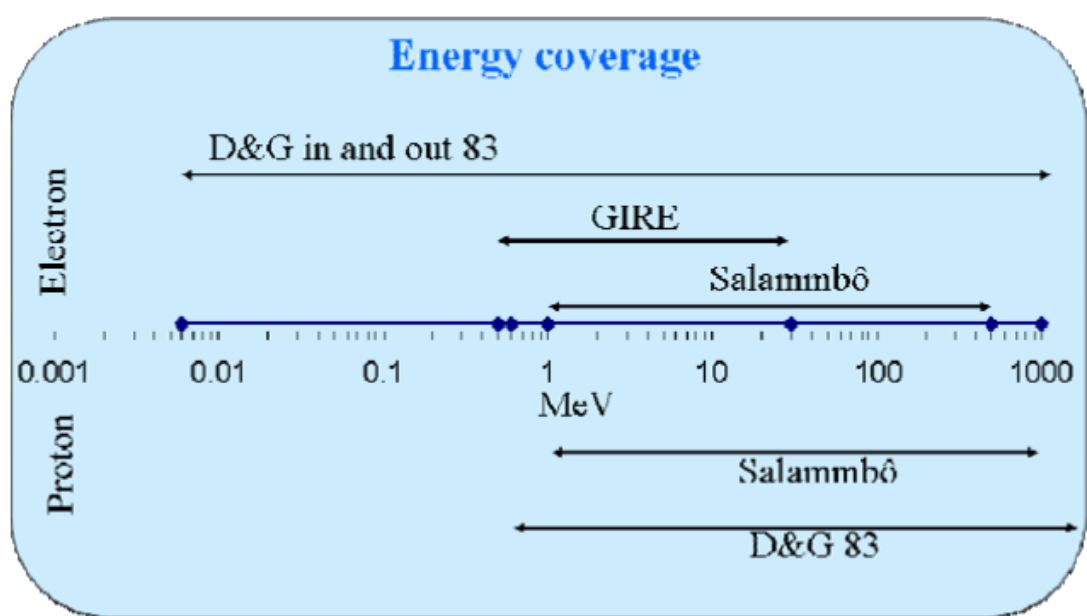


Figure 3.5: Energy spectrum of proton and electron fluxes

3.3 Ionizing Dose and Shielding Results

To validate all scenarios, an examination of some research papers, coming from previous mission studies, has been performed to get a better insight of the problem and risks ([16], [10], [8]). For this purpose the mission can be divided into two main segments: the interplanetary travel to Jupiter and the insertion and operational lifetime on orbit around Ganymede. The analysis process has been kicked off with the SPENVIS software by ESA, to integrate the doses in the overall time frame.

A complete model of Ganymede's magnetosphere and radiation conditions is not completely developed yet. Therefore, to simulate as much as possible the real mission environment, the orbit of Ganymede around Jupiter has been selected for the second mission phase. During the operational phase, a study on the number of doses and the needed Al protection layer thickness has been performed. The results are represented in Fig. 3.6 and 3.7 as the spectrum of electron and proton fluxes, at the Ganymede orbit, during the whole 2 years of mission.

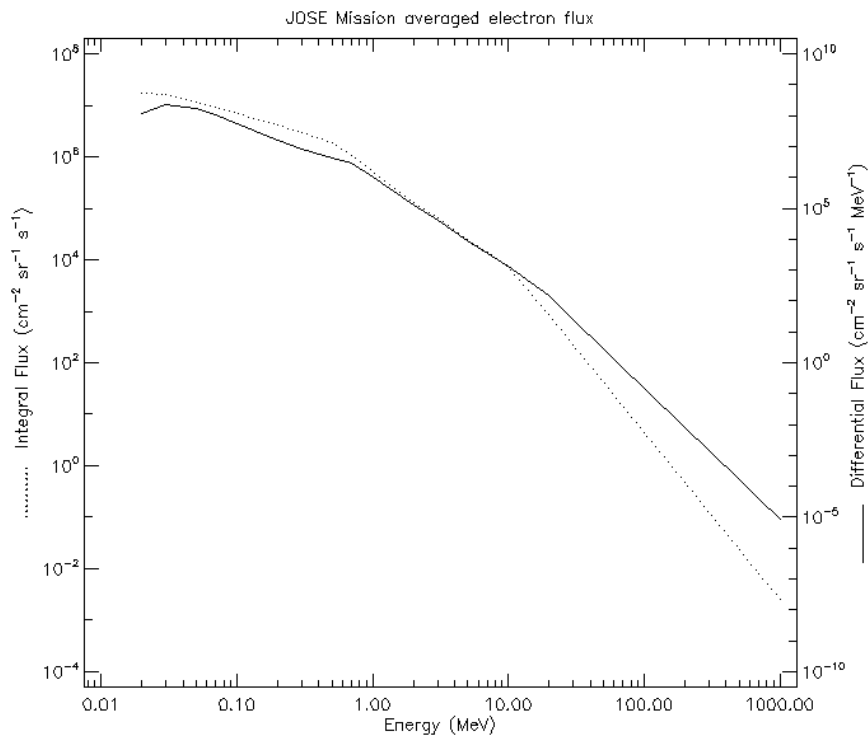


Figure 3.6: Ganymede orbit electron flux spectrum

The number of doses impacting on internal components, made by Silicon and Aluminum, under an Aluminum shielding, are represented in Fig. 3.8 and 3.9. A minimum protection of 7 mm is necessary to consistently reduce the failure risk against the 10^4 rad of total radiation.

The first mission phase, the interplanetary travel, lasts 8 years at least, with multiple fly-by of Venus and Earth and eventually even of Mars. We can see in Fig. 3.10 an interplanetary transfer example taken as reference from previous missions scenarios. SPENVIS cannot estimate such a complex path, therefore a near Earth interplanetary trajectory at 1 AU has been considered to ensure average results as first approximation. The amount of Doses reaching internal components, under a similar Aluminum protection, are about one order of magnitude less than the ones during the second mission phase. Accordingly, the formers could be considered negligible consistently also with available previous mission data. Doses into Silica and Aluminum components are plotted as function of the Al shielding thickness in Fig. 3.11 and Fig. 3.12 .

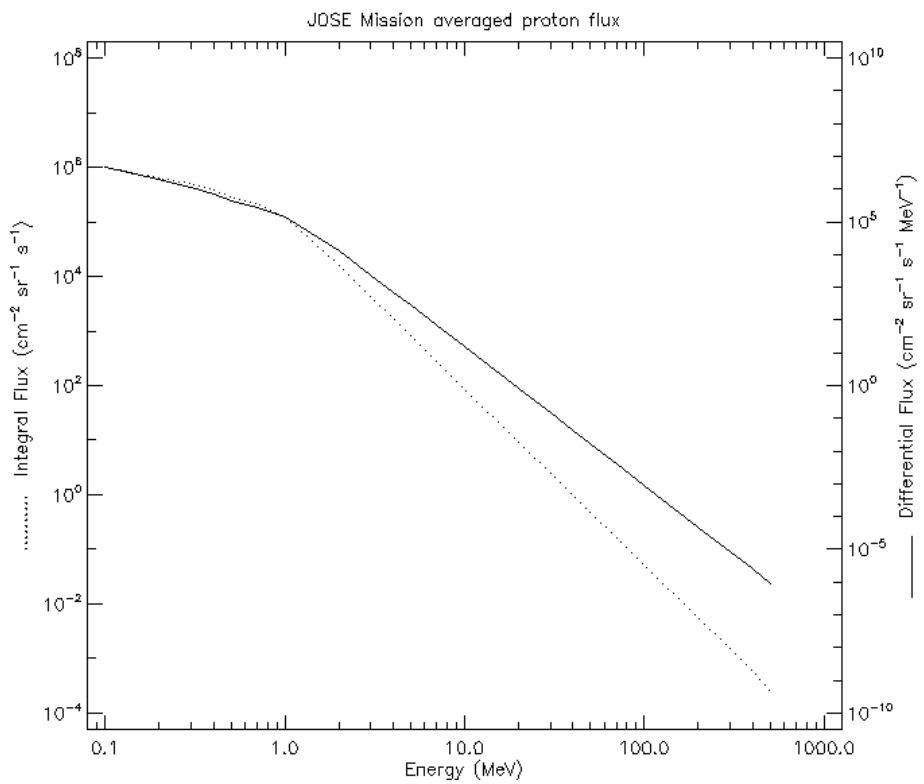


Figure 3.7: Ganymede orbit proton flux spectrum

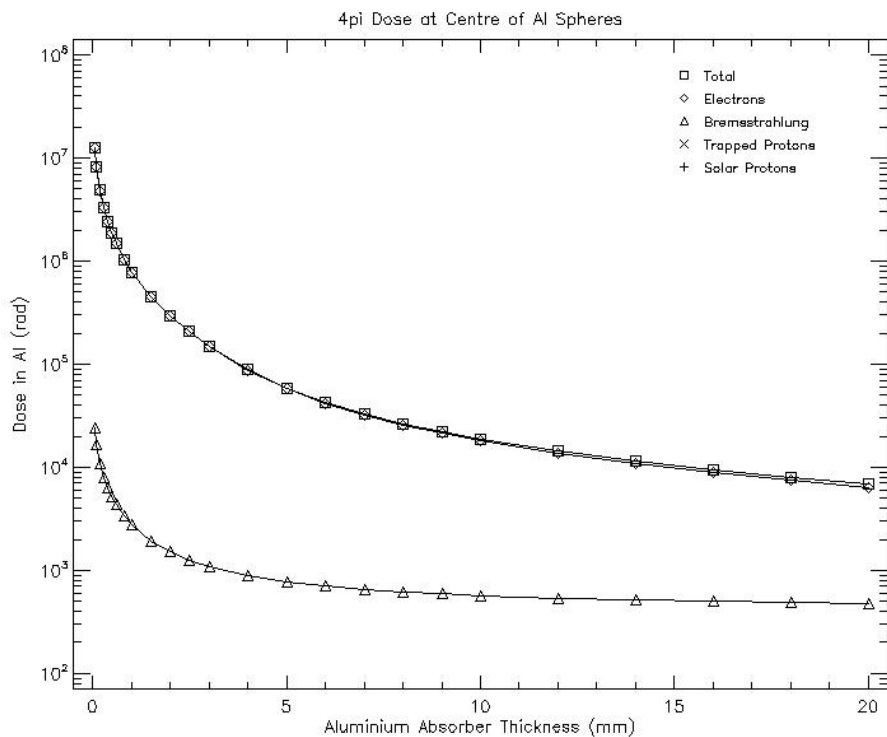


Figure 3.8: Doses into Ganymede orbit on Al components

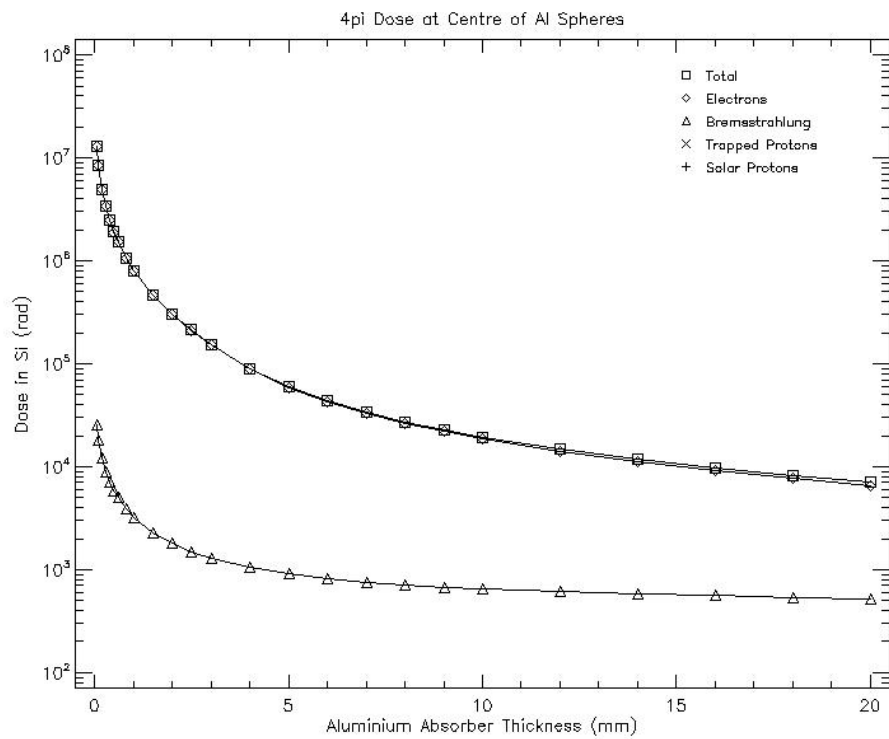


Figure 3.9: Doses into Ganymede orbit on electronics components (Si)

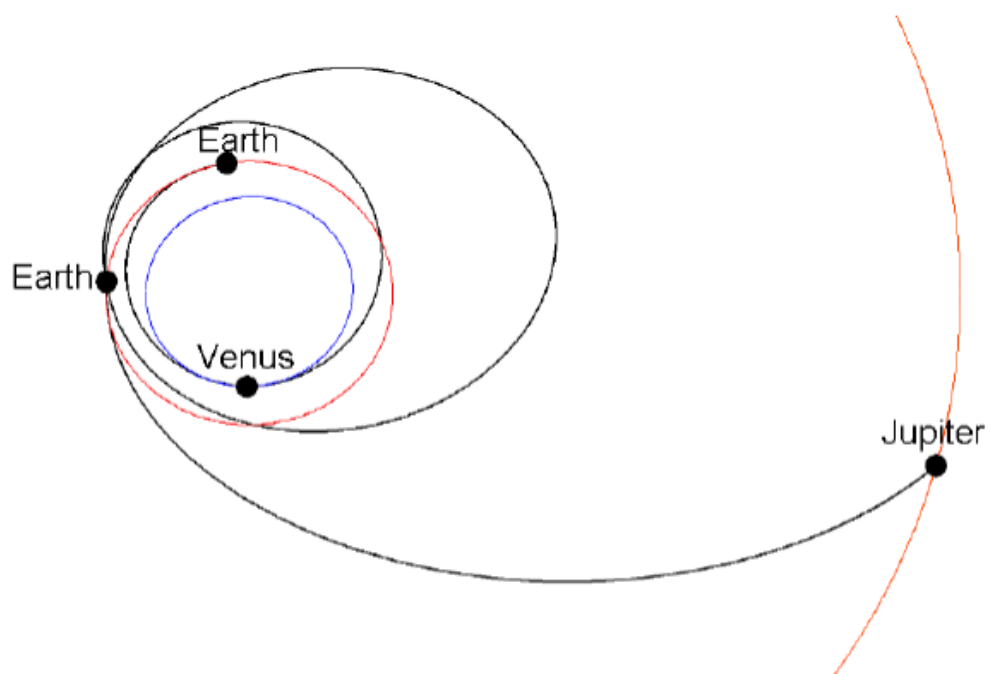


Figure 3.10: Venus-Earth-Earth gravity assist sequence of interplanetary transfer to Jupiter

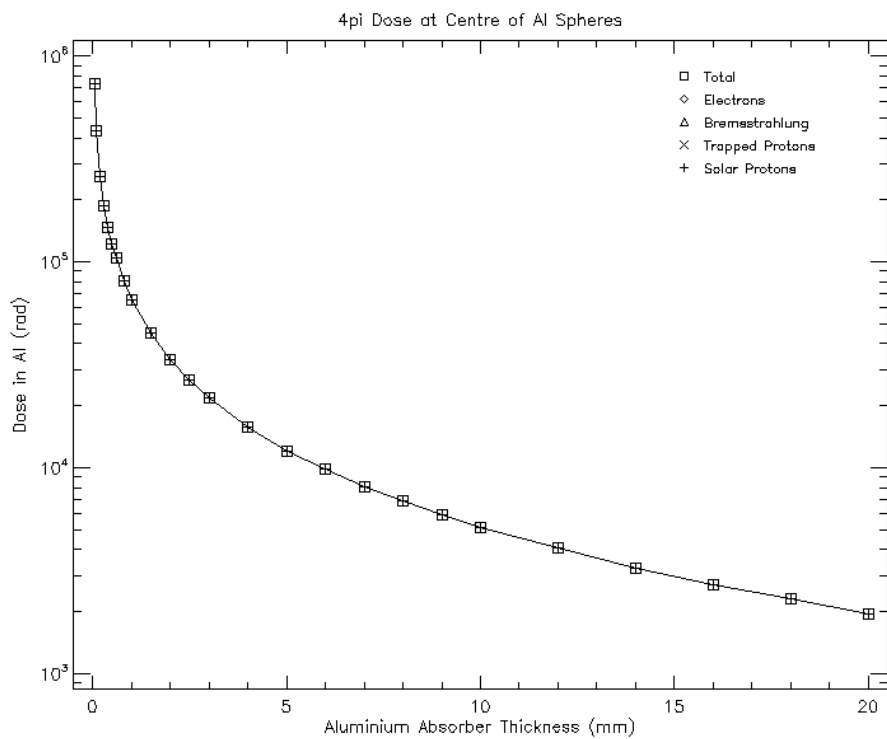


Figure 3.11: Doses during 8 year interplanetary transfer on electronics components (Si)

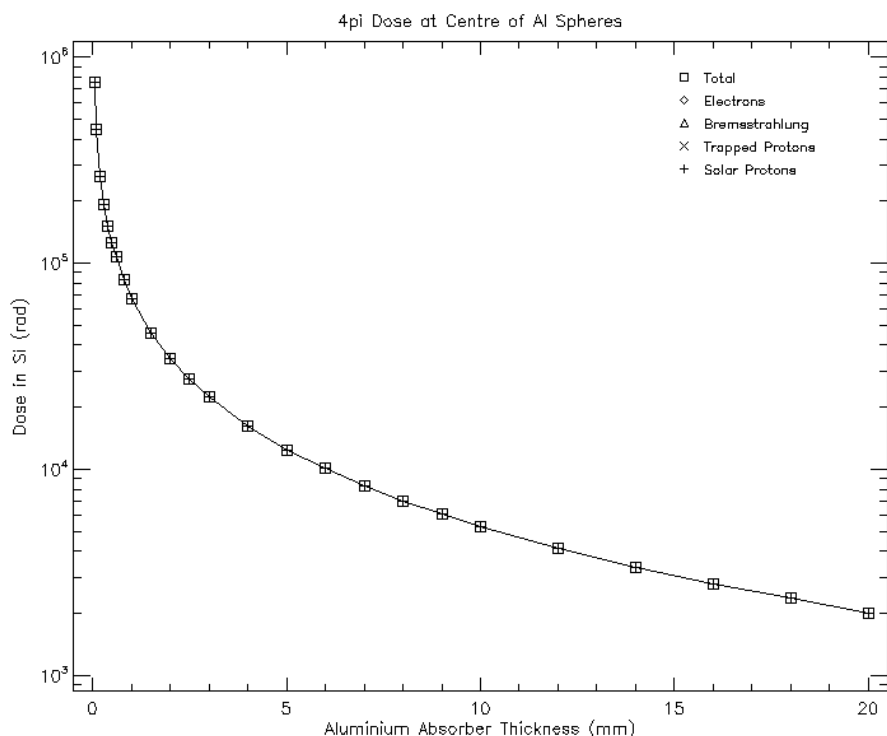


Figure 3.12: Doses during 8 years interplanetary transfer on Al components

3.4 Further improvements

In the most commonly cited computations, the shielded material is normally taken to be Aluminium. A more sophisticated approach can be used to consistently reduce the shielding mass. Direct tantalum coating of existing Aluminum materials augments radiation shielding to space environment. Tantalum-based shielding is therefore recommended when the required aluminium thickness exceeds 4mm, as shown in Table 3.2 (it must be noted that Tantalum is difficult to machine). In this approach it is taken into account that electrons and secondary radiation are better blocked by a high Z material, where Z is the atomic number, and protons are better blocked by a low Z material. A triple layer of low-density material, such as Copper, Titanium or Aluminum, then an high density material such as Tantalum or Tungsten, and another low-density material in the end, could meet the goal. In the end, the variation in Z number creates an effective filter along a broad spectrum of radiation mitigating both primary and secondary radiation damage effects, including Bremsstrahlung [11]. Tantalum can be integrated into 3D printed aluminum structures such as satellite structural components. Thus, the structure and the radiation shield can be combined into one multi-functional monolithic panel [9].

Table 3.2: Equivalent Tantalum shielding

Environment	4 mm shielding (Al)	8 mm shielding (Al)	10 mm shielding (Al)
Dose	5.3 Mrad	1.5 Mrad	770 krad
Equivalent Ta shielding	0.651 mm	1.1 mm	1.3 mm
Mass gain in percents	~ 0 %	> 12 %	20 %

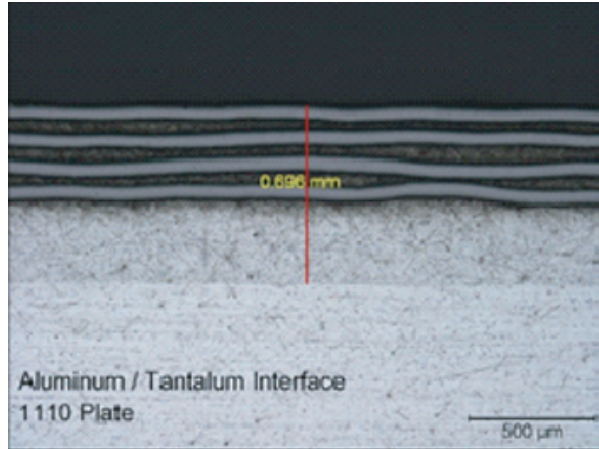


Figure 3.13: Tantalum-based shielding

4. System Architecture

Table 4.1: Interface Requirements

ID	Statement
R-INT-010	The instrument shall receive power from spacecraft power bus
R-INT-010.1	The power coming from the spacecraft power bus shall be converted voltages of the components
R-INT-060	The instrument shall be interfaced with the telemetry and telecommand subsystem of the spacecraft
R-INT-070	The laser headbox shall be connected directly to the spacecraft power bus
R-INT-080	The TCU shall be interfaced with all the other subsystems
R-INT-090	The instrument shall receive commands from the spacecraft
R-INT-100	The TCU shall receive the temperatures of all components

In this chapter the overall architecture of the instrument is defined. Fig. 4.1 presents a sketch of it to guide the reader around the different subsystems.

The main subsystems, such as the transmitter unit, the receiver unit and the electronic unit, can be identified. From this it is possible to state the first preliminary technical requirements and the connections between parts.

The transmitter unit must produce a laser beam, which shall operate in the near infrared in order to assure reflection by the planet's surface. The instrument shall also be able to direct the laser beam towards the desired spot on the planet's surface using an appropriate optics system.

Into the receiver unit the instrument shall collect the reflected laser beam coming from the surface using another optics system with noise filters. Successively, the instrument shall direct the collected beam towards the detector. Both the laser source and the detector parts need a thermal control to perform in their operational conditions.

The thermal control unit consists in a distributed net of thermal sensors able to get information on the components survival parameters.

The instrument's power shall be granted by the spacecraft's power bus. To fulfil the mission objective, the instrument shall provide data to enable determination of surface ranges with the right resolution. This implies the necessity of an electronic unit. The transmitted pulse shall be tagged in time and its characteristics shall be provided as well.

All the acquired data shall be sent to the ground base on Earth, where they will be processed to obtain the desired altitude mapping, so the instrument shall be interfaced with the telemetry and telecommand subsystem on board of the spacecraft. This implies that the information shall be firstly digitalized, then linked to other parameters of interest, and encoded in the end. An on-board memory is provided to permit data storage and periodically transmission to the ground station.

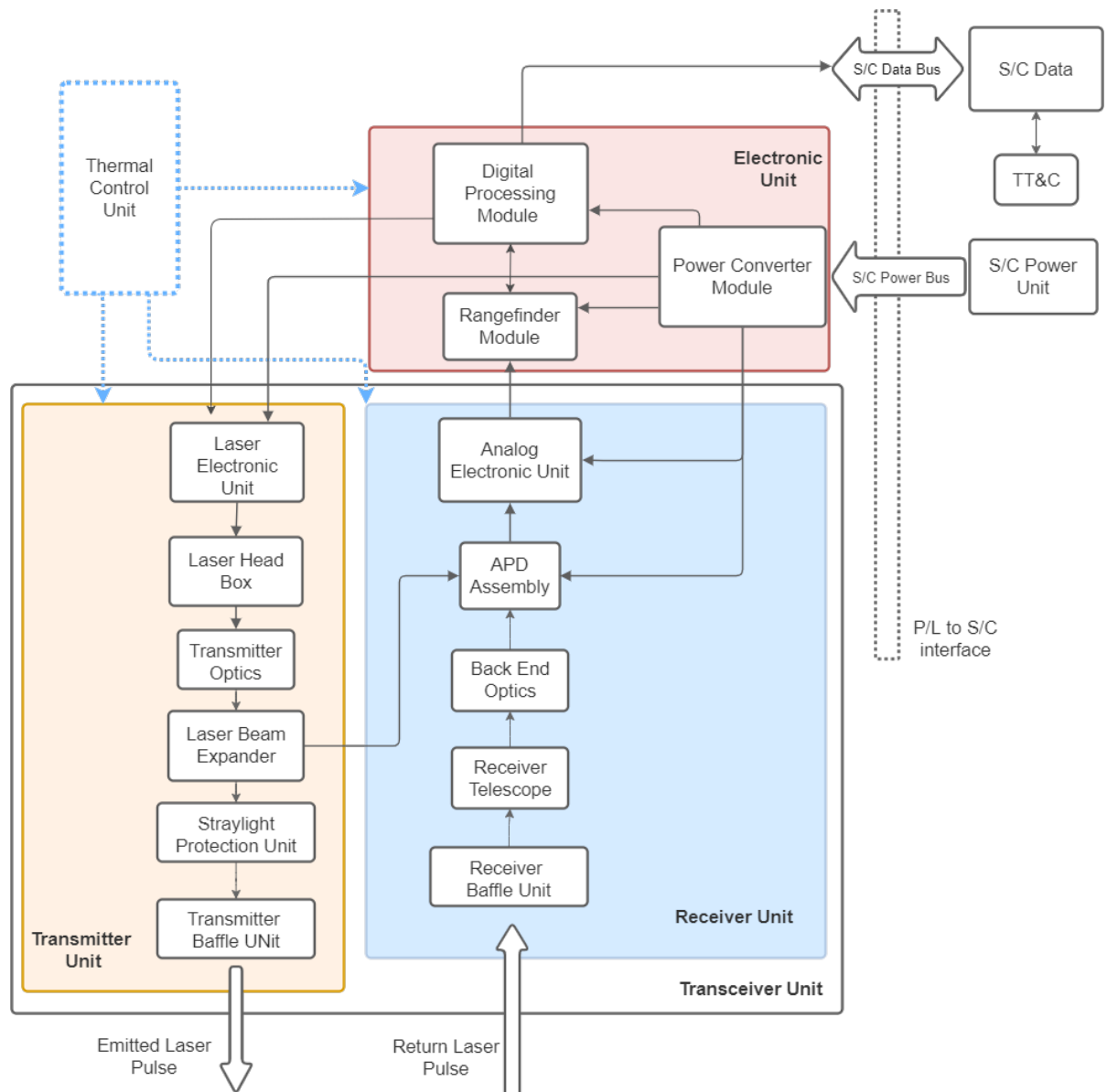


Figure 4.1: Overall system architecture

5. Operational Scenarios

Table 5.1: Operational scenarios requirements

ID	Statement	Subsection
R-REL-050	The instrument should keep in storage the temperature data of the last hour of operation	5.1
R-FUN-060.2	The instrument shall store 12.3 Mb of data during operative mode	5.2
R-FUN-060.1	The instrument shall transmit the data to the TT&C of the spacecraft	5.3
R-INT-090	The instrument shall receive commands from the spacecraft	5

The instrument can be operated through 4 modes of operation, which can be activated at any moment during the mission by the spacecraft on-board computer, either through preset algorithmic decision, or by ground's override command. The modes are designed to guarantee the operability of the instrument through any conditions the spacecraft might encounter.

5.1 Safe Mode

During the *Safe Mode*, only the diagnostic tasks are executed by the instrument's subsystems to guarantee components survival through harsh conditions encountered during the mission. This mode is activated by default in the first phase of the mission, after the spacecraft is deployed on its parking orbit around the Earth, before entering the interplanetary orbital leg, which lasts for about 8 years. In the safe mode the laser subsystem is in standby and the only thermal subsystem is activated to collect and store temperature data, transmitted upon request to the spacecraft. For this reason, the power consumption is very limited.

5.2 Operative Mode

The main *Operative Mode* of the instrument is activated once the final circular orbit around Ganymede is reached. The laser subsystem is operated at nominal conditions, emitting pulses at a constant frequency and predefined power; the instrument data-acquisition & processing components execute their programmed functions to obtain the altitude ranges and store them in a data storage device continuously for 16 hours. The sampling frequency of the converter and the laser pulse rate are such to guarantee the minimum commissioned mapping resolution. Active thermal control on the photon sensor, namely an avalanche photo-diode, is activated to keep the sensor within the working temperature range. The power consumption reaches nominal levels.

5.3 Data Transfer Mode

The *Data Transfer Mode* switches with the operative one when the memory is full and the data is transmitted to the spacecraft's data handling unit. This mode will be operative for about 8 hours at least to complete all the transfer between periods of operativity.

5.4 Focus Mode

The *Focus Mode* is an optional operative mode which allows a higher mapping resolution by exploiting the converter's maximum performances in terms of sampling frequency. The power consumption reaches the maximum levels of the mission and therefore it drives the interface requirements with the spacecraft power bus.

The status of the subsystems for each mode is summarized in Table 5.2. A more detailed power budget comprehensive of specific margins for the components can be seen in Fig. 5.1 and is further specified in section 9.1.

Table 5.2: Operative modes

	Safe Mode	Operative Mode	Data Transfer Mode	Focus Mode
Thermal Control Unit	ON	ON	ON	ON
Transmitter Unit	OFF	ON	OFF	POWERED
Receiver Unit	OFF	ON	OFF	POWERED
Electronic Unit	LIMITED	ON	ON	ON

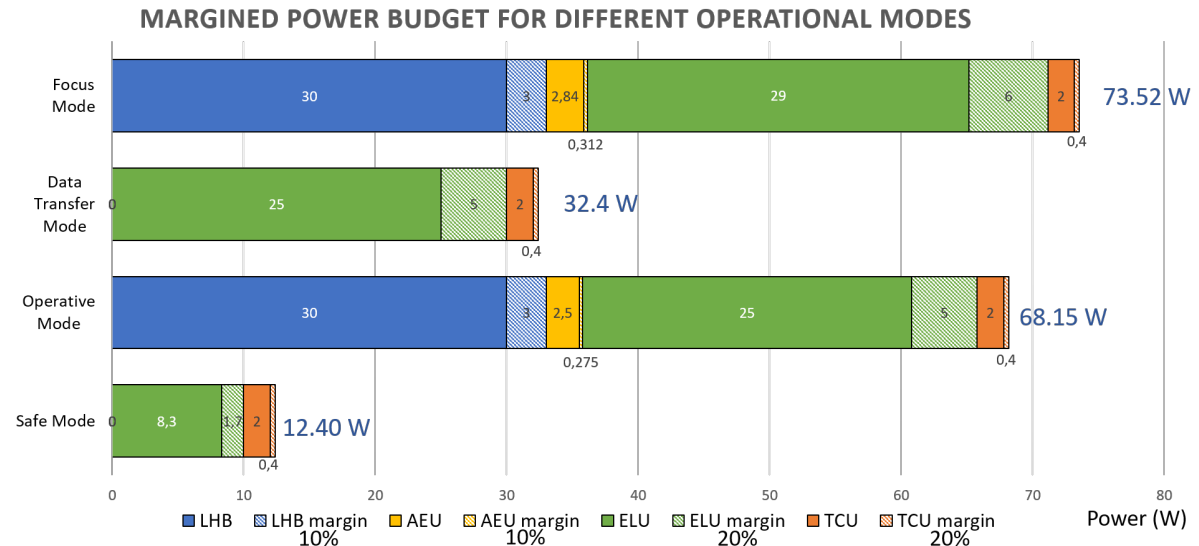


Figure 5.1: Power budget for every mode

6. Components Design

6.1 Transmitter Unit

Table 6.1: Transmitter Unit requirements

ID	Statement	Subsection
R-FUN-090	The transmitter shall have a baffle	6.1.1
R-FUN-010	The instrument shall produce a laser beam	6.1.2
R-FUN-015	The emitted laser wavelength shall be 1064 nm	6.1.2
R-FUN-050.3	The instrument shall provide the characteristics of the transmitted pulse	6.1.2
R-FUN-050.4	The instrument shall provide time tagging of the transmitted pulse	6.1.2
R-FUN-080	The start pulse shall be delivered from the TX to the APD-assembly by optical fibers	6.1.2
R-FUN-100	The instrument shall have a Nd:YAG side pumped laser emitter	6.1.2
R-FUN-120	The pulse width should be inferior to 50 ns	6.1.2
R-FUN-130	The energy distribution of the laser pulse shall have a Gaussian shape	6.1.2
R-PER-070	The repetition rate of the pulse shall be between 20 and 30 Hz	6.1.2
R-PER-080	The pulse's width should be inferior to 5 ns	6.1.2
R-INT-070	The laser headbox shall be connected directly to the spacecraft power budget	6.1.2
R-FUN-110	The beam expander shall produce spotsize on the surface of 70 m from 500 km altitude	6.1.3

The transmitter unit is composed by the transmitter baffle unit, the straylight protection unit, the laser box, the transmitter optics, the beam expander and the laser electronics unit. All the subsystems are displayed in Fig. 6.1 and are described in details in the following sections.

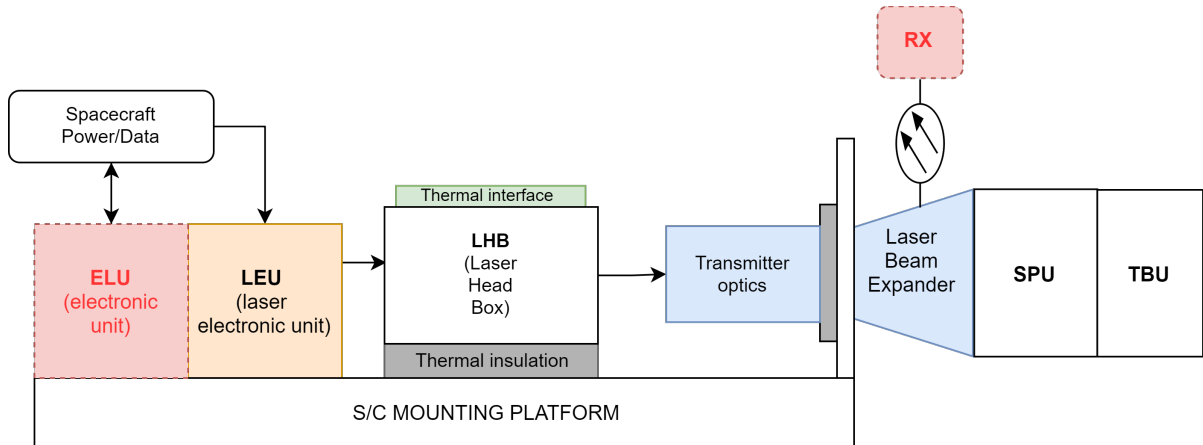


Figure 6.1: Architecture of transmitter unit

6.1.1 Transmitter Baffle Unit and Straylight Protection Unit

The transmitter baffle unit protects the inner side of the transmitter from direct sunlight. It has been modelled as a simple monocoque cylinder with the dimensions reported in Fig. 6.2. The straylight protection unit (on the right in Fig. 6.2) provides additional protection against contamination and straylight by absorbing the other disturbances that were able to pass through the baffles, reducing the heat flux toward the laser.

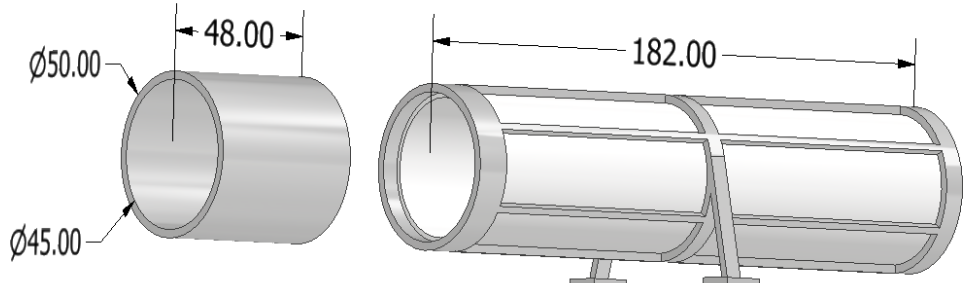


Figure 6.2: Transmitter baffle and straylight protection unit

6.1.2 Laser Head Box and Laser Electronic Unit

The laser system design consists of the laser head box (LHB) and its controller, which are isostatically mounted onto the instrument baseplate, and the laser electronic unit (LEU), mounted on the spacecraft bench. The LEU (Fig. 6.3) provides laser voltage and current supply, as well as control communication for the LHB on one side and a command interface to the electronics unit of the instrument on the other side.

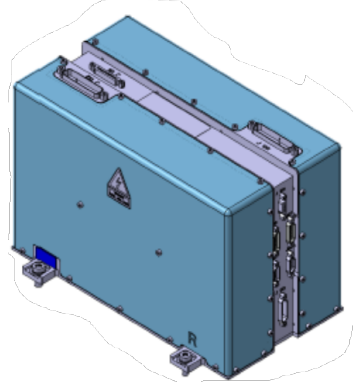


Figure 6.3: Laser Electronic Unit

The design of the laser unit is based on the M-NANO Nd:Yag diode pumped solid state laser from *Montfort Laser GmbH* ([14]) shown in Fig. 6.4, which has the compact driver separated from the laser head. In order to guarantee the double redundancy on the laser pump it is possible to exploit a custom design with two laser heads connected to a single controller/driver unit, thus saving in mass and occupied space. Both the module weight less than 1 kg and are very compact: the laser head is 150 x 70 x 60 mm³ and the controller module is 132 x 78 x 64 mm³.



Figure 6.4: M-NANO 80mJ 10Hz Nd:YAG DPSSL w/ Separate Compact Driver [PR179]

The laser box contains two Nd:YAG (neodymium-doped yttrium aluminum garnet) lasers in cold redundancy that emit at 1064 nm with an energy of minimum 50 mJ and a repetition rate of 25 Hz. The box is pressurized with synthetic air to protect the laser optics from laser-induced damage effects [13] and sealed in order to facilitate a low pressure drop over the time.

The schematic of a single-stage, actively q-switched, diode laser side-pumped Nd:YAG rod laser system with unstable resonator geometry is illustrated in Fig. 6.5. The laser diode assemblies emit at about 808 nm wavelength with an electrical-to-optical efficiency of about 50%. The pump light is converted with an optical-to-optical efficiency of about 10% to laser radiation by means of a pump cavity of diffusing reflectors made from purified polytetrafluorethylene material. In order to extract the stored energy at this high efficiency into a short laser pulse at 1064 nm, an electro-optic crystal (Pockels cell) switches from non-polarizing to quarter-wavelength condition within less than 30 ns rise time to actively open the optical path in the laser resonator. This electro-optic switch is driven by a miniaturized 3 kV transistor cascade in close proximity to the laser resonator inside the LHB. With this active q-switch, typical pulse durations of 5 ns are achieved at 1064 nm as required by the application.

During its few round trips, the stimulated laser beam pulse at 1064 nm expands in diameter.

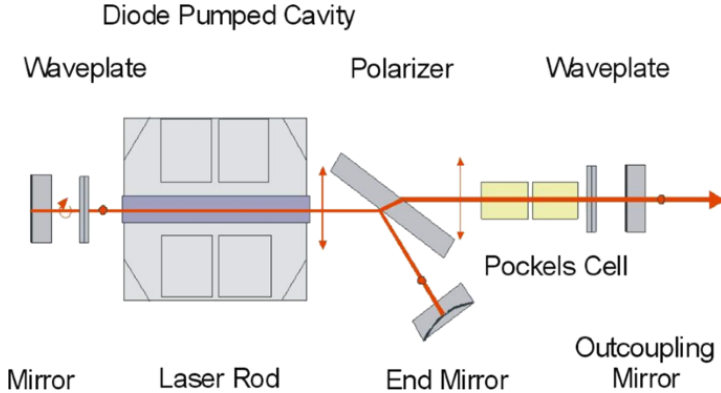


Figure 6.5: Laser scheme

This allows for subsequent stimulation of radiation from the entire laser rod volume. An out-coupling mirror with radially variable reflectivity determines the mode profile and establishes a near Gaussian mode shape of the laser pulse leaving the resonator in direction of the beam expander (BEX) optics. The outgoing laser beam has a divergence of $140 \mu\text{rad}$ after leaving the BEX and reaches Ganymede's surface with an average spot sizes of 70 m. An optical fiber leading to the receiver is connected to the BEX, providing a reference to the outgoing laser pulse and the start signal for the altimetry measurement.

The diode lasers are the primary font of ohmic dissipation (see Fig. 6.6), thus they are directly mounted onto the LHB structure in order to minimize thermal gradients and consequent deformations. From the laser head box housing, which is made of highly thermally conductive AlBeMet alloy, the heat flows via a highly thermally conductive flexible link to the heat pipe thermal sink provided by the spacecraft. Quasi-isostatic bipod flexures connect the LHB structure to the instrument baseplate, in order to provide for opto-mechanical stability. These bipods have a low thermal conductivity and transfer only very small torques to the instrument baseplate to avoid thermo-mechanical deformation. In order to not provide thermal stress on the instrument the LHB is lifted up with a layer of insulated polystyrene foam.

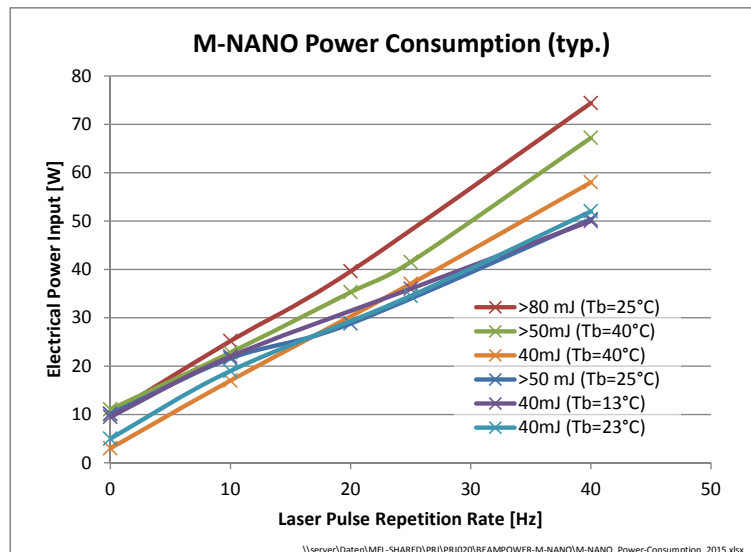


Figure 6.6: M-NANO Power consumption

6.1.3 Transmitter Optics and Beam Expander

To prevent sunlight from directly entering, the laser box is positioned in a different region from the exit one, so the transmitter optics are needed to convey the beam to the exit area. Specifically, two 45° mirrors are implemented since the beam has to be rotated twice by 90 degrees.

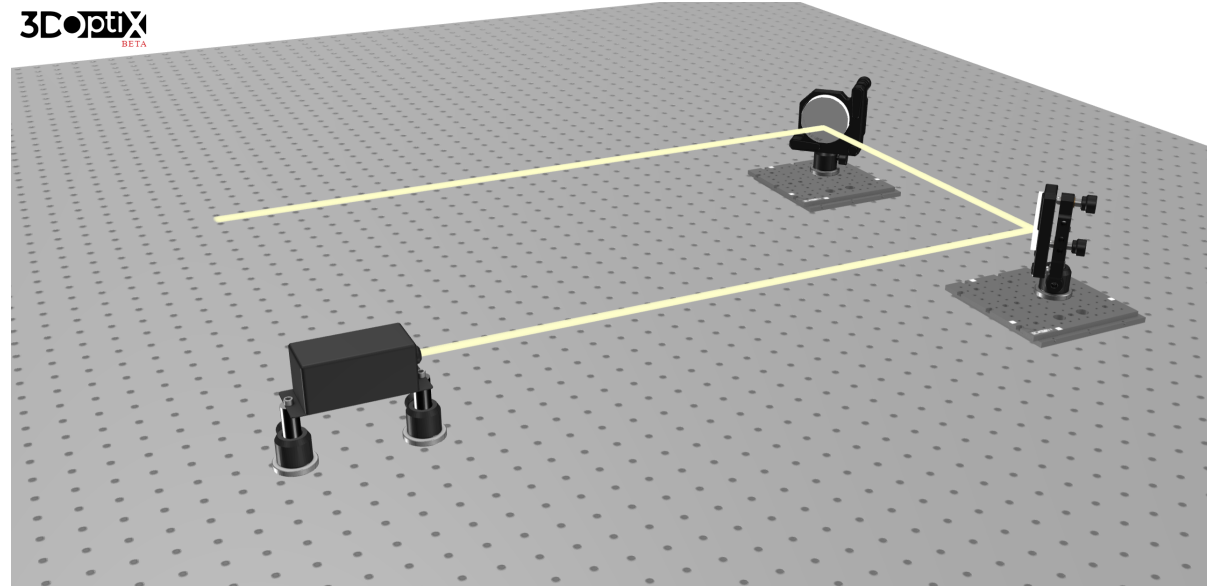


Figure 6.7: Transmitter optics

Once in the exit area, the laser passes through the beam expander, where it is expanded in order to increase the diameter of the collimated light. The beam expander has been designed such that the spotsize on the surface is exactly 70 m. To this aim, a field of view of 140 μrad was considered. The design of the beam expander in *Zemax* is summarized in Fig. 6.8 and Fig. 6.10.

The pointing of the laser with respect to the receiver is determined mainly by the pointing of the BEX optics. In order to separate critical optics from the deformation of the laser head box, a precise design with the BEX supported by quasi-isostatic mounts attached to the base unit of the LHB is needed. An optical fiber from the receiver is connected to the beam expander, providing a reference to the outgoing laser pulse and the start signal for the altimetry measurement.

	Surface Type	Comment	Radius	Thickness	Material	Coating	Clear Semi-Dia	Chip Zone	Mech Semi-D	Conic	TCE x 1E-6
0	OBJECT	Standard ▾		Infinity	Infinity		0,000	0,000	0,000	0,000	0,000
1		Standard ▾		Infinity	14,600		2,000 U	0,000	2,000	0,000	0,000
2	STOP (aper)	Standard ▾		Infinity	2,000	N-BK7	3,000 U	0,000	3,000	0,000	-
3	(aper)	Standard ▾		5,680	85,004 V		3,000 U	0,000	3,000	0,000	0,000
4	(aper)	Standard ▾		594,200	3,500	SF2	20,000 U	0,000	20,000	0,000	-
5	(aper)	Standard ▾		55,340	11,000	N-BK7	20,000 U	0,000	20,000	0,000	-
6	(aper)	Standard ▾		-48,479	10,000		20,000 U	0,000	20,000	0,000	0,000
7	IMAGE	Standard ▾		Infinity	-		10,895	0,000	10,895	0,000	0,000

Figure 6.8: Beam expander data

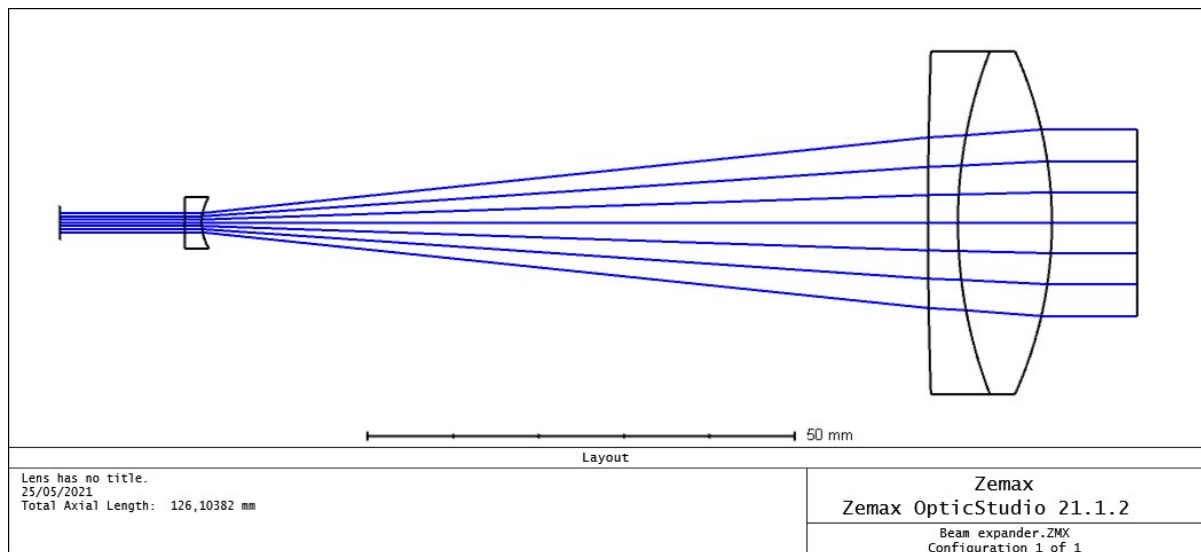


Figure 6.9: Beam expander architecture

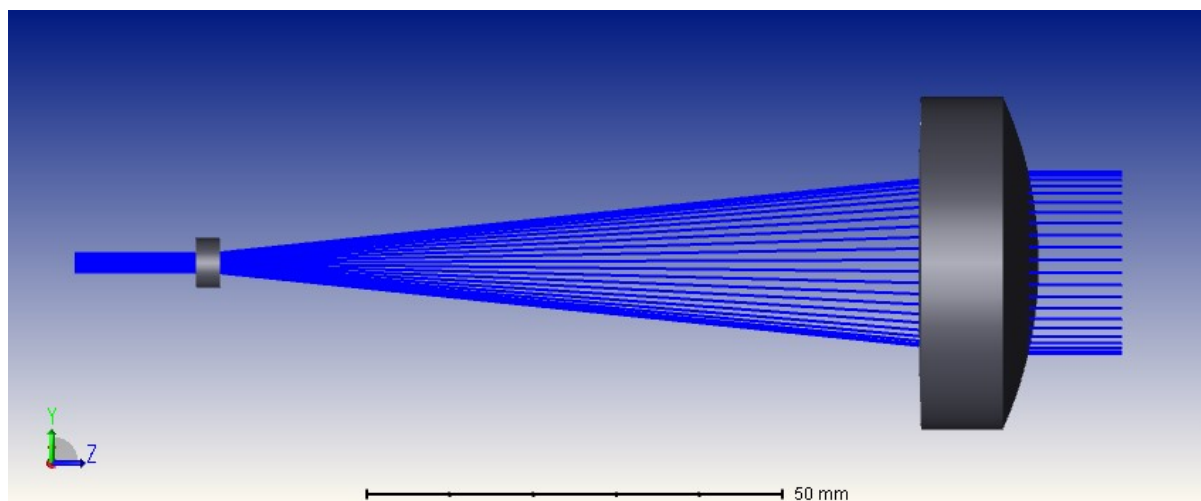


Figure 6.10: Beam expander 3D architecture

6.2 Receiver Unit

Table 6.2: Receiver Unit Requirements

ID	Statement	Subsection
R-FUN-150	The receiver shall have a baffle	6.2.1
R-FUN-150.1	The baffle shall weight less than 1 kg	6.2.1
R-PER-010	The instrument shall reject 90% of incoming radiation other than the laser beam	6.2.1
R-FUN-160	The receiver telescope axial length shall be less than 15 cm	6.2.2
R-FUN-170	The receiver telescope configuration shall be a Ritchey-Chretien Cassegrain	6.2.2
R-FUN-180	The receiver field of view shall be $500 \mu\text{rad}$	6.2.2
R-PER-020	The receiver telescope reflectivity shall be at least 85%	6.2.2
R-PER-030	The back of the secondary mirror shall reflect at least 80% of the incoming radiation	6.2.2
R-FUN-040	The instrument shall direct the collected beam towards the detector	6.2.3
R-FUN-050.5	The receiver unit shall isolate the laser wavelength	6.2.3
R-FUN-080	The start pulse shall be delivered from the transmitter to the APD assembly by optical fibers	6.2.4
R-FUN-140	The instrument shall incorporate an avalanche photo diode detector	6.2.4
R-FUN-140.1	The operating voltage of the APD shall be less than 375 V	6.2.4
R-FUN-140.2	The active diameter of the APD detector shall be at least 0.8 mm	6.2.4
R-FUN-140.3	The APD detector should have a single pixel	6.2.4
R-PER-040	The total dark current in the APD shall be less than 55 nA	6.2.4
R-PER-050	The responsivity of the APD shall be at least 36 A/W	6.2.4
R-PER-060	The gain of the APD shall be at least 120	6.2.4
R-PER-190	The A/D converter shall work at a 200 MHz	6.2.5
R-FUN-050.1	The instrument shall digitalize the returned pulse	6.2.5
R-FUN-050.2	The instrument shall tag in time the return pulse	6.2.5

A schematic diagram of the receiver unit is shown in Fig. 6.11, where the basic connections with the transmitter and electronic unit are highlighted:

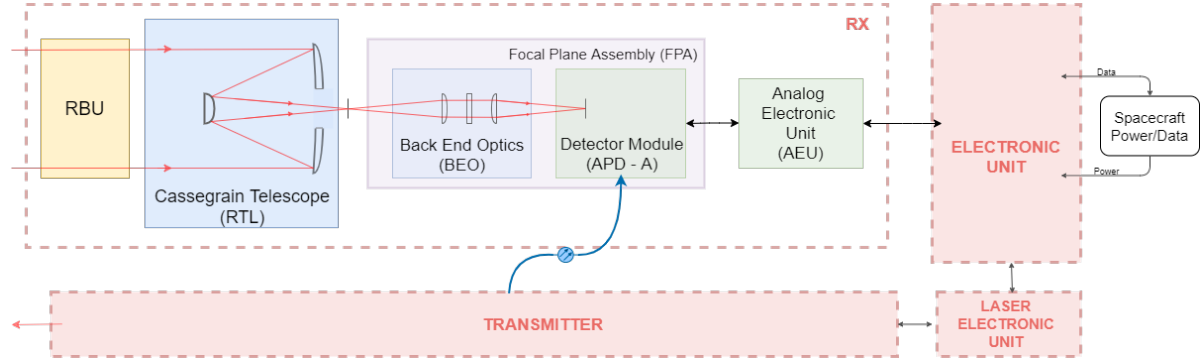


Figure 6.11: Architecture of receiver and electronic unit

6.2.1 Receiver Baffle Unit

The mean solar irradiance at Jupiter is 50.26 W/m^2 , almost thirty times lower than the one at Earth. Still, for active optical payloads with an internal light source like a laser altimeter it is of paramount importance to suppress most of the solar and thermal infrared power that may otherwise pass through the 25 cm large front aperture. With this aim, a reflective Stavroudis baffle is designed to protect the receiver telescope. This kind of reflective baffle exploits a sequence of ellipses and hyperbolae, alternating between outer and inner diameter, as shown in Fig. 6.12. The optical design is completely determined with the definition of the inner and outer diameter, the payload field of view and a length constraint as defined in Table 6.3. The receiver field of view (full cone) is fixed by the diameter of the field stop aperture and the focal length of the telescope. The transmitter has a beam divergence of $140 \mu\text{rad}$.

The receiver has to capture the return pulse and thus its field of view must be larger than the beam divergence. Moreover, the alignment between transmitter and receiver must be stable. The value of $500 \mu\text{rad}$ for the receiver field of view accounts for the beam divergence and includes margins for cross-alignment and thermo-elastic distortions. The overall final design of the baffle is presented in Fig. 6.13

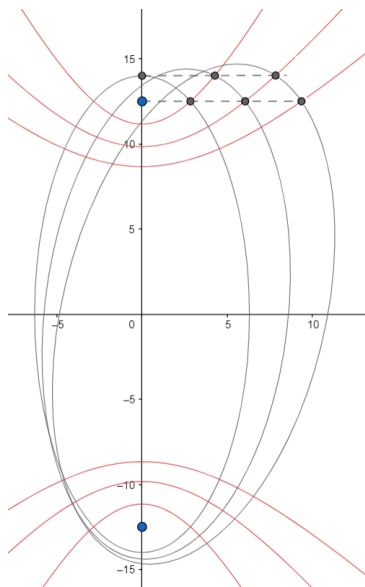


Figure 6.12: Baffle construction

Table 6.3: Receiver reflective baffle data

Inner diameter [mm]	Outer diameter [mm]	FOV [μrad]	Max Length [mm]
250.0	280.0	500	10.0

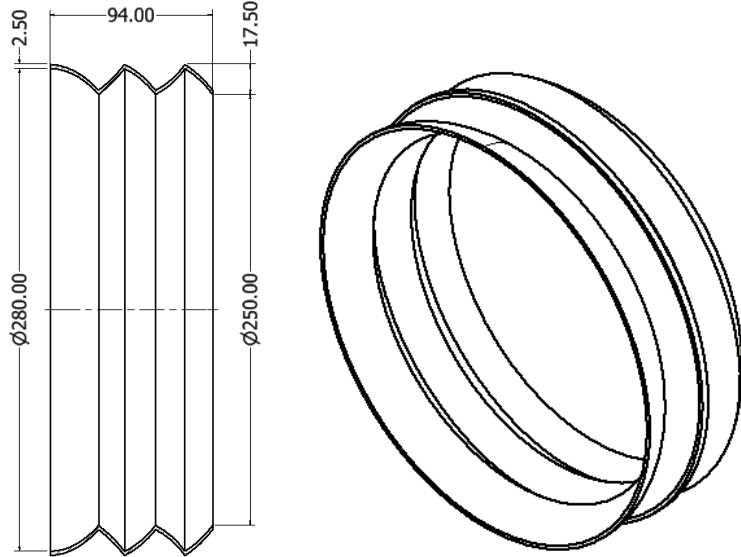


Figure 6.13: Stavroudis baffle design

6.2.2 Receiver Telescope

The telescope is a Ritchey-Chrétien Cassegrain configuration with two hyperbolic mirrors, that has been chosen since it has a larger field of view free of optical errors. The initial computations were done by applying the pin-hole model to obtain the total focal length of the system starting from the orbit's altitude and the footprint. The aperture diameter (25 cm) and the distance between the mirrors (10 cm) have been chosen from the baseline. The magnification (10) has been imposed considering typical values and the stop radius (90 nm) has been set in order to obtain a contained volume for the telescope structure. With these data, the preliminary calculations that led to a first approximate model for the telescope have been performed.

The second step in the design was developed in *Zemax Optic Studio*, starting from the values given by the previous calculations. During this stage, a few parameters like the magnification have been changed to obtain a more compact configuration but the results are similar to the ones from the draft model and the result is reported in Fig. 6.14.

The RTL is designed as an all Beryllium telescope, as the Cassegrain receiver of the *Bepi Colombo Laser Altimeter*, (except for specific structural attachments and the field stop aperture) to achieve the required low mass while providing sufficient stiffness [5]. A thin Cr-Au layer covers completely the two mirrors: the gold coating was applied to satisfy the optical requirements of reflectivity at the working wavelength as well as over the solar and thermal spectrum while chrome is applied for adhesion.

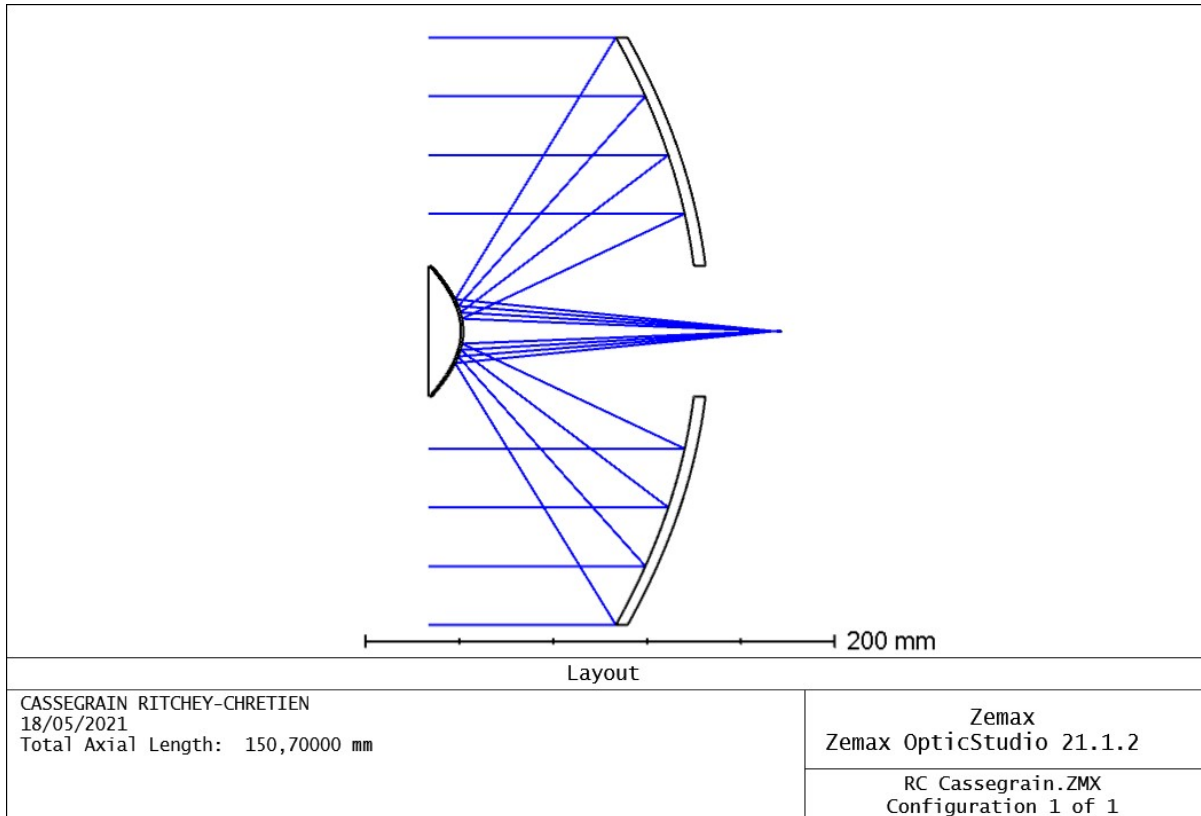


Figure 6.14: Telescope architecture

Table 6.4: Telescope Data

Primary Mirror Diameter [mm]	250.0
Primary Mirror Curvature Radius [mm]	223.6
Secondary Mirror Diameter [mm]	55.6
Secondary Mirror Curvature Radius [mm]	25.9
Magnification	11.5
System Focal Length [m]	1.2858

6.2.3 Back-End Optics

The rays exiting the telescope enter the Back End Optics unit. A field stop is placed at the focus of the telescope as the first step in removing straylight. The instrument operates over both the nightside and the dayside of Ganymede, hence a narrowband filter to isolate the laser wavelength was incorporated into the design. Rays coming from the image plane of the telescope enter the first lens, the collimating objective, and pass as a collimated beam through the filter. The second part of the BEO, the imaging objective, focuses the light onto the avalanche photodiode detector, passing through a fused silica window [7]. The aperture stop of the all receiver system is located in the collimated beam of the BEO, such that the entrance pupil is located on the surface of the primary mirror. Fig. 6.15 shows the proposed BEO architecture, while Table 6.5 summarizes the important parameters.

Table 6.5: Back End Optics Data

	Surface Type	Radius [mm]	Thickness [mm]	Material	Semi-Diameter [mm]
0	Object	Infinity	12.000		0.350
1	(aper)	Infinity	2.243	F. Silica	3.000
2	(aper)	-7.320	4.902		3.000
3	(aper)	Infinity	2.000	F. Silica	3.000
4	(aper)	Infinity	2.902		3.000
5	Stop	Infinity	2.000		2.000
6	(aper)	3.799	2.861	F. Silica	3.000
7	(aper)	Infinity	4.000		3.000
8	(aper)	Infinity	1.016	F. Silica	3.000
9	(aper)	Infinity	3.500		3.000
10	Image	Infinity	-		0.400

In optics, fused silica offers exceptional UV transmission, and can be manufactured to facilitate the transmission of infrared wavelengths. Coupled with low refractive index variations, it exhibits ideal optical qualities for high-precision optics applications. In addition, the physical properties and extremely high-temperature resistance of fused silica glass make it particularly useful for high-performance applications in harsh conditions.

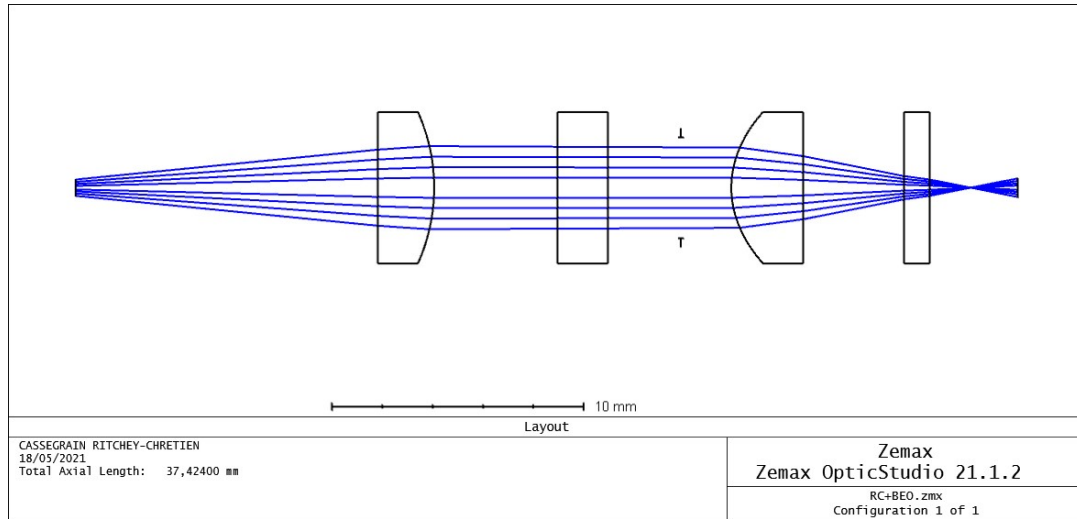


Figure 6.15: Back-End Optics architecture

The complete model of the telescope and back-end optics is presented in Fig. 6.16, where its overall dimensions can be appreciated. The combination of the two produces the footprint on the detector shown in Fig. 6.22.

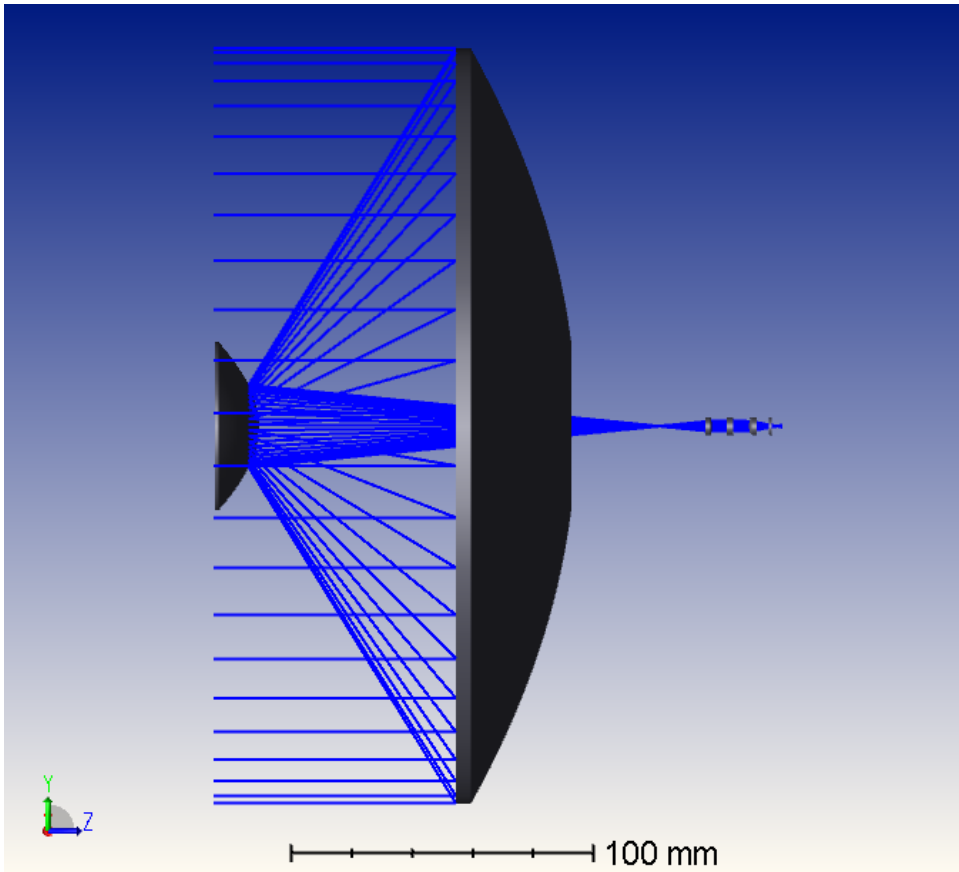


Figure 6.16: 3D model of Receiver Telescope and Back-End Optics

6.2.4 Avalanche Photo Diode-Assembly

The Avalanche Photo Diode-Assembly (APD-A) is the detector assembly that is responsible for the detection of both the start and return laser pulses and, together with the BEO, forms the Focal Plane Assembly (FPA). The start pulse is delivered from the transmitter to the diode assembly by optical fibers, and it is used to determine the emitted energy. The return pulse reaches the detector through the receiver telescope and the back-end optics.

The most important component of the assembly is the detector itself, which is an Infrared Enhanced Silicon Avalanche Photo Diode with a single pixel. The C30954EH Long-Wavelength, Enhanced Silicon Avalanche Photodiode (Si APD) [6] provides a 0.8 mm active area diameter and high quantum efficiency at 1060 nm, thus it has flown on several laser altimeters, including BELA, LOLA and MOLA [12].

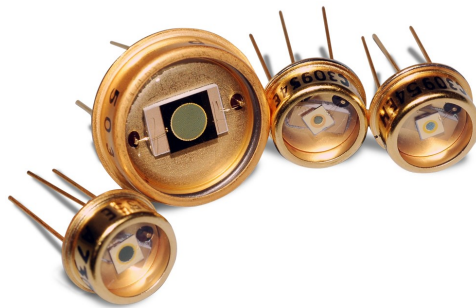


Figure 6.17: Excelitas' 1064 nm Si APD

Avalanche photo diodes rely on the generation of additional electrical charges through a

multiplication mechanism initiated by an external electric field, which accelerates the electrons in the conductive band to the positive pole. As a result, the electrons gain kinetic energy and can generate other electrons by collision, sustaining an avalanche process. The electrical field, and thus the magnitude of the avalanche process, depend on the bias voltage on the photodiode and on the ambient temperature and as the multiplication process is limited by the device properties, there is an upper limit for the voltage too (Fig. 6.18, Fig. 6.19).

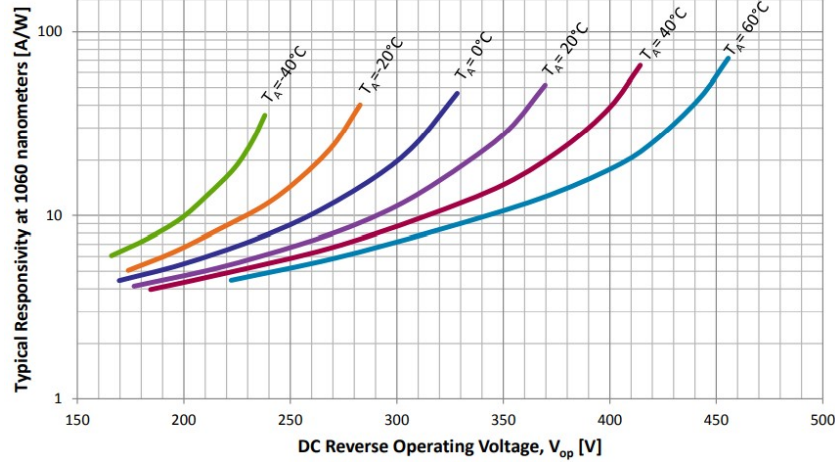


Figure 6.18: Typical Responsivity at 1060 nm as a function of Operating Voltage

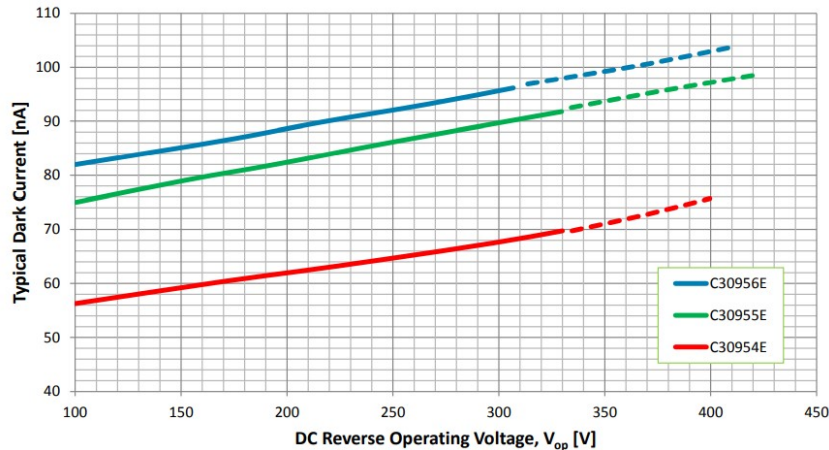


Figure 6.19: Typical Dark Current as a function of Operating Voltage

The specification on the APD performances have been selected considering the value obtained from a study on the *GAnymede Laser Altimeter* in the NASA mission *JUICE* [3], and the values are reported in Table 6.6. The responsivity has been determined from Fig. 6.20, considering 1064 nm and the proper detector (the red one) and resulted in 40 A/W. From the datasheet of the component (appendix B) the typical responsivity is set to 36 A/W, thus this value has been considered. The noise current has been set to $1 \text{ pA}/\text{Hz}^{\frac{1}{2}}$, therefore the gain has been chosen accordingly from Fig. 6.21.

A trade-off between high avalanche process and low dark and noise current has to be done and as a result, the diode's working temperature has been set to 20 °C. For this reason, a temperature sensor and a specific active element have to be added in the avalanche photodiode assembly to allow for thermal control. A more in depth description of the thermal subsystem will be presented in chapter 7.

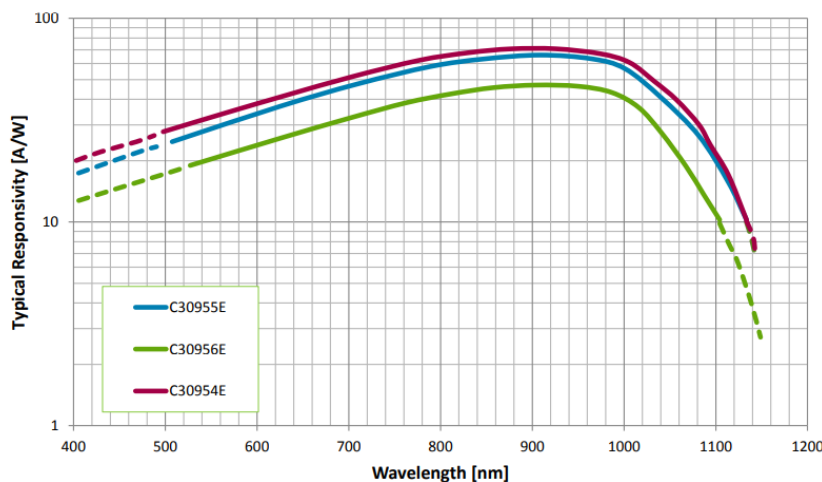


Figure 6.20: Typical Responsivity of APD as function of wavelength

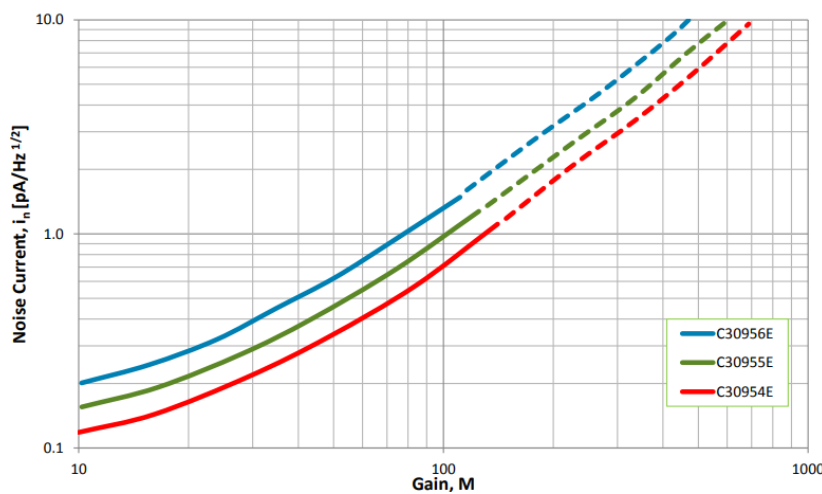


Figure 6.21: Typical Noise Current as function of gain

Table 6.6: Avalanche Photo Diode specifications

Photosensitive surface: area [mm ²]	0.5
Photosensitive surface: diameter [mm]	0.8
Breakdown voltage [V]	375
Quantum efficiency [%]	36
Gain [-]	110
Responsivity [A/W]	36
Noise current [pA/Hz ^{1/2}]	1

The start pulse fibres have to deliver a small fraction of the laser pulse to the APD active area and, in order to have a stable pulse energy, single mode fibres were selected rather than multi-mode ([12]). A small mirror within the FPA is used to deliver the light emerging from the fibres in the focal plane of the receiver to the APD. The optical fibres, manufactured by Diamond, successfully passed radiation testing.

The laser footprint on the detector meets the specification on the 0.8 mm active diameter, as shown from the optical model in Zemax shown in Fig. 6.22:

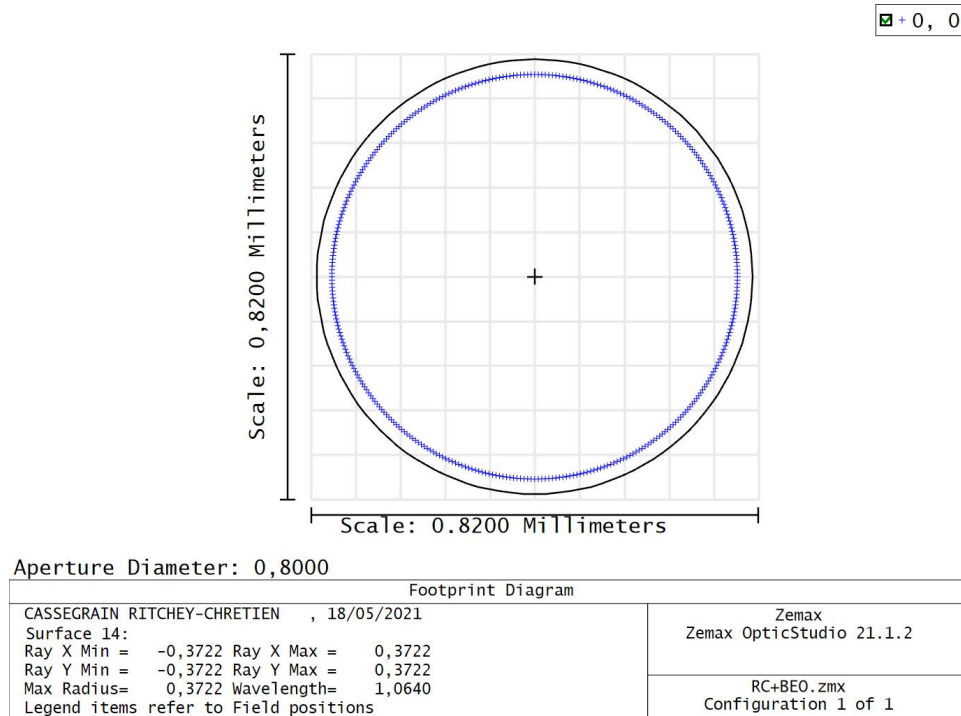


Figure 6.22: Back End Optics Footprint

6.2.5 Analog Electronic Unit

The analog electronics unit amplifies, filters and digitalized the diode-assembly output, carrying both the start and return pulse. As for the laser electronic unit, it is connected to the main electronic unit.

In relation to the capabilities of the space-graded instruments available on the market, it consists of one 14 bit converter, providing a maximum sampling frequency of 400MHz, based on the Texas Instrument ADS5474-SP [20], due to its high radiation hardness (up to TID 100krad). During the nominal mission execution, the sampling is carried out at 200MHz, corresponding to one sample in 5ns which provides a height resolution of 0.8m. In the Focus Mode the A/D converter works at higher sample rates (up to the maximum one) in order to take more detailed measurement of specific regions.

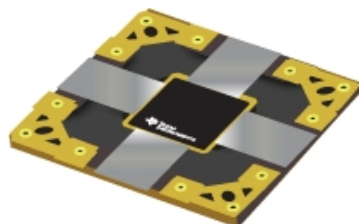


Figure 6.23: Texas Instrument ADS5474-S

6.3 Electronic Unit

Table 6.7: Electronic Unit Requirements

ID	Statement	Subsection
R-FUN-060	The instrument shall transmit the acquired data to the ground base on Earth	6.3.1
R-FUN-060.1	The instrument shall transmit the data to the TT&C of the spacecraft	6.3.1
R-FUN-060.2	The instrument shall store 12.3 Mb	6.3.4
R-FUN-070	The thermoresistors shall acquire temperature values from the components with a frequency of 5 Hz	6.3.4
R-INT-010	The instrument shall receive power from spacecraft power bus	6.3.3
R-INT-060	The instrument shall be interfaced with the telemetry and telecommand subsystem of the spacecraft	6.3.1
R-INT-090	The instrument shall receive commands from the spacecraft	6.3.1
R-THE-010.1	The avalanche photo diode assembly should include a temperature sensor	6.3.4
R-REL-050	The instrument should keep in storage the temperature data of the last hour of operation	6.3.4

This unit has a direct electrical interface to the S/C. The electronic unit module contains the following modules:

- 1 Digital Processing Modules (plus a redundancy)
- 1 Range-finder Module
- 1 Power Converter Modules (plus a redundancy)

6.3.1 Digital Processing Module

The Digital Processing Module is the instrument processing and control front-end and contains the on-board software responsible for the mission execution. The Digital Processing module performs the following tasks:

- Reception of telecommands from the spacecraft onboard computer and their decoding
- Reception and processing of the digitalized receiver signal control of the sensor operations
- Telemetry formatting and transmission
- Housekeeping data acquisition
- Instrument health check

Concerning the on-board software: it consists of two parts, the Booting application and the Operations application. The sole purpose of the Booting application is to switch on the instrument after the critical launch phases have been overcome, it is initiated by the firmware installed in the system's CPU and it launches the Operations application. The latter manages the instrument's operations.

6.3.2 Range-finder Module

The Range-finder module is the digital receiver part of our payload. It receives the digitalized diode sensor data from the A/D converter installed in the analog electronics unit module, controlled in a master-slave arrangement, calculates the range and manages the sequence of instructions to combine the range data with the time-tags.

6.3.3 Power Converter Unit

The Power Converter module is responsible for generating regulated supply voltages for all the payload instrument subsystems from the spacecraft regulated bus voltage. Also in this case, it consists of two independent boards (main and redundant) in cold spare configuration, connected to the S/C Power system.

6.3.4 Data volume

Since the S/C in its orbit has an altitude of about 500km, the time that the light takes to travel back and forth is about 3ms. In addition to that, it should be also considered the time that it takes to compute the maximum intensity of the return pulse and its respective time instant, and the time that it takes to compute the range. Considering all these contributions, and considering the fact that during this time interval the S/C should not cover a distance higher than the footprint, it can be considered a total cycle duration of 40ms (Fig. 6.24). Since it is collected one measurement for each laser cycle, the range processing frequency is 25Hz.

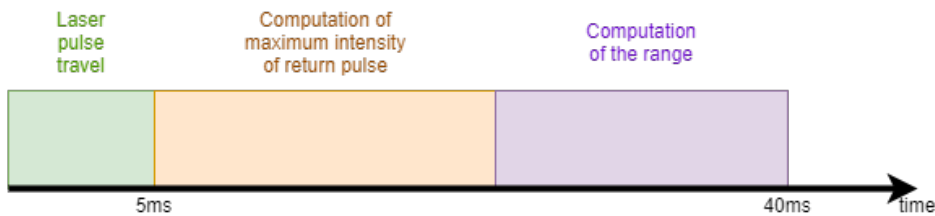


Figure 6.24: Laser cycle timing

With a single-precision floating-point representation, each measurement will be represented with 32 bits. Moreover, for each measurement it is necessary to associate a time tag, that will be expressed in number of clock tic and it will be reset every time the payload interrupts its operations during the S/C-Ground data transmission windows. It will be represented in single-precision floating-point too, in format long, and so with 32 bits. That will lead to a telemetry data volume of 64 bits for each sample. Considering the frequency sample, during the 16 hours of nominal operation for each day it will be necessary to store and transmit 10.9Mb of data.

In case of diagnostic mode the instrument must be capable of providing the last-hour-temperatures of critical points within the instrument. Since fast temperatures excursions are not expected, the temperature sampling frequency is set to 5Hz. The critical components that have to be monitored are the two DPMs, the two PCMs, the RFM, the LEU, the AEU and the FPA. Due to the redundancy, there will be 3 thermoresistors for the first four component and 2 for the others, taking to a total of 20 thermoresistors. Since each temperature would be represented in floating-point single-precision, and then with 32 bits, that will take to a data volume of 1.4Mb. These data will be constantly stored in the data storage, and occasionally sent to the S/C in case of diagnostic mode.

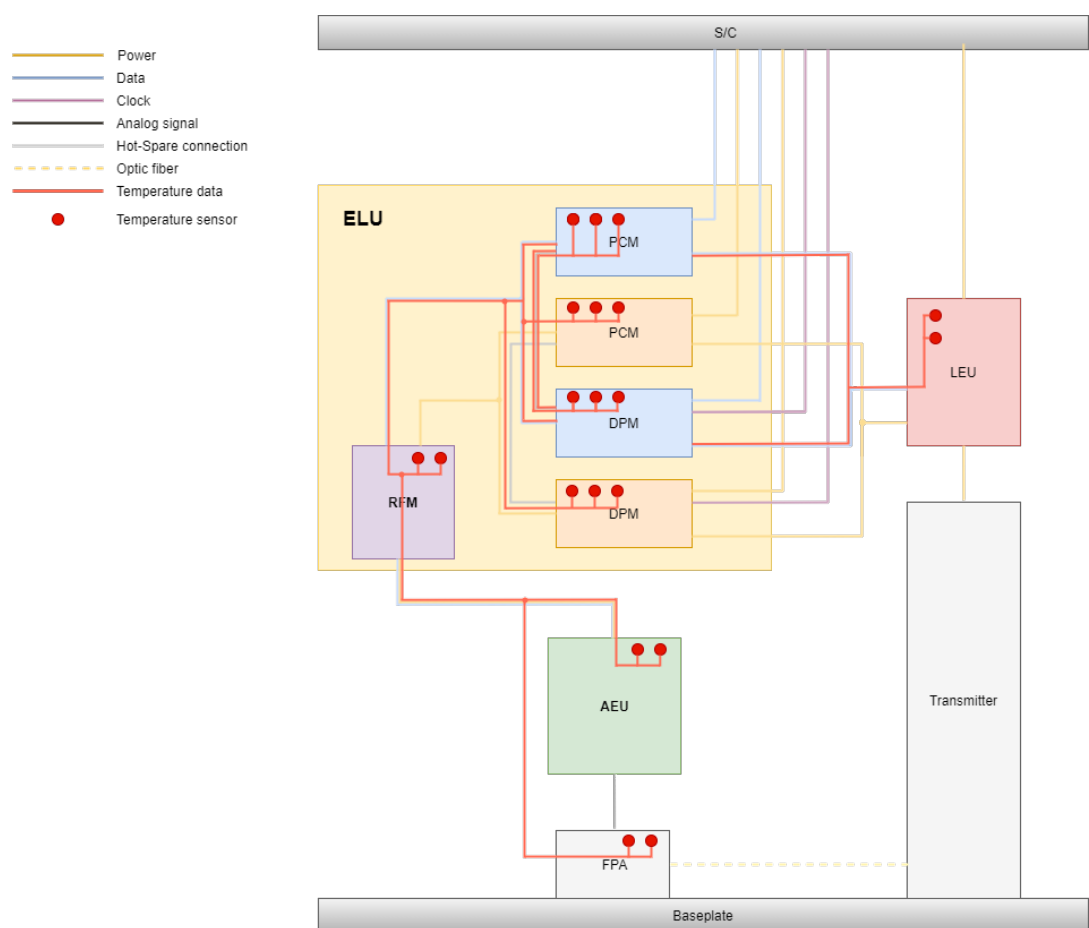


Figure 6.25: ELU

7. Thermal Analysis

Table 7.1: Thermal requirements

ID	Statement	Section
R-MIS-020	The orbit around Ganymede shall have an altitude of 500 km	7
R-INT-010	The instrument shall receive power from spacecraft power bus	7
R-INT-080	The TCU shall be interfaced with all the other subsystems	7
R-INT-100	The TCU shall receive the temperatures of all components	7
R-SAF-010	The instrument shall be designed according to the standards	7
R-ENV-030	The instrument shall survive to the hottest Venus fly-by	7
R-ENV-040	The instrument shall survive to the coldest position in Jupiter shadow	7
R-THE-010	The avalanche photo diode should be kept at 20°	7
R-THE-010.1	The avalanche photo diode assembly should include a temperature sensor	7
R-THE-010.2	The avalanche photo diode assembly should include a dedicated heater	7
R-THE-020	The avalanche photo diode's temperature shall stay between -40 and 70°C	7
R-THE-030	The laser emitter's temperature shall stay between 0 and 40°C	7
R-THE-040	All electronic components temperature shall stay between -20 and 50°C	7
R-THE-050	The baffle unit's temperature shall stay between -165 and 130°C	7
R-THE-060	The telescope's mirrors temperature shall stay between -269 and 260°C	7
R-THE-070	All components made of Al 2014-T6 temperature shall not exceed 210°C	7
R-THE-080	All components made of Ti-6Al-4V temperature shall not exceed 427°C	7

The payload must operate in the cold environment of Ganymede, in the Jupiter System, and must face quite different conditions during the interplanetary travel. All the working components must be kept in their right temperature range to ensure good survival conditions, fair functional properties in all the operational modes, and the best interface setting with the spacecraft. The thermal control has been designed starting from architecture and components, allocating them in the minimum space possible. The payload inside the spacecraft has been shaped as an Aluminum cubic structure of almost 41 cm side and 7 mm of radiation protection layer, following this approach. It is allocated in the spacecraft inner section to permit the best interface, avoiding high temperature gradients with the latter. Only one face is in direct contact with the external and cold deep space, where the outer section of the telescope receiver and transmitter unit are placed. This surface must be in view of the planet and perpendicular to the orbiter velocity, as it is reported in Fig. 7.1.

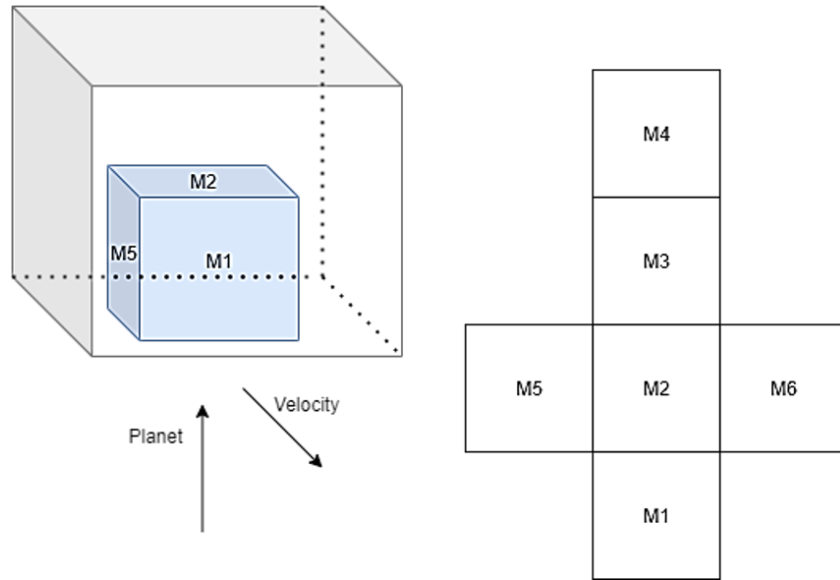


Figure 7.1: Payload configuration in the thermal model

Each face of the box has been shaped as a thermal mass, a node in the thermal resistance diagram (M1, M2, M3, M4, M5 and M6) Fig. 7.2. All the neighboring cuboid faces are connected by means of multiple conductive resistances, and the payload to spacecraft interface is established similarly, but accounted as a constant boundary temperature. The only external surface, M4, is radiating towards the deep space, which is considered as a cold sink at 4K. To undertake the analysis, the two critical conditions during the whole mission, hottest and coldest, have been investigated. The former befalls the payload during Venus flyby, the closest position to the Sun; here the instrument is offline, but it is communicating its status to the spacecraft. Whereas, the coldest one was considered on the orbit around Ganymede behind Jupiter, therefore in complete shadow, when the laser source is shut down but the electronics are still working. An internal power dissipation of 10W on M2 was considered for the electronics in both states, because the laser headbox is not operating even during the interplanetary transfer. On the exposed surface, M4, the albedo of Venus is present during the fly-by, and its infrared radiation is present too. On the other hand, for the cold case around Ganymede, its albedo radiation was neglected (S/C on the shadow side), but its infrared emission is lighting up M4. All the thermal fluxes are make clear in Table 7.2.

The resulting equilibrium temperatures, under the previous conditions, are not satisfactory, in particular regarding the most critical face. To ensure a good interface with the spacecraft, the minimum temperature gradient is necessary especially in the operative phase of the mission. The MLI (Multi-Layer Insulator), as passive thermal control device, is applied on the exposed

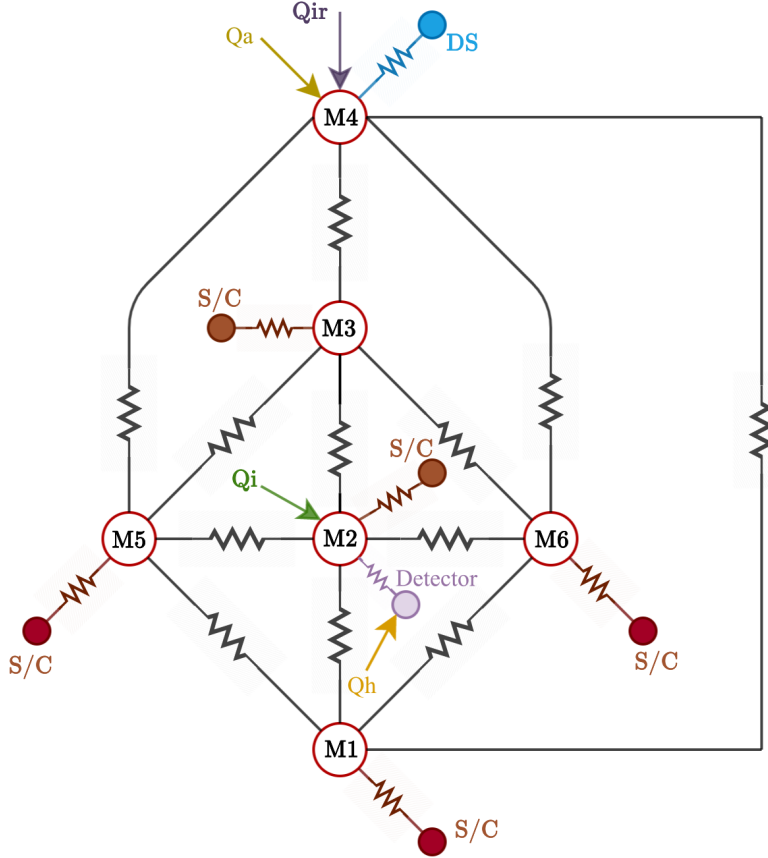


Figure 7.2: Thermal Control Scheme

Table 7.2: Heat Fluxes

Condition	Qa [W]	Qir [W]	Qi [W]	Qh [W]
Hot Case	12.16	95.59	10	-
Cold Case	-	0.22	10	2

side of the payload out of the spacecraft, apart from the entrance and exit area of the laser, to cut the heat exchange with the deep space. It should be optimized (in term of efficiency vs. mass) with a number of layers between 15 to 25 [1]. MLI is composed of an outer cover in Kapton 160 XC with aluminium backing, an inner cover in aluminized polyimide with fiberglass backing, interior layers in aluminized Kapton, and separator layers in Dacron web as shown in Fig. 7.3. The material's properties are reported in Table 7.3.

Results are now more uniform and are spell out in Table 7.4. A key-point is the detector temperature range of operation. Its performances are really influenced by the temperature noises; therefore, it needs to be kept at nominal 20 °C (293 K). A small heater of 2W needs to be added, limited to this additional node, in the thermal resistance diagram. Hence, it is possible to reach a suitable equilibrium temperature even in the coldest conditions.

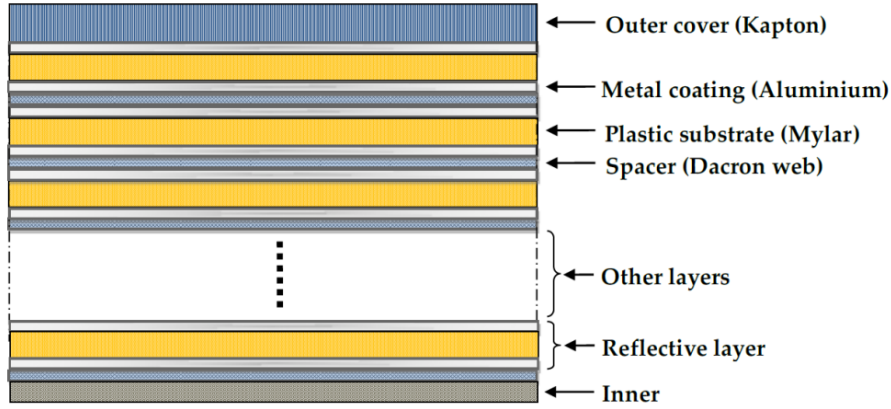


Figure 7.3: MLI composition

Table 7.3: MLI materials properties

Layer	Thickness	Absorbance	Emissivity	Temperature range °C
Kapton	0.127	0.54	0.18	-73/65
Aluminized polyimide	0.01	-	0.04	-
Aluminized Kapton	0.025	0.12	0.028	-250/288
Dracon web	0.16	-	-	-70/177

Table 7.4: Equilibrium Temperatures

Conditions	M1	M2	M3	M4	M5	M6	Detector
Hot Case	308 K	308 K	308 K	316 K	308 K	308 K	308 K
Cold Case	273 K	273 K	273 K	272 K	273 K	273 K	293 K

An equilibrium temperature validation with a more precise model is necessary at the final stage of our design. This analysis relies on the structural model created on Inventor, Autodesk. All the components and instrument parts are modeled in the right position with their precise dimensions and the detector temperature is fixed at 20°C. The results are comparable with the ones from the previous analysis made by Simulink, MatLab and all the requirements temperature ranges are fulfilled. In Fig. 7.4 and Fig. 7.5 the thermal gradient representations for both hot and cold cases can be seen. At the detector, a more sophisticated approach for further improvements, could be considered using a Peltier thermo-electric module [17] instead of a simple heater. It could guarantee temperature control in both the cold and the hot case, keeping the detector at 20°C and thus maximizing its performances.

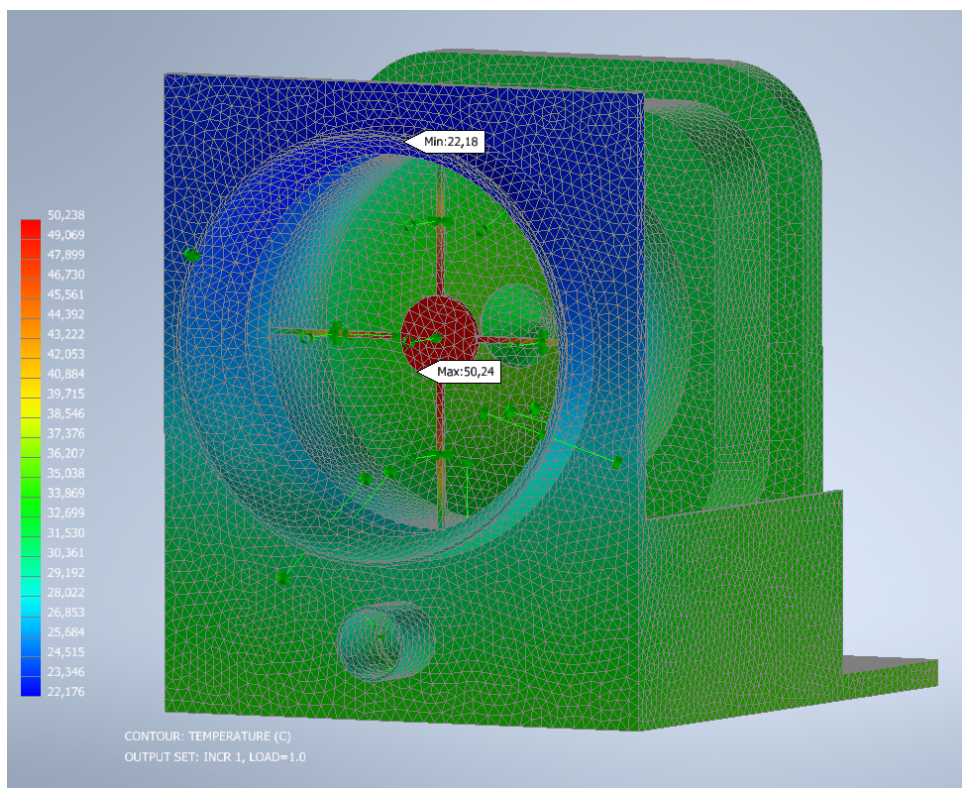


Figure 7.4: Thermal analysis for hot case

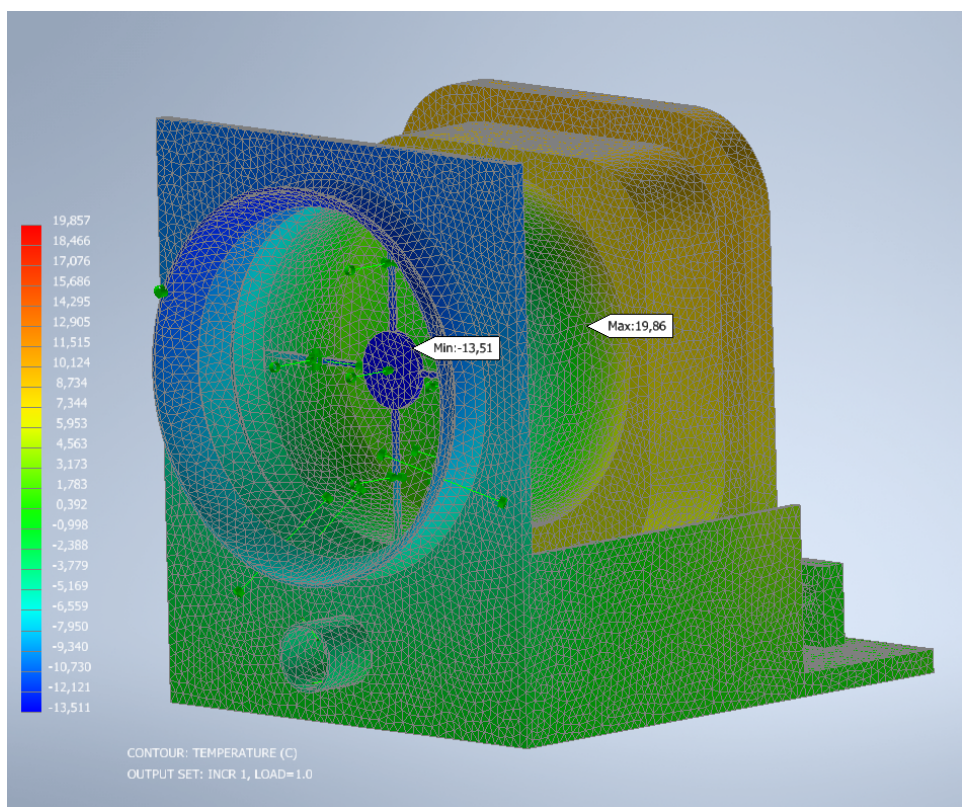


Figure 7.5: Thermal analysis for cold case

8. Structural Analysis

Table 8.1: Structural Requirements

ID	Statement	Section
R-LAN-010	The launch vehicle shall be Ariane 5	8.3
R-LAN-020	The instrument mass shall fit the launcher capability	8.3
R-LAN-025	The instrument volume shall fit the launcher capability	8.3
R-LAN-030	Launch site shall be CGS (Kourou, French Guyana)	8.3
R-STR-010	The instrument shall support the launch environment	8.4
R-STR-020	The instrument structure shall support the mechanical static and dynamic loads encountered during its entire life	8.4
R-STR-030	Lateral frequencies of the instrument shall be greater than 8 Hz	8.4
R-STR-040	Longitudinal frequencies of the instrument shall be greater than 27 Hz	8.4

8.1 3D model

Fig. 8.1 shows the 3D model in its isometric and lateral view, where colors have been used to distinguish the different components. Specifically, starting from the upper left, the receiver Stravroudis baffle is shown in red. After that, the receiver unit is composed by the Ritchey-Chretièn Cassegrain (light blue), the analog electronic box (cyan), and the opto-mechanical bench (purple). The Back-End Optics unit and the APD assembly are not visible as they are centred inside a hole in the AEU right after the telescope.

On the transmitter side there are two yellow laser head boxes and a single controller (orange). The laser beam travels inside the transmitter optics, shown in grey, then enters the beam expander (black), the straylight protection unit (white) and finally exits through the green transmitter baffle. Finally, the structural bench is shown in clear green. The electronic boards, which are not displayed in this model, are thought to be positioned behind the transmitter optics, fixed on the bottom platform.

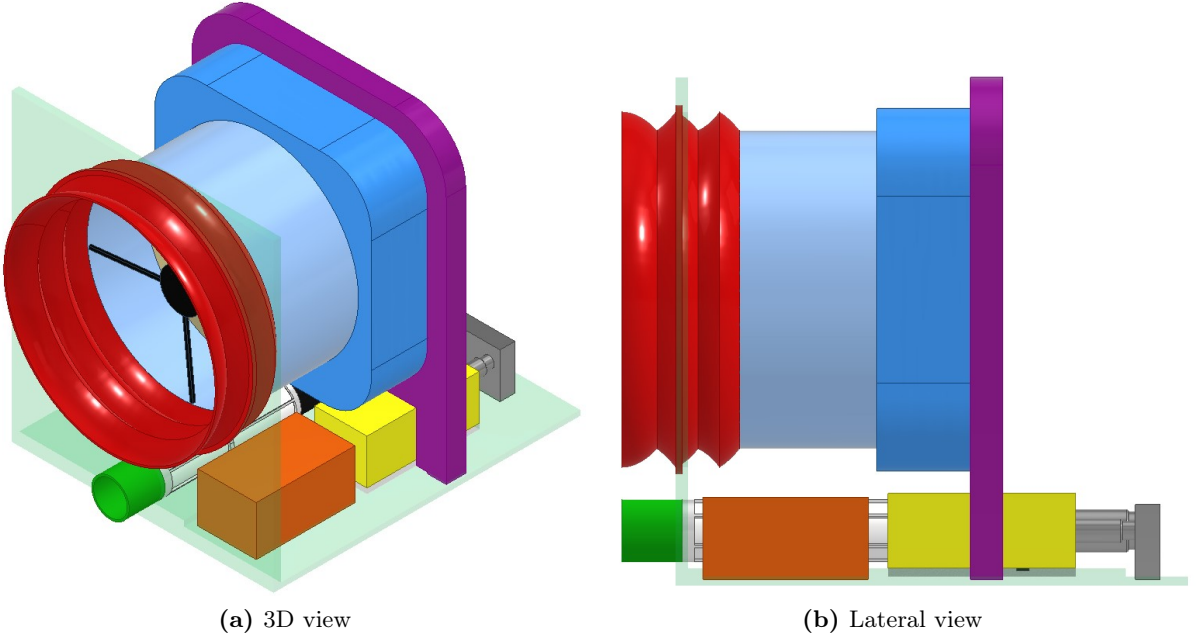


Figure 8.1: Assembly model

8.2 Materials selection

Al 2014-T6 [2] is a precipitation hardening alloy in the T6 temper. To achieve this temper, the metal is solution heat-treated and artificially aged until it meets standard mechanical property requirements. It has been used for the modelling of all the components, apart from the telescope and the structural parts.

The structural components that need a high strength vs weight with a low thermal expansion coefficient have been modelled in titanium alloy. Specifically, Ti-6Al-4V [21] is a two-phase alloy, containing both alpha and beta phase crystalline structures. This high strength alloy can be used at cryogenic temperatures to about 427°C. It is most widely used for structural purpose as both sheet and forgings. The alloy is age hardenable by heat treatment to achieve higher strengths. Some of the mechanical and thermal properties of the two materials are summarized in Table 8.2.

Table 8.2: Materials properties

Material	Magnetic property	E	G	Melting Range	C_p
Al 2014-T6	Nonmagnetic	73 GPa	27.4 GPa	505-640 °C	0.869 J/gK
Ti-6Al-4V	Nonmagnetic	110 GPa	41-45 GPa	1604-1660 °C	0.526 J/gK

8.3 Launcher

From all the possible available launchers, the Ariane 5 by Arianespace was chosen since it has been used for other missions to Jupiter. The total mass of the spacecraft has been considered for the choice of frequency threshold values in the modal analysis. Starting from this, some Launcher requirements are underlined to be taken into account in further structural analysis.

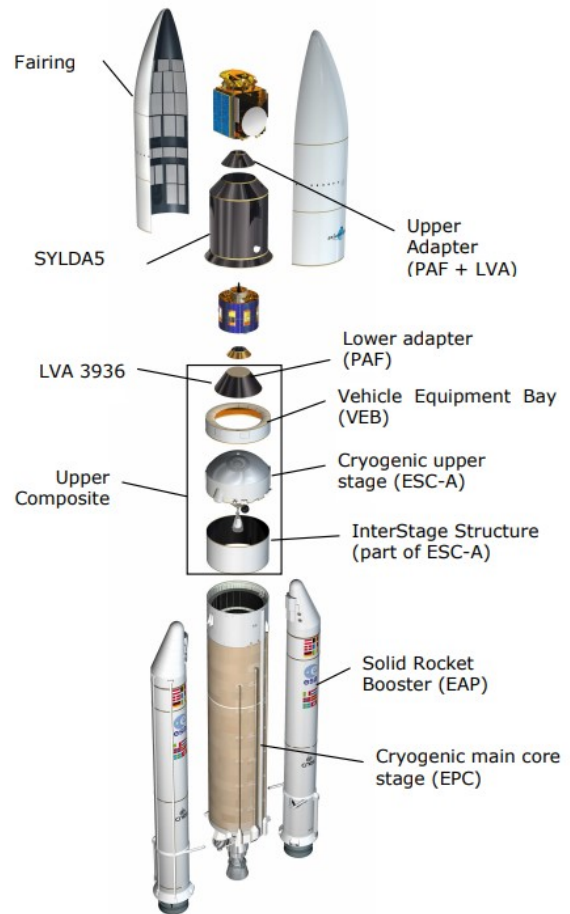


Figure 8.2: Ariane 5 launcher vehicle by Arianespace

The fundamental (primary) frequency in the lateral axis of a spacecraft cantilevered at the interface must be major than 8 Hz considering an average spacecraft mass of 5300Kg.

The fundamental frequency in the longitudinal axis of a spacecraft cantilevered at the interface must be major than 27 Hz.

8.4 Stress analysis

8.4.1 Static loads

Fig. 8.3 shows a typical longitudinal static acceleration-time history for the L/V during its ascent flight. The highest longitudinal acceleration occurs at the end of the solid rocket boost phase and does not exceed 4.55 g, thus in the load analysis this maximum value has been considered. The highest lateral static acceleration may be up to 0.25 g [18].

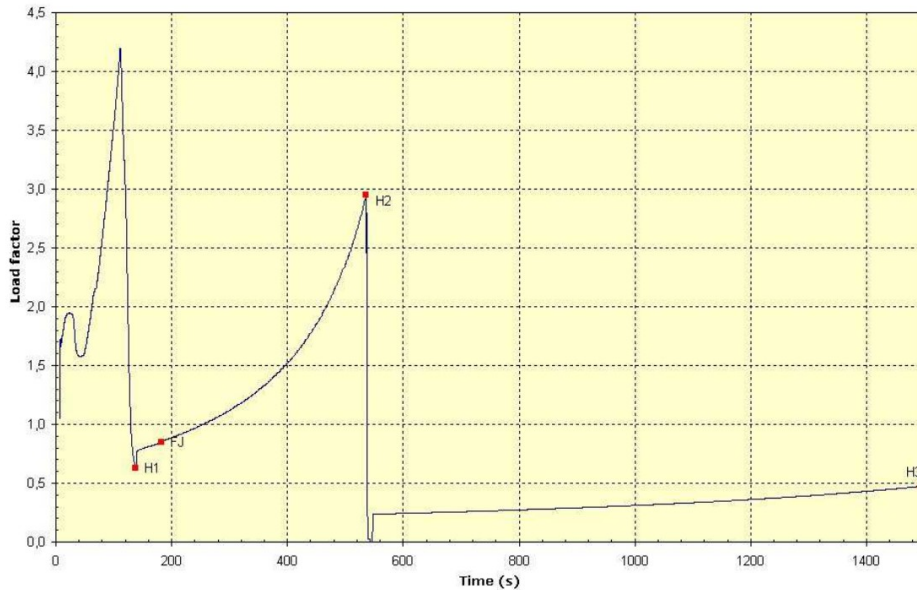


Figure 8.3: Typical longitudinal static acceleration

8.4.2 Random loads

Under 100 Hz, the random environment is covered by the sine environment defined in Fig. 8.4. The acoustic spectrum defined in section 8.4.3 covers excitations produced by random vibration at the spacecraft base for frequency band above 100 Hz.

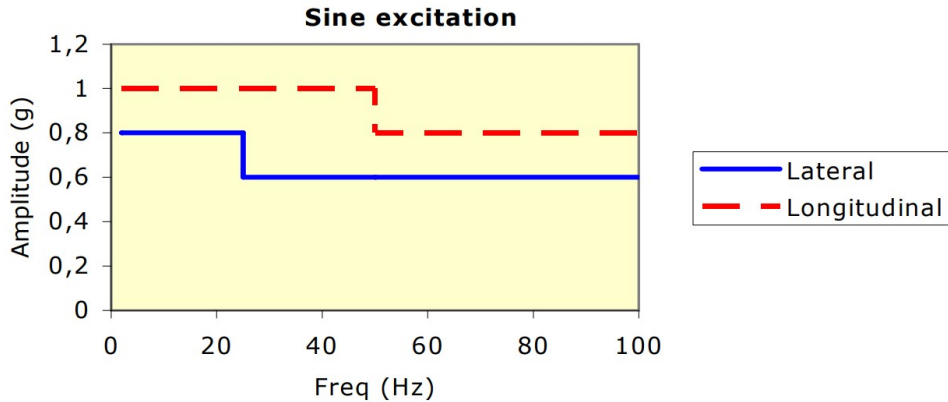


Figure 8.4: Sine excitation at spacecraft base

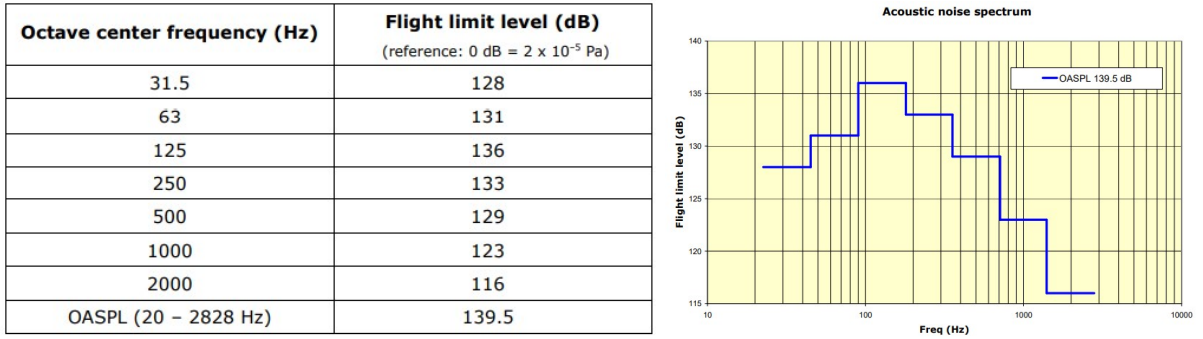
8.4.3 Acoustic loads

The envelope spectrum of the noise induced inside the fairing during flight is shown in Fig. 8.5a and Fig. 8.5b. and it corresponds to a space-averaged level within the volume allocated to the spacecraft stack.

The measured root mean squared sound pressure p_{rms} can be computed from the equation below, where $p_{ref} = 2 \times 10^{-5}$ is the reference pressure.

$$OASPL = 10 \log \left(\frac{p_{rms}^2}{p_{ref}^2} \right) \quad (8.1)$$

As a result, the sound pressure level contributes to the loads with a total $p_{rms} = 188.3649$ Pa.



(a) Sound Pressure Level table

(b) Acoustic noise spectrum

Figure 8.5: Acoustic noise load

8.4.4 Design loads

The design and dimensioning of the spacecraft primary structure and/or evaluation of compatibility of existing spacecraft with Ariane 5 launch vehicle shall be based on the design load factors. The design load factors are represented by the Quasi-Static Loads (QSL) that are the more severe combinations of dynamic and static accelerations that can be encountered at any instant of the mission (ground and flight operations). The QSL reflect the line loads at the interface between the spacecraft and the adapter. The flight limit levels of QSL for a spacecraft launched on Ariane 5 and complying with the previously described frequency requirements and with the static moment limitation are given in Fig. 8.6.

Acceleration (g)	Longitudinal		Lateral
	Static	Dynamic	Static + Dynamic
Critical flight events			
Lift-off	- 1.8	\pm 1.5	\pm 2
Aerodynamic phase	- 2.7	\pm 0.5	\pm 2
Pressure oscillations / SRB end of flight	- 4.40	\pm 1.6	\pm 1
SRB jettisoning *	-0.7	\pm 3.2	\pm 0.9

Figure 8.6: Design loads

8.4.5 Results

The stress analysis of the structure under longitudinal and lateral loads has been carried out using Inventor Nastran. The structure has been constrained to be fixed on the bottom face and the quasi static loads have been applied as equivalent accelerations to the overall structure.

As a first approximation, all the cylindrical components (RX and TX baffle, straylight protection unit, Cassegrain telescope) can be modelled as monocoque cylinders, while the structural parts of laser head, controller, analog electronic and electronic boxes can be considered as skin-frame structure.

Concerning the longitudinal loads, the design acceleration was set to 5.5g, which results from the sum of the maximum static (Fig. 8.3) and random loads (Fig. 8.4). The resulting Von Mises stresses are shown in Fig. 8.7, expressed in MPa.

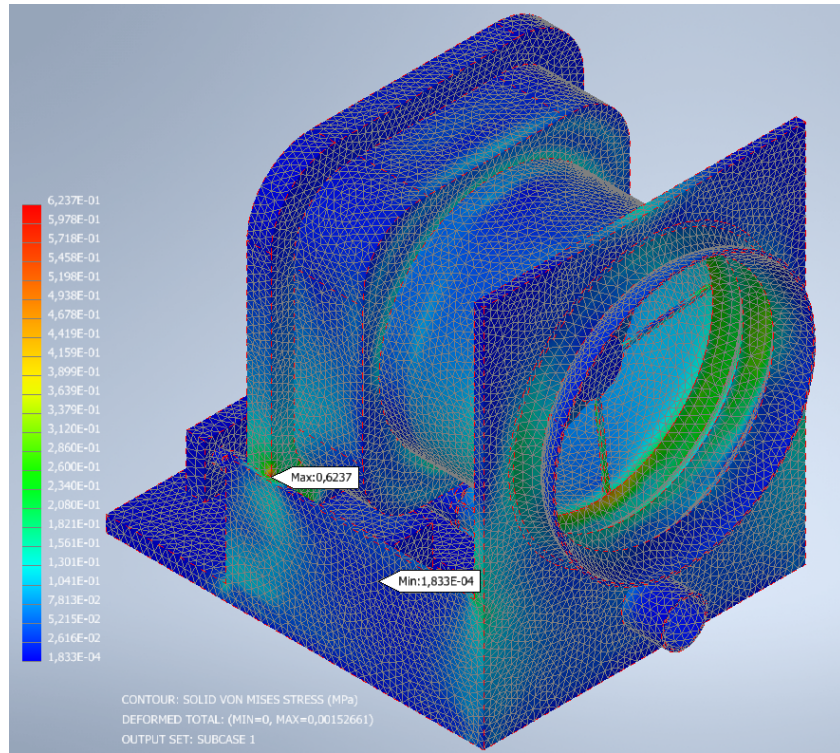


Figure 8.7: Von Mises stresses due to longitudinal acceleration

As it can be seen from the zoom in Fig. 8.8, the maximum stress occurs in correspondence of the bench corner, which is subjected to 0.62 MPa. Fig. 8.9 shows that this value is well inside the elastic region of the aluminum alloy 2014-T6 [15].

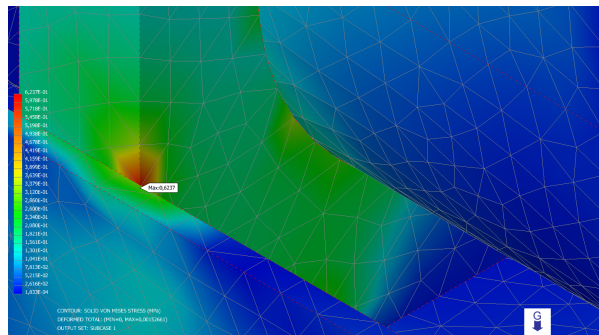


Figure 8.8: Zoom on maximum stress

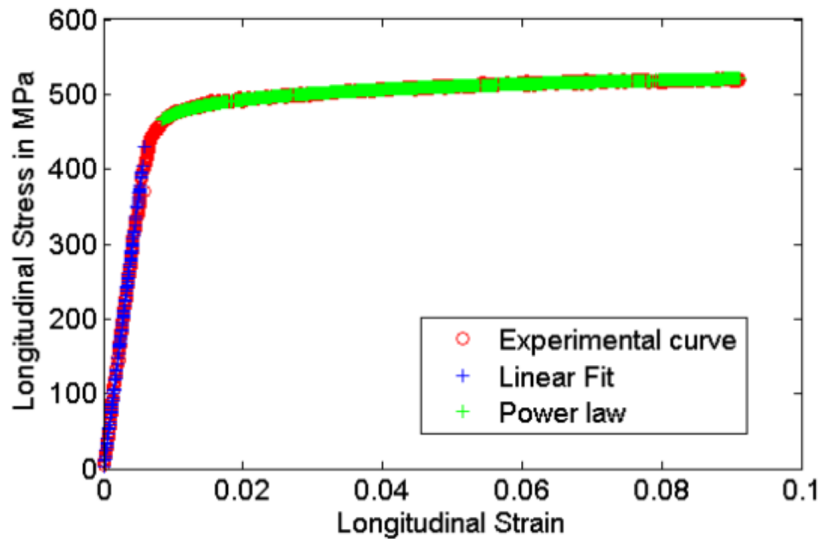


Figure 8.9: Stress-strain curve of Al 2014-T6

Fig. 8.10a shows the structure displacements due to the longitudinal acceleration. The most critical part is the secondary mirror, which is attached to the telescope cylindrical shell through titanium sustains. As it can be seen, the maximum displacement is 0.0015 mm, which is still compatible with the requirement on the alignment of the two mirrors. Infact, from a simulation in Zemax it can be seen that a such a displacement does not visibly influence the footprint on the detector.

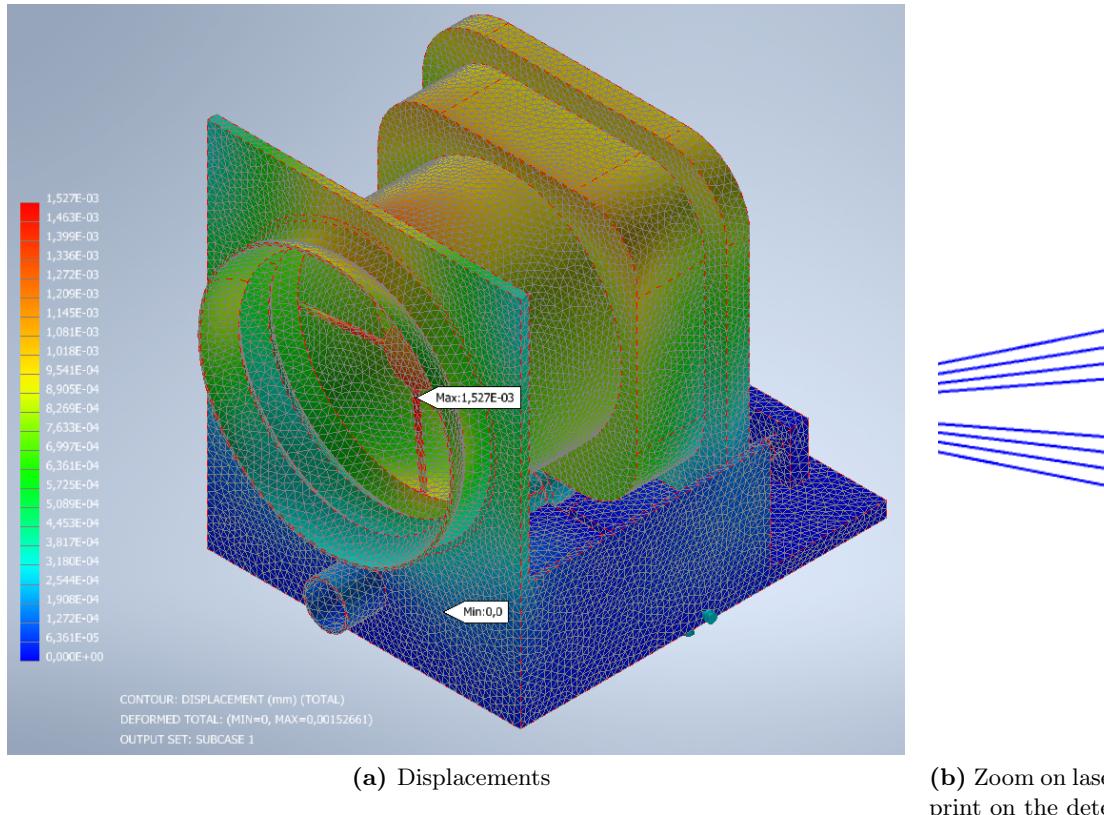


Figure 8.10: Displacements due to longitudinal acceleration

Regarding the maximum lateral acceleration, a maximum of 2 g has been considered from Fig. 8.6 and the results are shown in the following figures. Fig. 8.11 displays the structure's Von Mises stresses, with the highlighted maximum (Fig. 8.12) on the secondary mirror's sustains. As expected, this part is the most critical since the 25 cm aperture must be left as clear as possible but still guaranteeing a sufficient mechanical resistance to the loads.

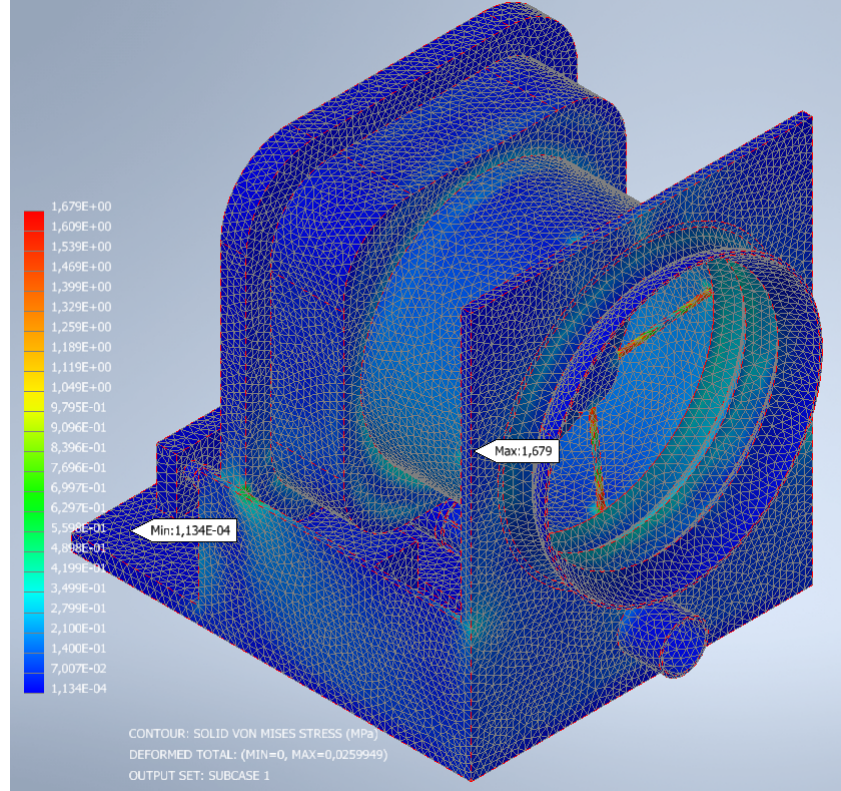


Figure 8.11: Von Mises stresses due to lateral acceleration

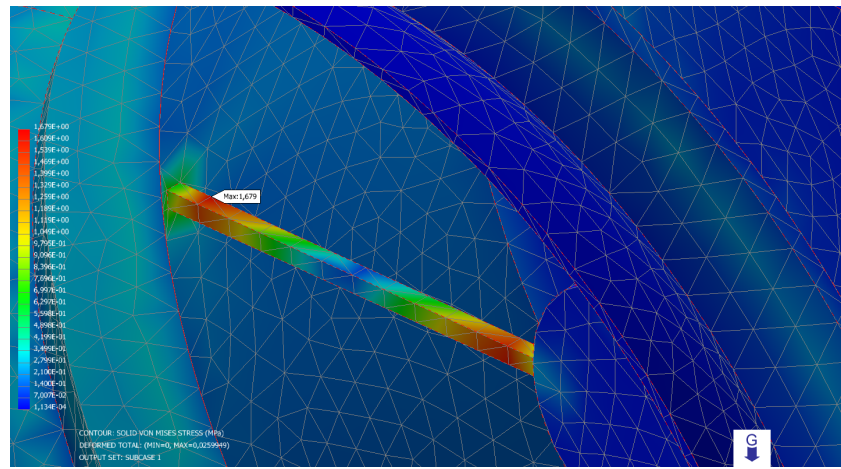


Figure 8.12: Zoom on maximum stress

Specifically, the maximum stress is 1.7 MPa, which also in this case is well inside the elastic region for the Titanium alloy Ti-6Al-4V, as shown from the stress-strain curve in Fig. 8.13.

For what concerns the displacements, the secondary mirror is subjected to a maximum of 0.026 mm (Fig. 8.14a). As it can be seen from Fig. 8.14b, optical systems are very sensitive and the footprint on the detector would be modified. Thus it is of paramount importance to ensure

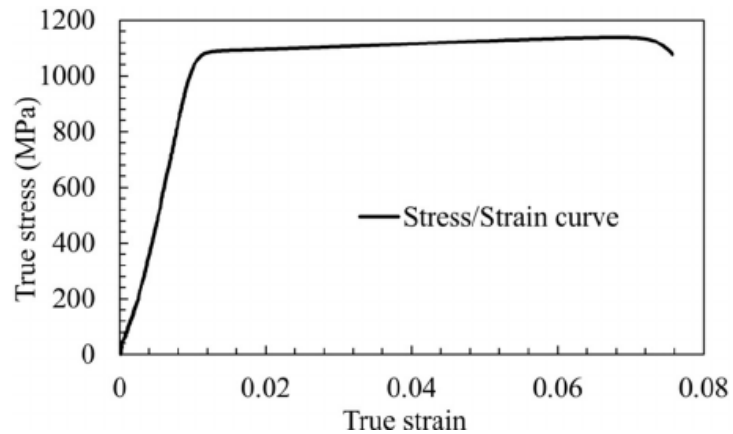


Figure 8.13: Stress-strain curve of Ti-6Al-4V

that the instrument would not be subjected to a lateral load of this magnitude while operating. Otherwise, an increment in the supports' size would have to be taken into account.

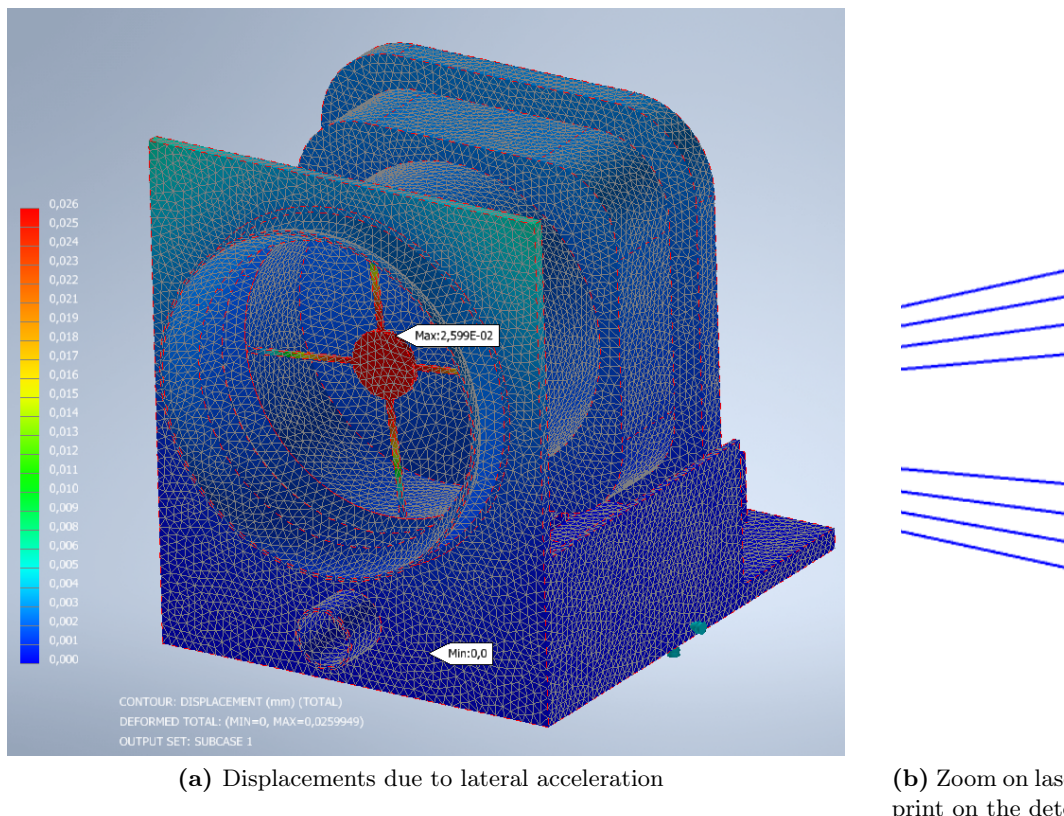


Figure 8.14: Displacements due to lateral acceleration

8.5 Frequency analysis

Modal analysis is a powerful tool to identify the dynamic characteristics of structures. Every structure vibrates with high amplitude of vibration at its resonant frequency. It is imperative to know the modal parameters-resonant frequency, mode shape and damping characteristics of the structure at its varying operating conditions for improving its strength and reliability at the design stage [4].

Since the most critical component of the instrument structure is the Cassegrain receiver telescope, a preliminary frequency analysis has been conducted on this component only, using *Autodesk Inventor Professional*. The telescope has been fixed on the bottom side and the results in Fig. 8.15 show that the first mode (99.04 Hz) is well beyond the minimum value of 27 Hz, imposed by the launcher.

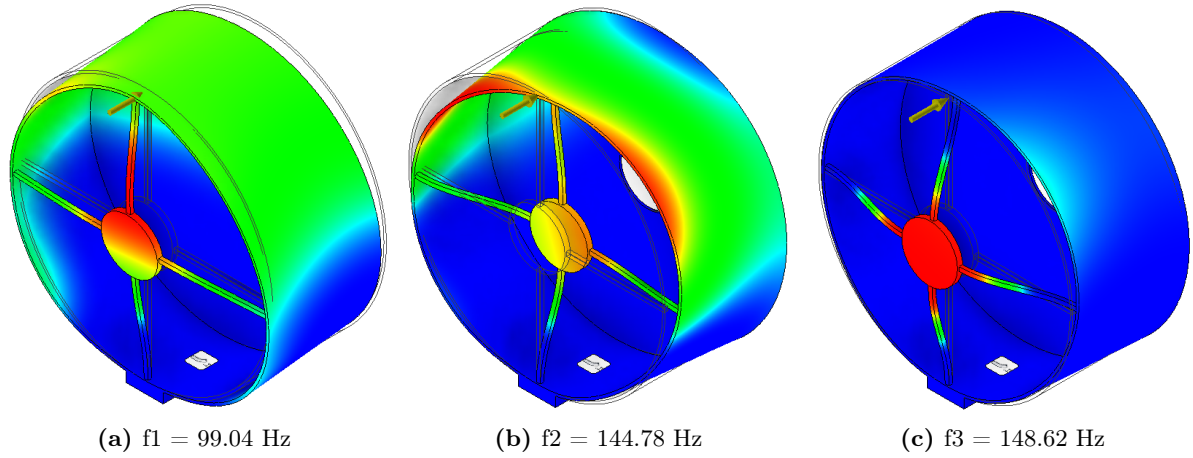


Figure 8.15: Modal frequency analysis of the receiver telescope: fixed at bottom side

A second analysis has been performed fixing the telescope on the lateral ring. In this case, the resulting frequencies are even higher and thus will not cause any resonance problem. Fig. 8.16 shows the first three mode shapes.

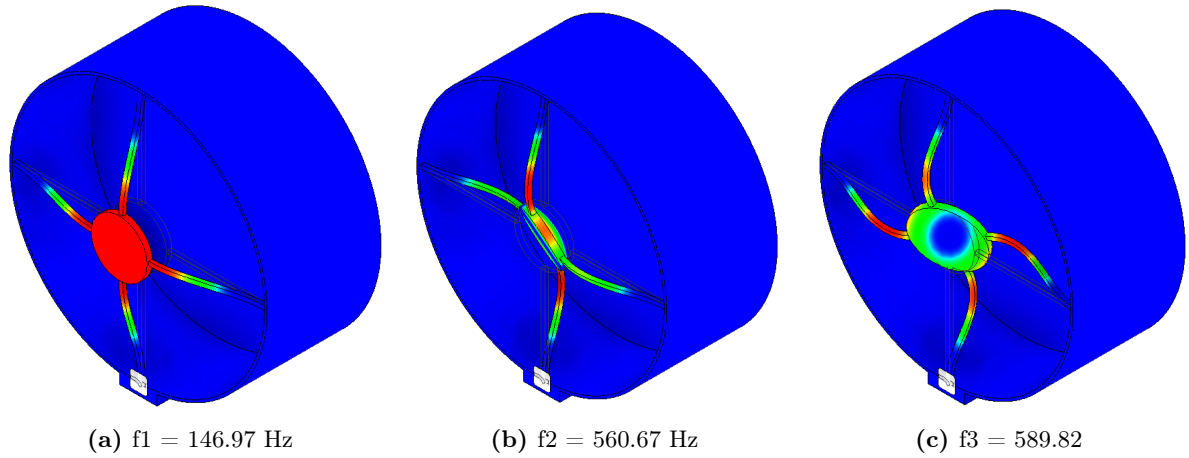


Figure 8.16: Modal frequency analysis of the receiver telescope: fixed on lateral ring

For what concerns the natural frequencies of the complete model, the same approach has been applied. Firstly, the model has been fixed on the bottom side: as expected, the most critical dynamic is the one associated to the secondary mirror of the receiver telescope (Fig. 8.17a). After that, the successive modes are the ones associated to torsion and bending of the vertical plate where the baffles are jointed, as shown in Fig. 8.17b, Fig. 8.17c, and Fig. 8.17d.

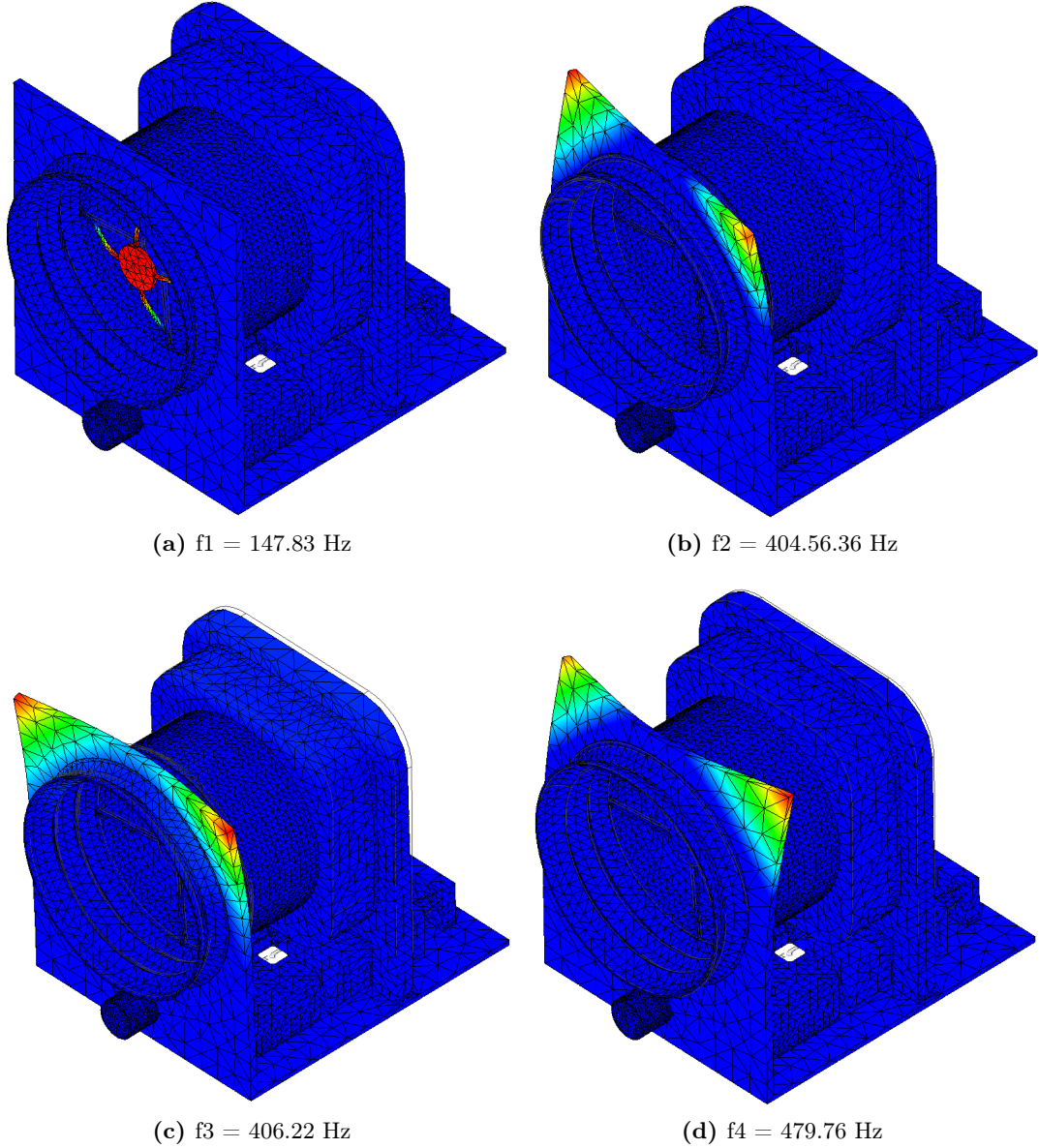


Figure 8.17: Modal frequency analysis of the assembly: fixed at bottom side

If instead we consider the fixed constraint on the vertical plate and leave the bottom one free, the results show that the most critical component is still the Cassegrain receiver telescope (Fig. 8.18a) but now the assembly is subjected to some other important dynamics (Fig. 8.18b, Fig. 8.18c, Fig. 8.18d). It is therefore of paramount importance to constraint the instrument also on the bottom plate, as dynamics like these could cause misalignment between the two mirrors. The mounting bipod supports are show in Fig. 8.19.

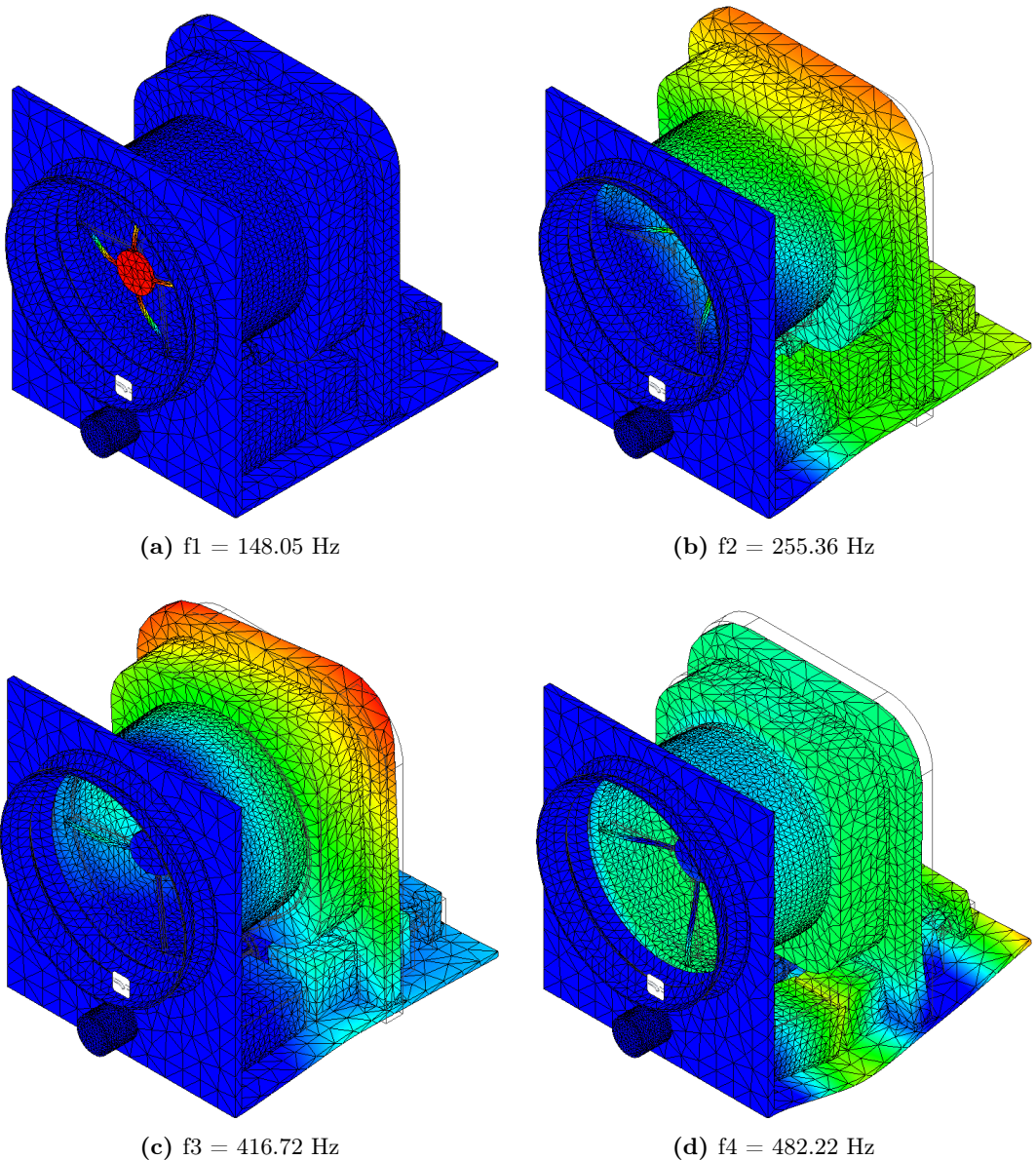


Figure 8.18: Modal frequency analysis of the assembly: fixed on lateral plate

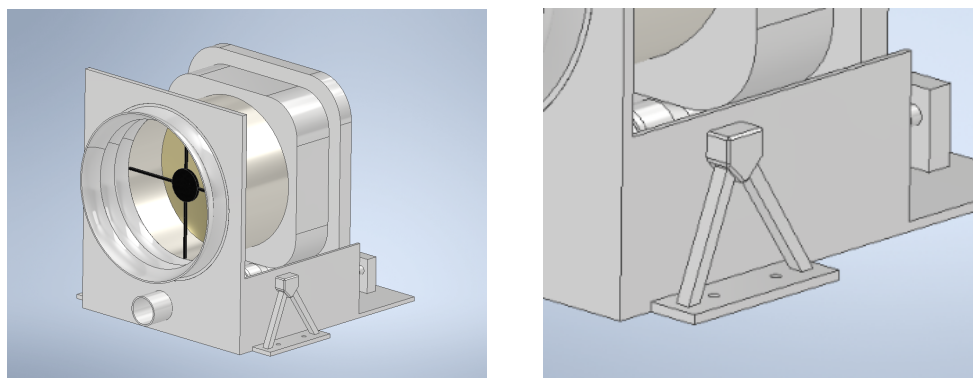


Figure 8.19: Final assembly with a close up on the mounting supports

9. Conclusions

9.1 Mass and power budget

The mass budgets for the every subsystems are summarized in the following tables: Table 9.1 for the transmitter unit, Table 9.2 for the receiver unit, Table 9.3 for the electronic unit. Lastly, all the remaining structural parts are summarized in Table 9.4. Every component have been margined based on the technology readiness level.

Table 9.1: Mass budget: Transmitter Unit

Component	Nominal mass [kg]	Margin [%]	Margined mass [kg]
Transmitter Baffle Unit	0.050	25	0.061
Straylight Protection Unit	0.138	25	0.173
Beam Expander	0.224	25	0.280
Transmitter Optics	0.851	20	1.021
Laser Head Box	0.917	10	1.009
Controller/Driver	0.607	10	0.668
Total mass	2.787	-	3.212

Table 9.2: Mass budget: Receiver Unit

Component	Nominal mass [kg]	Margin [%]	Margined mass [kg]
Receiver Baffle Unit	0.621	25	0.776
Receiver Telescope	0.976	25	1.220
Converter	0.200	20	0.240
Total	1.797	-	2.236

Table 9.3: Mass budget: Electronic Unit

Component	Nominal mass [kg]	Margin [%]	Margined mass [kg]
Electronic Unit	0.500	10	0.550
Laser Electronic Unit	0.500	20	0.600
Total	1.00	-	1.15

Moreover, a further margin has been added at subsystem level: since the technologies for laser altimeters are well known and already space proven, a 10% margin has been considered.

Table 9.4: Mass budget: Structural Unit

Component	Nominal mass [kg]	Margin [%]	Margined mass [kg]
Opto/mechanical bench	2.820	20	3.384
Structure	5.742	20	6.890
Total	8.562	-	10.274

Table 9.5: Mass budget: Subsystems

Subsystem	Nominal mass [kg]	Margin [%]	Margined mass [kg]
Transmitter Unit	3.212	10	3.533
Receiver Unit	2.236	10	2.4596
Electronics Unit	1.15	10	1.265
Structural Unit	10.274	10	11.3014
Total			18.559

As a last step in the mass budget definition, a further 10% margin at system level has been considered, reaching a final mass of 20.415 kg.

For what concerns the power, the budget for the nominal operating mode is summarized in Table 9.6 while Table 9.7 shows the power budget for the different operative modes:

Table 9.6: Operative Mode Power Budget

Component	Nominal power [W]	Margin [%]	Margined power [W]
Laser Head Box	30	10	33
Analog Electronic Unit	2.5	10	2.75
Electronic Unit	25	20	30
Thermal Control Unit	2	20	2.4
Total			68.15

Table 9.7: Margined power budget for different operational modes

Component	Margin [%]	Safe mode [W]	Operative mode [W]	Data transfer mode [W]	Focus mode [W]
LHB	10	0	33	0	33
AEU	10	0	2.75	0	3.12
ELU	20	10	30	30	35
TCU	20	2.4	2.4	2.4	2.4
Total		12.4	68.15	32.4	73.52

9.2 Final considerations

At the end of this preliminary design phase, a baseline model of an instrument suited for the required mission has been obtained. The architecture and components fulfill all the mandatory

requirements and still leave some flexibility on the preference ones. For example, in successive design phases, further tests on the materials may lead to a more optimized mass budget and a more in depth thermal analysis may lead to a more accurate choice of the heater or Peltier element for the detector. The integration of the instrument with the spacecraft would also need a more accurate study, considering the needs and characteristics of the spacecraft itself, not known in this design phase. Costs have not been considered as a limitation in this study but they should be taken into account in a hypothetical further development of the project. For example in the choice of a lighter more performing material, such as Tantalum, with respect to Aluminum, costs would play an important part.

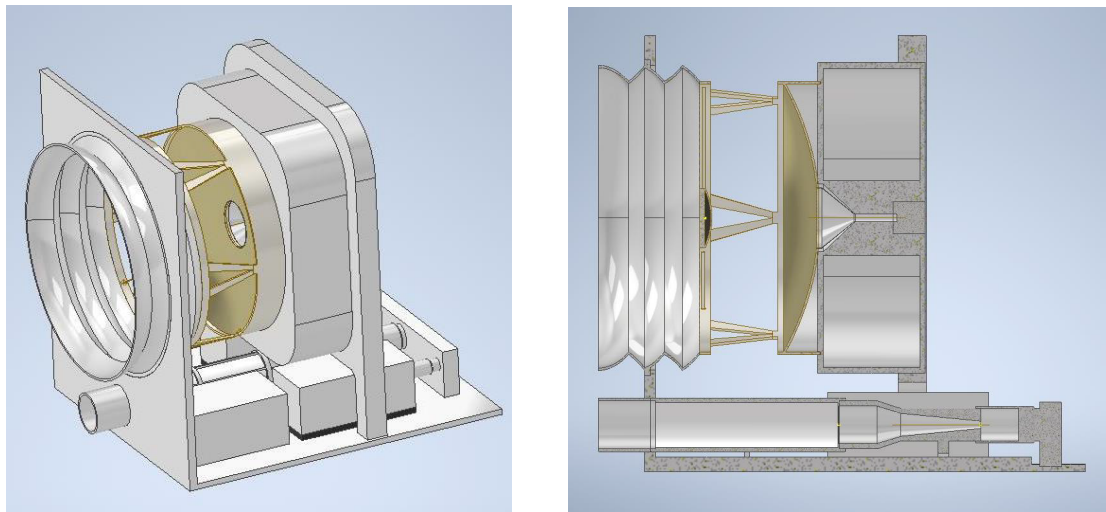


Figure 9.1: Final assembly and section view

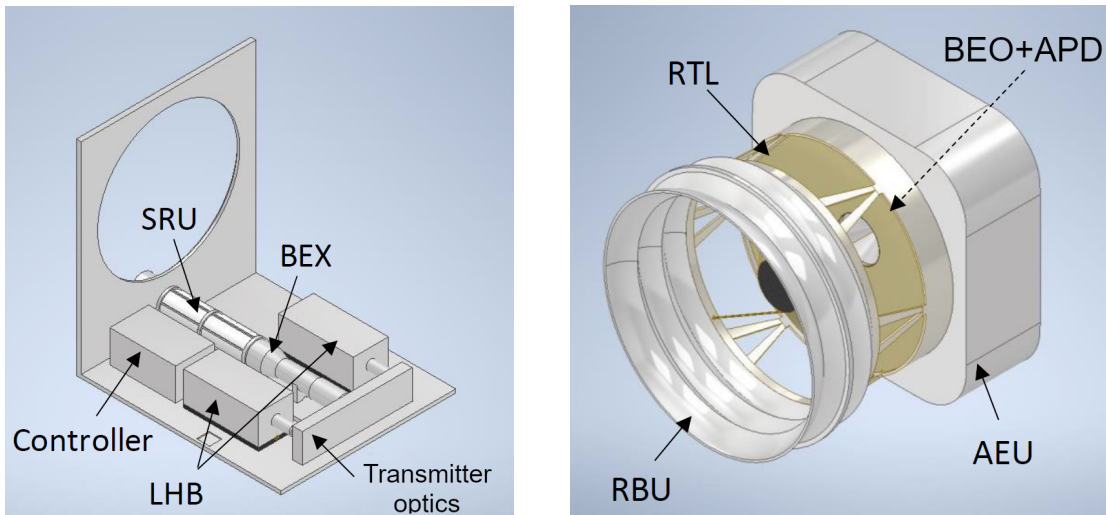


Figure 9.2: Details of transmitter and receiver units

Appendix A

Mass budget graphical representations

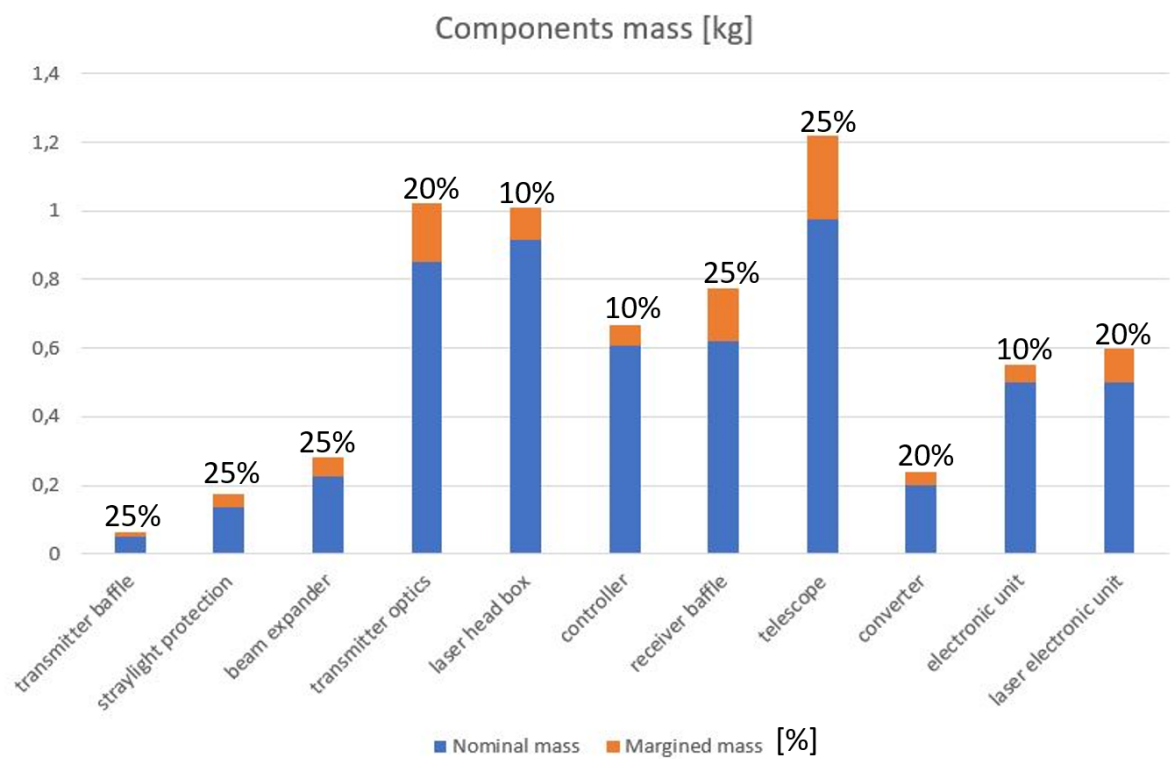


Figure A.1: Components mass

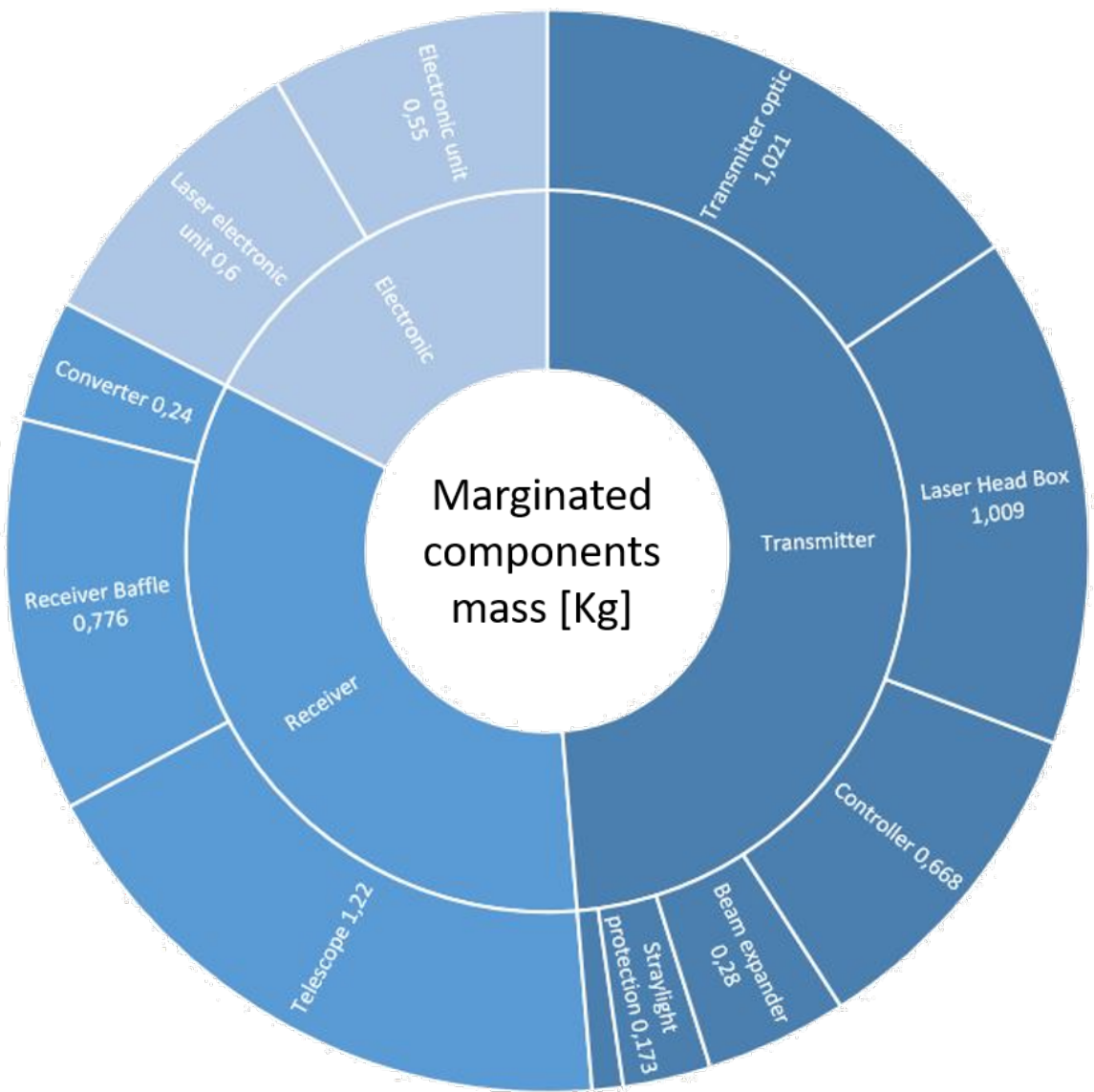


Figure A.2: Marginated components mass divided in sub-systems

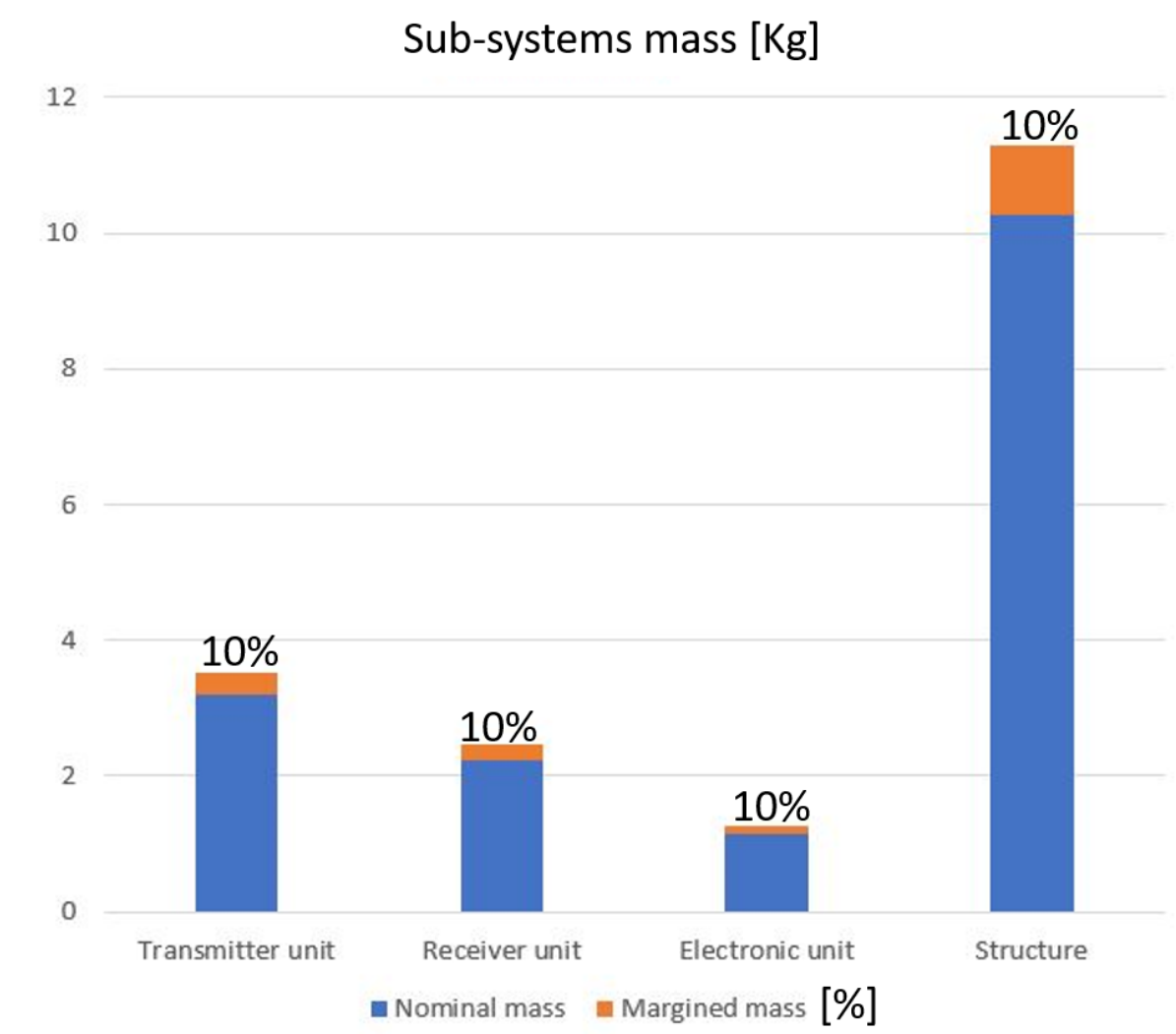


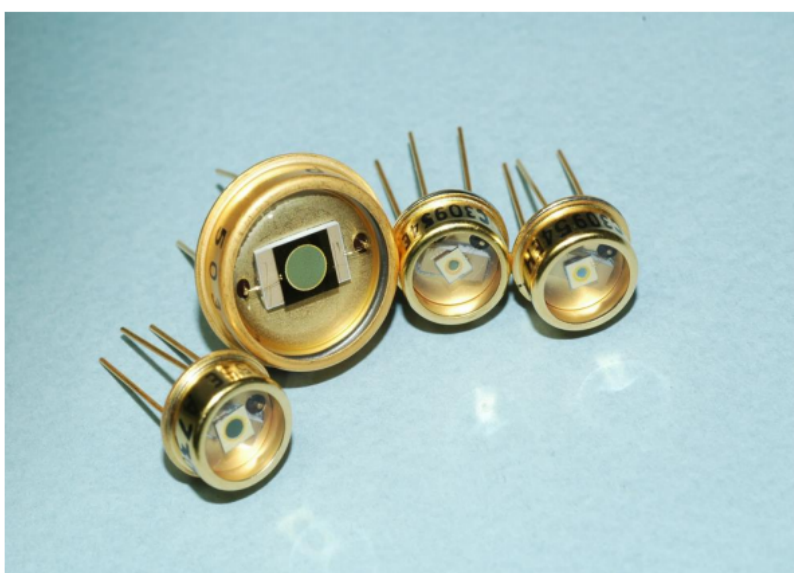
Figure A.3: Sub-systems mass

Appendix B

Excelitas Long Wavelength Enhanced Silicon Avalanche Photodiodes



C30954EH, C30955EH and C30956EH Series **Long Wavelength Enhanced Silicon Avalanche Photodiodes**



Reach through 1064nm quantum efficiency enhanced silicon avalanche photodiode.

Key Features

- High Quantum Efficiency at 1060nm
- Fast Response Time
- Wide operating Temperature Range
- Hermetically sealed packages

Applications

- Range finding
- LIDAR
- YAG Laser Detection

Figure B.1: C30954EH, C30955EH and C30956EH Series

Excelitas' C30954EH, C30955EH, and C30956EH are general purpose silicon avalanche photodiodes made using a double-diffused "reach through" structure. The design of these photodiodes is such that their long wave response (i.e. > 900 nm) has been enhanced without introducing any undesirable properties. These APDs have quantum efficiency of up to 40% at 1060 nm. At the same time, the diodes retain the low noise, low capacitance, and fast rise and fall times characteristics. Standard versions of these APDs are available in hermetically-sealed, flat top glass TO-5 packages for the smaller area C30954EH and C30955EH, and a TO-8 package for the larger area C30956EH. To help simplify many design needs, these Si APDs are

also available in Excelitas' high-performance hybrid preamplifier module, C30659 Series, as well as the preamplifier and Thermo-electric (TE) cooler incorporated module, the LLAM Series. Recognizing that different applications have different performance requirements, Excelitas offers a wide range of customization options for these APDs to meet your design challenges. TE cooler-packaged versions are available on a custom basis. Operating and breakdown voltage selection, dark current and NEP screening, custom device testing and packaging are among the many application-specific solutions available.

Parameter	Symbol	C30954EH	C30955EH	C30956EH	Unit
Shape		Circular	Circular	Circular	
Package		TO-5	TO-5	TO-8	
Photosensitive Surface:					
Useful area	A	0.5	1.77	7	mm ²
Useful diameter	d	0.8	1.5	3	mm
Field of View:					
Nominal field of view α (see Figure 10)	FoV	110	104	135	Degrees
Nominal field of view α' (see Figure 10)		125	130	150	

Figure B.2: Mechanical and Optical Characteristics

Parameter	Symbol	C30954EH			C30955EH			C30956EH			Unit
		Min	Typ	Max	Min	Typ	Max	Min	Typ	Max	
Breakdown Voltage	V _{br}	300	375	475	315	390	490	325	400	500	V
Temperature Coefficient of V _{op} for Constant M	V _{op}		2.4			2.4			2.4		V/°C
Gain	M		120			100			75		
Responsivity at 900 nm at 1060 nm at 1150 nm	R	65 30 4	75 36 5		55 26 4	70 34 5		36 20 2.8	45 25 3.5		A/W
Quantum Efficiency at 900 nm at 1060 nm at 1150 nm	Q.E.		85 36 5			85 40 5			85 40 5		%
Total Dark Current	I _d		50	100		100	200		100	200	nA
Noise Current $f=10\text{kHz}, \Delta f=1.0\text{Hz}$	i _n		1	2		1	2		1.1	2.2	pA/VHz
Capacitance	C _d		2	4		3	5		10	12	pF
Series resistance	R _s			15			15			15	Ω
Rise/Fall Time, R _L = 50Ω: 10% to 90% points 90% to 10% points	t _r t _f		2 2	3 3		2 2	3.5 3.5		2 2	3.5 3.5	ns

Figure B.3: Electro-Optical Characteristics - Case Temperature TA = 22 °C; at the DC reverse operating voltage V, V_{op}

Parameter	Symbol	Minimum	Typical	Maximum	Unit	Remarks/Conditions
Reverse Bias Current				200	μA	
Photocurrent Density : average value peak value	J_p			5 20	mA/mm^2	Continuous operation
Forward Current: average value peak value	I_F			5 50	mA	Continuous operation (For 1 second duration, non-repetitive)
Storage Temperature	T_{stg}	-60		100	$^\circ\text{C}$	
Operating Temperature	T_o	-40		70	$^\circ\text{C}$	
Soldering				260	$^\circ\text{C}$	5 seconds, leads only

Figure B.4: Absolute - Maximum Ratings, Limiting Values

For incident radiation at angles $\leq \alpha/2$, the photosensitive surface is totally illuminated.

For incident radiation at angles $> \alpha/2$, but $\leq \alpha'/2$, the photosensitive surface is partially illuminated

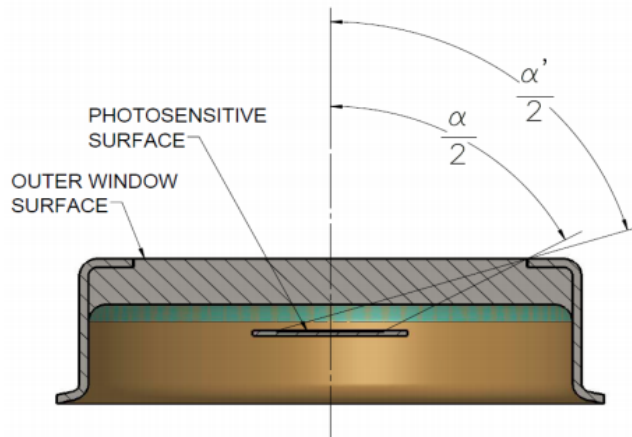


Figure B.5: Approximate Field of View

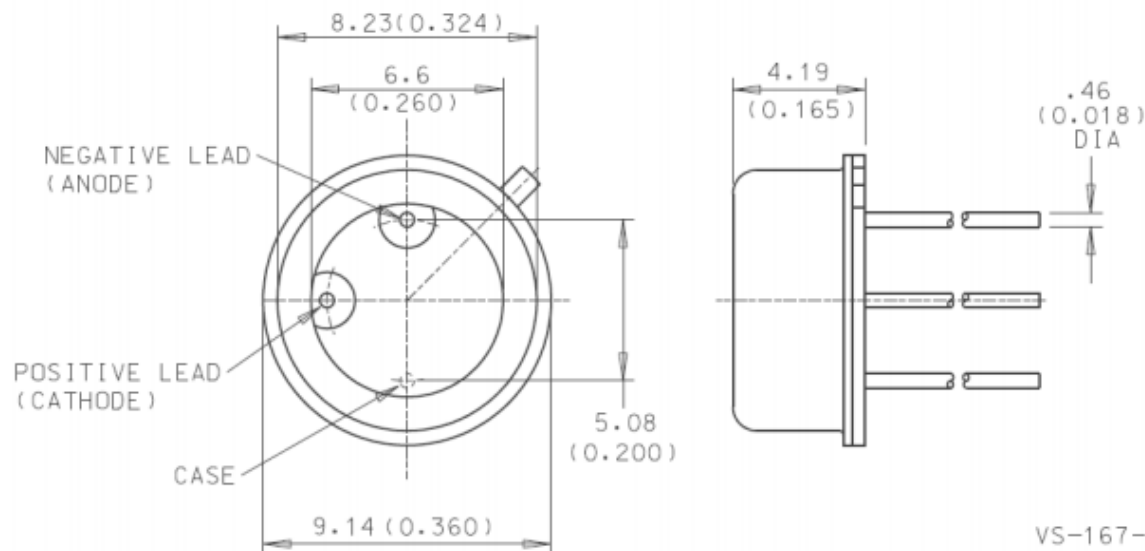


Figure B.6: Dimensional Outline (C30954EH, C30955EH Types) Low-Profile TO-5 Package, dimensions in mm (inch)

Appendix C

Montfort Laser GmbH M-NANO



M-NANO 80mJ 10Hz Nd:YAG DPSSL w/ Separate Compact Driver [PR179]

Even more compact and low weight (<1kg) 50-80mJ-level pulsed Nd:YAG laser head due to the separated control electronics/laser diode current driver and a flexible cable connection in between. Generates laser pulse energies of up to or >50mJ@20Hz or >80mJ@10Hz at pulse durations of <~8 ns, others on request.

Figure C.1: Introduction

Average output power	1 W
Pulse energy, max.	80 mJ
Pulse duration (FWHM)	3 ... 8 ns
Wavelength (center)	1064 nm

Figure C.2: Characteristics

Due to the separation of the electronics and the laser head module, this is an even more compact 50-to-80-mJ-level, pulsed Nd:YAG laser with separated control electronics and a flexible cable connection between electronics and laser head module.

Generates laser pulse energies up to >50...80 mJ, pulse durations of 8 ns and pulse repetition rates of 10 or 20 Hz, other values upon request.

This extremely small laser head is suited for space-constrained and handheld applications (total weight of laser head module <1 kg). The laser can be integrated in the user's setup and just needs to be mounted onto a sub-mount capable of taking the head away during operation to avoid heat accumulation. The user simply provides an external 24-28 VDC power supply and a pulse trigger (TTL).

Inquire about higher pulse energies, higher repetition rates, harmonics, burst mode, extended temperature ranges etc. Benefits: In contrast to existing flash-lamp-pumped Nd:YAG technologies, this laser is laser-diode-pumped and the conductively cooled laser diode stack is included in the laser head. Not only the compactness but also lower electrical power consumption, lower weight, maintenance-free operation and improved beam quality, divergence and focusability are achieved and result in improved application results.

Applications: The compactness and low weight enable applications that were not possible with existing flash-lamp pumped technologies, including handheld applications and other applications with critical space and/or weight constraints. Applications of these compact laser sources include - besides scientific applications - laser analytics, LIBS (Laser-induced breakdown spectroscopy), optical component damage testing, PIV (Particle image velocimetry), LIDAR (Light detection and ranging), Photoacoustic Imaging, Defense, optical amplification, etc.

The specifications of the module are summarized in Fig. C.3:

Average output power	up to >1 W @20Hz
Pulse energy	up to >80 mJ @10Hz, >50 mJ @20Hz
Pulse duration (FWHM)	8 ns (+/-5ns)
Wavelength (center)	1064 nm
Pulse repetition rate	10 Hz, 20 Hz (inquire for higher)
Beam quality M ² , typical	2 ~ 3
Size (laser head)	150 x 70 x 60 mm ³
Size separate controller/driver	132 x 78 x 64 mm ³
Cooling requirement	provide heat sink @ 0...40°C
Power supply	provide 24-28 VDC

Figure C.3: Specifications

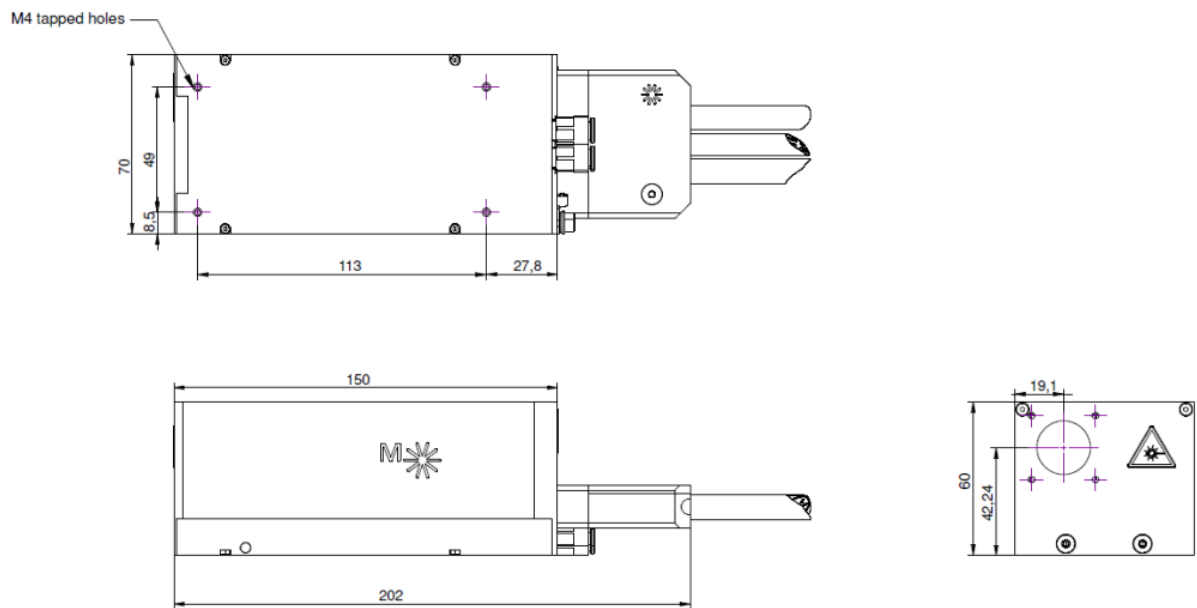


Figure C.4: Laser Head dimensions

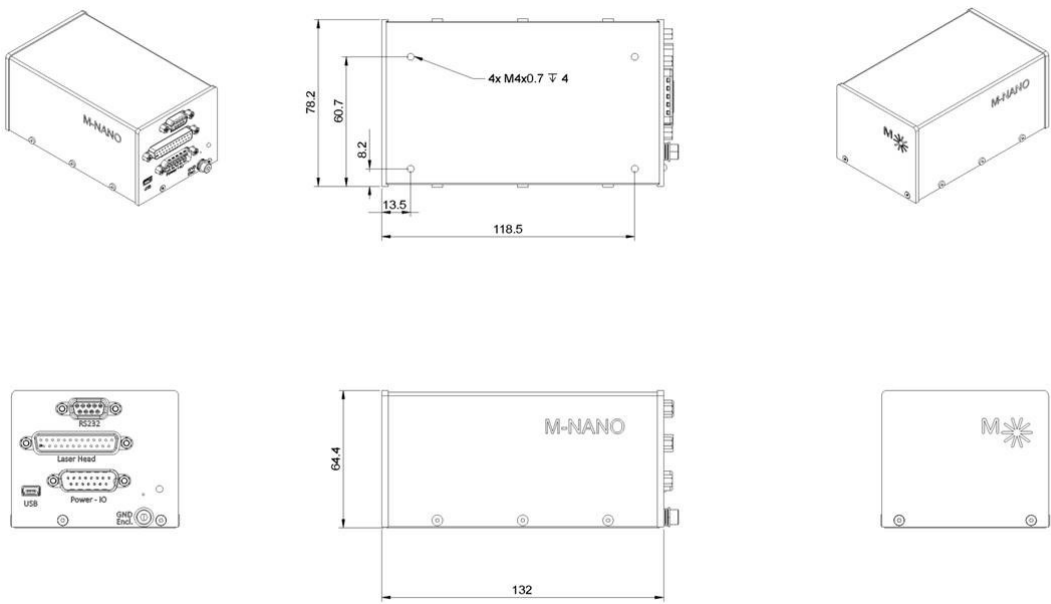


Figure C.5: Controller dimensions

Appendix D

Texas Instrument ADS5474-SP



ADS5474-SP

www.ti.com

SLAS574A –SEPTEMBER 2013–REVISED DECEMBER 2013

Class V, 14-BIT, 400-MSPS ANALOG-TO-DIGITAL CONVERTER

Check for Samples: [ADS5474-SP](#)

FEATURES

- 400 MSPS Sample Rate
- 14 Bit Resolution, 10.9 Bits Effective Number of Bits (ENOB)
- 5962R13208:
 - Radiation Hardness Assurance (RHA) up to TID 100 krad (Si)
 - Total Ionizing Dose 100 krad (Si)
 - ELDRS free 100 krad (Si)
 - SEL/SEU characterized
- 1.28 GHz Input Bandwidth
- SFDR = 78 dBc at 230 MHz and 400 MSPS
- SNR = 69.8 dBFS at 230 MHz and 400 MSPS
- 2.2 V_{PP} Differential Input Voltage
- LVDS-Compatible Outputs
- Total Power Dissipation: 2.5 W
- Power Down Mode: 50 mW
- Offset Binary Output Format
- Output Data Transitions on the Rising and Falling Edges of a Half-Rate Output Clock
- On-Chip Analog Buffer, Track-and-Hold, and Reference Circuit
- Available in a 84-Pin Ceramic Nonconductive Tie-Bar Package (HFG)
- Military Temperature Range: -55°C to +125°C T_{case}
- Engineering Evaluation (/EM) Samples are Available ⁽¹⁾
- Pin-Similar and Compatible With 12- and 14-Bit Family:
[ADS5463-SP](#) and [ADS5444-SP](#)

APPLICATIONS

- Test and Measurement Instrumentation
- Software-Defined Radio
- Data Acquisition
- Power Amplifier Linearization
- Communication Instrumentation
- Radar

(1) These units are intended for engineering evaluation only. They are processed to a non-compliant flow (e.g. No Burn-In, etc.) and are tested to a temperature rating of 25°C only. These units are not suitable for qualification, production, radiation testing or flight use. Parts are not warranted for performance over the full MIL specified temperature range of -55°C to 125°C or operating life.

Figure D.1: A/D converter features

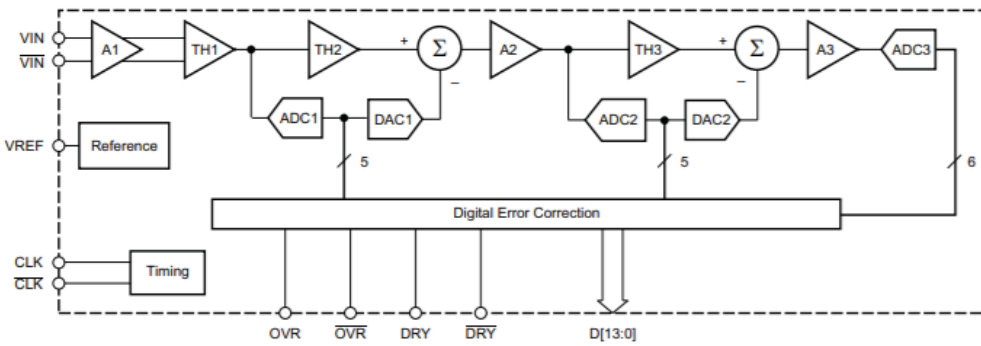


Figure D.2: A/D converter block scheme

	MIN	TYP	MAX	UNIT
SUPPLIES				
AVDD5 Analog supply voltage	4.75	5	5.25	V
AVDD3 Analog supply voltage	3.1	3.3	3.6	V
DVDD3 Output driver supply voltage	3	3.3	3.6	V
ANALOG INPUT				
Differential input range	2.2			V _{PP}
VCM Input common mode	3.1			V
DIGITAL OUTPUT (DRY, DATA, OVR)				
Maximum differential output load	10			pF
CLOCK INPUT (CLK)				
CLK input sample rate (sine wave)	20 ⁽¹⁾		400	MSPS
Clock amplitude, differential sine wave ⁽¹⁾	0.5		5	V _{PP}
Clock duty cycle ⁽¹⁾	40	50	60	%
T _c Operating case temperature range	-55		+125	°C

Figure D.3: A/D converter recommended operating conditions

PARAMETER	TEST CONDITIONS	MIN	TYP	MAX	UNIT
Resolution		14			Bits
ANALOG INPUTS					
Differential input range		2.2			V _{PP}
Analog input common-mode voltage	Self-biased; see VCM specification below	3.1			V
Input resistance (dc)	Each input to VCM	500			Ω
Input capacitance	Each input to GND	7.4			pF
Analog input bandwidth (-3dB)		1.28			GHz
CMRR Common-mode rejection ratio	Common-mode signal < 50 MHz (see Figure 28)	100			dB
INTERNAL REFERENCE VOLTAGE					
VREF Reference voltage		2.4			V
VCM Analog input common-mode voltage reference output	With internal VREF. Provided as an output via the VCM pin for dc-coupled applications.	2.9	3.1	3.3	V
VCM temperature coefficient		-0.8			mV/°C
DYNAMIC ACCURACY					
No missing codes		Assured			
DNL Differential linearity error	f _{IN} = 10 MHz	-0.99	±0.7	2.5	LSB
INL Integral linearity error	f _{IN} = 10 MHz	-7.0	±1.5	7.0	LSB
Offset error		-16		16	mV
Offset temperature coefficient		0.02			mV/°C
Gain error		-5		5	%FS
Gain temperature coefficient		-0.02			%FS/°C

Figure D.4: A/D converter electrical characteristics at T = 25°

HFG (S-CQFP-F84)

CERAMIC QUAD FLATPACK WITH NCTB

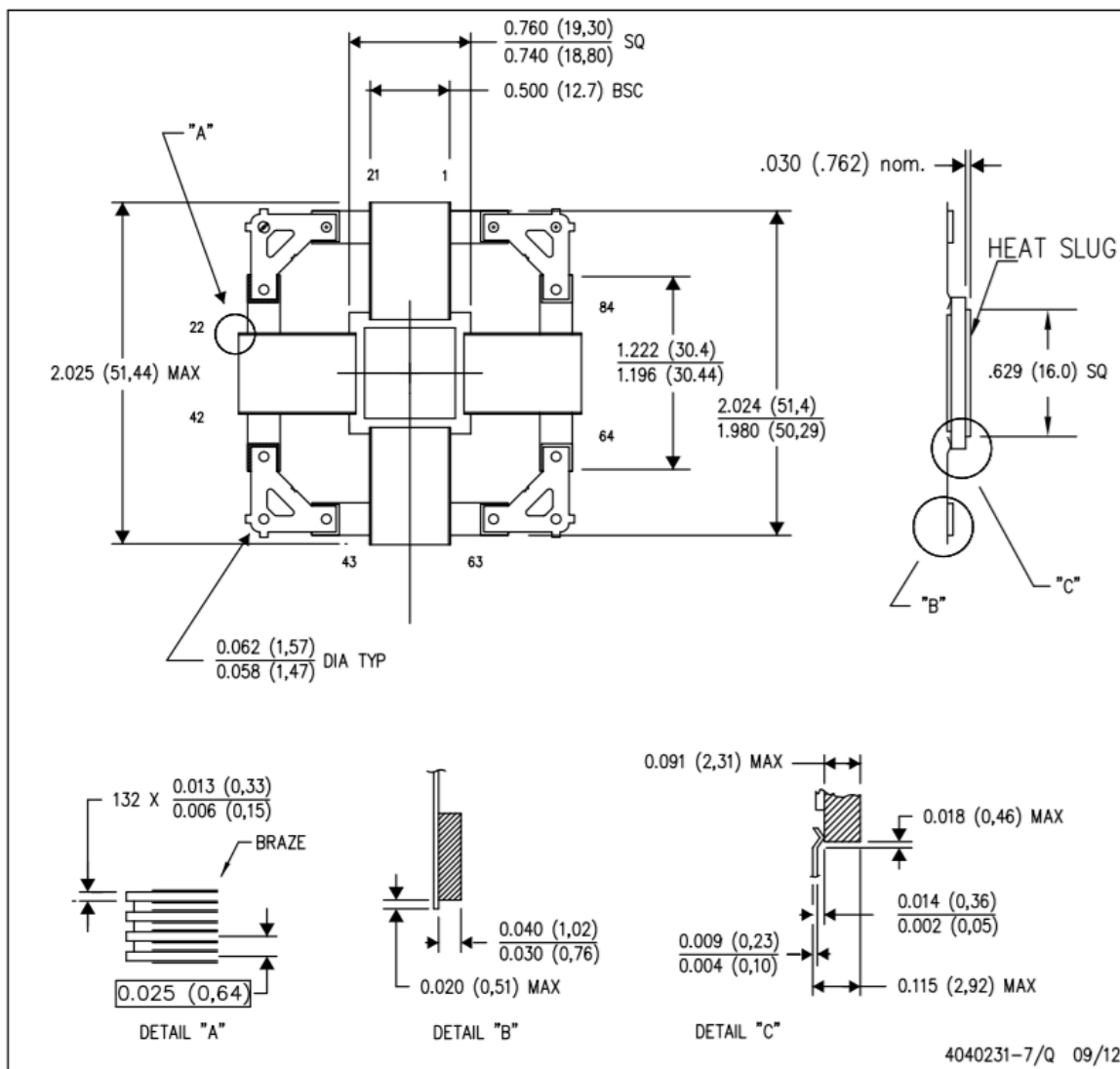


Figure D.5: A/D converter architecture

Bibliography

- [1] Peyrou-Lauga R. Darel A. *JUICE thermal architecture and performance*. Tech. rep. ESA ESTEC, AIRBUS Defence, and Space, 2017.
- [2] *Aluminum 2014-T6*. URL: <http://www.matweb.com/search/DataSheet.aspx?MatGUID=e5de9f1161d34f71a34ae016723d097f&ckck=1>.
- [3] Hiroshi ARAKI et al. “Performance Model Simulation of Ganymede Laser Altimeter (GALA) for the JUICE Mission”. In: *Transactions of the Japan Society for Aeronautical and Space Sciences* 17 (Jan. 2019). DOI: 10.2322/tastj.17.150.
- [4] A. Chandravanshi M. Mukhopadhyay. “Modal Analysis of Structural Vibration”. In: vol. 14. Nov. 2013. DOI: 10.1115/IMECE2013-62533.
- [5] Brush Beryllium & Composites. *Designing for Optics: Beryllium*. Tech. rep. Materion Corporation.
- [6] *Excelitas Technologies*. URL: <https://www.excelitas.com/product/c30954eh-si-apd-08mm-5-package>.
- [7] *Fused Silica in Optical Components*. URL: <https://www.opcolab.com/fused-silica-in-optical-components/>.
- [8] Stewart Sarah Gilbert. *Development of a database for rapid approximation of spacecraft radiation dose during Jupiter fly-by*. Tech. rep. University of Tennessee, Knoxville, 2016.
- [9] *Gradient material solutions*. URL: <https://fabrisonic.com/gradient-material-solutions/>.
- [10] Podzolko M. V. Getselev I. V. IAM IKI. *Radiation Conditions of a Mission to Jupiter’s Moon Ganymede*. Tech. rep. Skoletsyn Institute of Nuclear Physics, Lomonosov Moscow State University, Russia.
- [11] Donald L. T. Roberto J. Jensen B. Hales S. Alexa J. *Methods of making Z-shielding*. Tech. rep. United States Patent US 8,661,653 B2, 2014.
- [12] Thomas N. Hussmann H. Spohn T. Lara L.M. Christensen U. Affolter M. Bandy T. Beck T. Chakraborty S. Geissbuehler U. Gerber M. Ghose K. Gouman J. *The BepiColombo Laser Altimeter*. Tech. rep. Springer Nature, 2021.
- [13] Kallenbach R. Behnke T. Perplies H. Henkelmann R. Rech M. Geissbühler U. Péteut A. Lichopoj A. Schroedter R. Michaelis H. Seiferlin K Thomas N. Castro J. M. Herranz M. Lara L. “Electromagnetic compatibility of transmitter, receiver, and communication port of a space-qualified laser altimeter”. In: *2016 ESA Workshop on Aerospace EMC (Aerospace EMC)*. 2016, pp. 1–7. DOI: 10.1109/AeroEMC.2016.7504591.
- [14] *M-NANO 80mJ 10Hz Nd:YAG DPSSL w/ Separate Compact Driver [PR179]*. URL: https://montfortlaser.com/en/products-solutions/detail/M-NANO-NdYAG-80-10-2.5m-LH-EL_PR179.
- [15] Saranath K. M. Reddy K. R. Ramji M. “Material Characterization of Al 2014-T6 Aluminum Alloy Using Virtual Fields Method”. In: Nov. 2014. DOI: 10.13140/2.1.2765.9206.

- [16] Atzei A. Wielders A. Stankov A. Falkner P. *Overview of the ESA Jovian Technology Reference Studies*. Tech. rep. ESTEC, 2007.
- [17] *Peltier thermoelectric cooler*. URL: <https://tetech.com/peltier-thermoelectric-cooler-modules/>.
- [18] Lagier Roland. *Ariane 5 User's Manual*. Tech. rep. ArianeSpace, 2016.
- [19] Al Naber A. Balossi C. Bonfanti S. Corradetti M. Di Lazzaro C. Di Vitto M. Grusovin S. Lardo G. Mascetti S. “LASAGNA Mission Requirements Document”. In: June 2021.
- [20] *Texas Instruments*. URL: <https://www.ti.com/product/ADS5474-SP>.
- [21] *Titanium 6Al-4V*. URL: <https://www.zare.it/materiali/titanio-ti64al4v>.